OULU 2013
C 447

ACTA UNIVERSITATIS OULUENSIS

Marko Sonkki

WIDEBAND AND MULTI-ELEMENT ANTENNAS FOR MOBILE APPLICATIONS

UNIVERSITY OF OULU GRADUATE SCHOOL;
UNIVERSITY OF OULU,
FACULTY OF TECHNOLOGY,
DEPARTMENT OF COMMUNICATIONS ENGINEERING;
CENTRE FOR WIRELESS COMMUNICATIONS;
INFOTECH OULU

ACTA UNIVERSITATIS OULUENSIS
C Technica 447

MARKO SONKKI

WIDEBAND AND MULTI-ELEMENT ANTENNAS FOR MOBILE APPLICATIONS

Academic dissertation to be presented with the assent of the Doctoral Training Committee of Technology and Natural Sciences of the University of Oulu for public defence in Wetteri-sali (IT115), Linnanmaa, on 17 May 2013, at 12 noon

UNIVERSITY OF OULU, OULU 2013

Acta Univ. Oul. C 447, 2013

Supervised by
Doctor Erkki Salonen
Professor Miguel Ferrando Bataller

Reviewed by
Doctor Marta Martínez Vázquez
Doctor Clemens Icheln

ISBN 978-952-62-0107-8 (Paperback)
ISBN 978-952-62-0108-5 (PDF)

ISSN 0355-3213 (Printed)
ISSN 1796-2226 (Online)

Cover Design
Raimo Ahonen

JUVENES PRINT
TAMPERE 2013

Sonkki, Marko, Wideband and multi-element antennas for mobile applications.
University of Oulu Graduate School; University of Oulu, Faculty of Technology, Department of Communications Engineering; Centre for Wireless Communications; Infotech Oulu, P.O. Box 4500, FI-90014 University of Oulu, Finland
Acta Univ. Oul. C 447, 2013

Abstract

This dissertation presents wideband and multi-element antennas for mobile applications. It is divided into the following main parts: modal theory, wideband antennas, multi-element antennas, and wideband multi-element antennas.

The radiating fields are first studied in terms of spherical scalar and vector modes, and it is shown how these modes correlate with the characteristic current modes on a planar mobile ground plane. The theory part shows how it is possible to excite the same modes on a conventional sphere and a rectangular planar mobile ground plane. The theory refers to the novel wideband antenna structures presented in this dissertation, in terms of current and radiating modes.

After studying the modes, the dissertation shows how to excite a radiating antenna mode within a wide frequency bandwidth. To gain this, two main approaches are taken. First, a quasi-complementary antenna (QCA) structure with an electric conductor and magnetic slot is presented, and its characteristics are studied. A QCA UWB antenna, and a QCA element excited with a monopole or a dipole, is presented. The QCA structure compensates for the imaginary part of the input impedance on wide frequency bandwidth, when, at the same time, the fundamental mode is excited to ensure good radiating properties.

The second approach uses a symmetrical feeding with two antenna elements to gain a wide frequency bandwidth, the relative -6 dB impedance bandwidth between 37.5–80%. When a field is symmetrically coupled to the conducting ground plane, the excitation avoids the awakening of higher order modes which might disturb the performance of the antenna.

It is also shown, by using multiple feeding elements, that the excitation of orthogonal higher order modes on a small radiating ground plane is possible. As the modes are orthogonal to each other, they present a very low correlation. By using this kind of approach, radiation pattern diversity can be obtained in mobile applications within a small volume.

On the other hand, when combining two QCA elements to a one multi-element antenna structure, a wideband diversity antenna with an 87.5% relative -6 dB impedance bandwidth, and a wideband MIMO antenna with a 95.0% relative -6 dB impedance bandwidth, are presented with excellent radiation and correlation properties. Also mutual coupling is need to be counted when multi-element antennas are designed.

When designing an efficient radiator, it is important to consider an antenna feeding in terms of wideband impedance matching and wideband baluns, not to spoil the antenna performance. The efficient antenna structures and feeding mechanisms are obtained by using commercial 3D electromagnetic simulators to find the desired wideband antenna characteristics. Prototype antennas are measured in most of the presented structures to show their functionality in real.

In general, the dissertation presents wideband antenna structures with radiating antenna modes excited on a planar conducting ground plane. The idea is to find structures and feeding mechanisms to excite the fundamental mode, or a certain radiating antenna mode, at a wide frequency bandwidth, by avoiding the excitation of higher order modes which might disturb the antenna performance. It is also shown that, by using multiple feeding elements, it is possible to excite higher order modes on a small antenna.

Keywords: characteristic modes, complementary antenna, diversity techniques, MIMO, multi-element antenna, mutual coupling, slot antenna, small antennas, spherical modes, UWB, wideband antenna

Sonkki, Marko, Matkaviestinten laajakaista- ja monielementtiantenniratkaisuja.
Oulun yliopiston tutkijakoulu; Oulun yliopisto, Teknillinen tiedekunta, Tietoliikennetekniikan osasto; Centre for Wireless Communications; Infotech Oulu, PL 4500, 90014 Oulun yliopisto
Acta Univ. Oul. C 447, 2013

Tiivistelmä

Väitöskirjassa esitetään uusia laajakaistaisia ja monielementtiantenneja matkaviestimiin. Väitöskirja koostuu neljästä pääalueesta: pintavirtojen muototeoria, laajakaistaiset antennit, monielementtiantennit sekä laajakaistaiset monielementtiantennit.

Teoriaosassa säteilykenttiä on aluksi tutkittu pallon pinnalla sekä skalaaripotentiaaleina että pintavirtavektoreina, jonka jälkeen niitä on verrattu mobiilin laitteen maatason ominaispintavirtojen synnyttämiin säteilykenttiin. Teoriaosassa osoitetaan, että pallon pinnalla sekä tasomaisella suorakaiteen muotoisella pinnalla on mahdollista herättää samat säteilykentät. Myöhemmin väitöskirjassa esitettävien uudenlaisten antennirakenteiden ominaisuuksia verrataan teoriaosassa esitettyihin pintavirtoihin ja säteilykenttiin.

Teoriaosuuden jälkeen osoitetaan miten säteilevä sähkömagneettinen kenttä saadaan herätettyä laajalla taajuusalueella. Tähän on otettu kaksi eri lähestymistapaa, joista ensimmäisessä esitellään ja tutkitaan kvasikomplementaarista antennirakennetta (QCA). Kvasikomplementaarisessa antennirakenteessa sisääntuloimpedanssin imaginaariosa kompensoidaan yhdistämällä sähköinen johde ja magneettinen rako samaan antenniin. Samanaikaisesti perusmuoto herätetään laajalla taajuusalueella, jolla varmistetaan antennin hyvät säteilyominaisuudet koko toimintataajuusalueella.

Toisessa lähestymistavassa käytetään kahta symmetrisesti asetettua antennielementtiä, joita syötetään symmetrisesti samalla amplitudilla ja vaiheella. Kun sähkömagneettinen kenttä herätetään symmetrisesti, korkeamman kertaluvun muotojen herättäminen voidaan välttää laajalla taajuusalueella. Symmetrisesti syötetyillä antennirakenteilla saavutettu -6 dB suhteellinen impedanssikaistanleveys on 37.5–80 %.

Useita syöttöelementtejä käytettäessä voidaan mobiilin laitteen maatasossa herättää yhdellä pistetaajuudella monta toisistaan riippumatonta säteilykenttää. Koska herätetyt kentät ovat toisistaan riippumattomia, on niiden välinen korrelaatio myös pieni. Kyseisellä rakenteella on mahdollista toteuttaa säteilykuviodiversiteetti erittäin pienessä tilassa, kuten matkapuhelimessa.

Toisaalta, kun yhdistetään kaksi QCA-elementtiä yhdeksi monielementtiratkaisuksi, voidaan toteuttaa laajakaistainen diversiteettiantenni, jonka suhteellinen -6 dB impedanssikaistanleveys on 87.5 %. Vastaavasti kahdella laajakaistaisella QCA-elementillä toteutetulla MIMO-ratkaisulla päästään 95 % suhteelliseen -6 dB impedanssikaistanleveyteen. Molemmilla ratkaisuilla on erittäin hyvät säteilyominaisuudet sekä alhainen korrelaatio ja pieni keskinäiskytkentä antennielementtien välillä.

Suunniteltaessa toimivaa laajakaistaista antennirakennetta, on tärkeää ottaa huomioon antennisyötön impedanssisovitus, jotta antennin suorituskyky ei heikkenisi. Lisäksi balansoidussa rakenteissa tulee olla laajakaistainen baluni, jolla vältetään säteilykuvion vääristyminen. Väitöskirjan syöttöratkaisuissa on käytetty kaupallisia sähkömagneettisia simulaattoreita, joilla antennirakenne voidaan mallintaa kolmiulotteisesti, ja joilla laajakaistainen syöttö saadaan optimoitua haluttuun antenniin. Suurin osa esitellyistä antennirakenteista on simulointien lisäksi myös mitattu, jolloin niiden toimivuus käytännössä pystytään todentamaan rakentamalla prototyyppiantenni.

Yleisesti väitöskirjassa esitellään tasomaisia antenniratkaisuja johtavassa maatasossa, joissa säteilevät pintavirrat herätetään mahdollisimman laajalla taajuusalueella. Ideana on löytää laajakaistaisia antenni- ja syöttörakenteita, joilla saadaan herätettyä perusmuoto tai jokin muu haluttu muoto. Ajatuksena on välttää korkeamman kertaluvun muotojen herättäminen, jotka voivat pilata antennin suorituskyvyn. Väitöskirjassa osoitetaan myös, että pienikokoisella antennilla on mahdollista herättää korkeamman kertaluvun muotoja pistetaajuudella käyttämällä useita heräte-elementtejä.

Asiasanat: diversiteettitekniikat, keskinäiskytkentä, komplementaarinen antenni, laajakaistainen antenni, MIMO, monielementtiantenni, pienet antennit, rakoantennit, *UWB*

Dedicated to my Family

Preface

My carrier in the field of radio engineering began at the University of Oulu in 2002 under the supervision of Prof. Erkki Salonen. After receiving my M.Sc degree in December 2004, I began my Ph.D. studies in 2005. As I was mostly carrying out research with antenna measurements by developing a measurement system for adaptive antennas in the department of Electrical Engineering, I began to focus my research on mutual coupling and mobile terminal antennas at the beginning of the Ph.D. studies.

During the first year of the Ph.D. studies, I received a three year project manager task (2005–2007) in a Tekes funded project "Future Active Multi-Frequency Antennas - TAMTAM". This naturally slowed down the progress of my research and PhD studies. After this three year period of project management, a new Tekes funded project called "Adaptation of Antennas to Usage Environments - AATE" was established in 2008–2010. The project studied different effects in a usage environment and how to compensate for them. This was the point where I began my research exchange period.

Previously, before the AATE-project started, I contacted Prof. Miguel Ferrando Bataller at the Universitat Politècnica de València in Spain to open up a new research contact with him and his antenna research team. The funding was first scheduled for nine months during 2008, but because of the fruitful cooperation, the exchange period finally took 18 months till the end of 2009, with a grant from the Universitat Politècnica de València. During the exchange period, antenna structures that are less sensitive to the user vicinity were studied. The research was chosen to carry out on wideband and multi-element antennas in mobile applications, which finally came to the title of my dissertation.

Later, a seven month research exchange period took place during 2010–2011 in a Tekes funded project "MIMO Terminal Testing Over-the-Air - MIMOTA". In the project, a wideband dual-polarized probe for a MIMO OTA test system was developed. During the visit, on the advice of Prof. Ferrando Bataller, I began the writing process of my dissertation and to think about the contents. At the beginning of 2012, Prof. Ferrando Bataller was officially accepted as the second supervisor to my dissertation by the management board of the University of Oulu Graduate School (UniOGS).

At the time of finalizing the dissertation for the review process, I was pleased to work for a three weeks exchange period in cooperation with Drexel University in Philadelphia.

A Tekes funded project "Reconfigurable Antenna Based Enhancement of Dynamic Spectrum Access Algorithms - RADSA" took place at the beginning of 2012. The project was focusing on Cognitive Radio, where my task was to design a wideband antenna array to a WAPR (Wireless Open-Access Research Platform) demonstrator. As a part of the project, a research exchange with the antenna research community in Drexel was established.

The Ph.D. research work was funded by the Finnish Funding Agency for Technology and Innovation (Tekes) during the years 2005–2012. Additionally, the year 2012 was financially supported by the Infotech Oulu Graduate School.

As there are a numerous number of people who have had a great role in my research and finalizing the dissertation, I would first like to thank my supervisors Dr. Erkki Salonen and Prof. Miguel Ferrando Bataller for providing me with an interesting research topic and by sharing their scientific knowledge through kind and innovating supervision.

I would also like to thank my instructor Dr. Eva Antonino Daviu, for providing help and support with topics related to the mobile antenna research and scientific writing.

My deepest gratitude for my present and former research colleagues, Prof. Pentti Leppänen, Dr. Marta Cabedo Fabrés, Dr. Daniel Sánchez Escuderos, Dr. Juha-Pekka Mäkelä, Dr. Markus Berg, Dr. Esperanza Alfonso Alós, Dr. Seppo Karhu, Lic. Tech. Timo Kumpuniemi, Lic. Tech. Risto Vuohtoniemi, Lic. Tech. Pekka Lilja, M.Sc. Ana Rodríguez Pérez, M.Sc. Jukka Kyröläinen, M.Sc. Veikko Hovinen, M.Sc. Juha Pihlaja, M.Sc. Antonio Berenguer Verdú, M.Sc. Tommi Tuovinen, M.Sc. Emmi Kaivanto, B.Sc. Tuomas Jääskö, and B.Sc. Mikko Heikkinen for offering priceless scientific background and help to my work.

My compliments to Anssi Rimpiläinen, Jari Pakarinen, Antti Nevantalo, Vesa Kaltio, Antonio Vila Jiménez, and Bernat Bernardo Clemente of manufacturing prototype antennas. Without their professional skills, complicated prototype antenna structures could not be fabricated. Also, laboratory engineer Jari Sillanpää and department secretary Varpu Pitkänen deserve warm thanks for organizing practical things related to my research work and PhD studies.

Acknowledgement to the University of Oulu, the Universitat Politècnica de València, the Nokia Foundation, the Tauno Tönning foundation, COST ASSIST IC0603, the Seppo Säynäjäkangas foundation, and the Ulla Tuominen foundation for financially supporting my PhD studies.

Finally, I would like to thank all my family members for their endless support and understanding towards my research work and encouraging my career.

Abbreviations

1G	*First generation analog mobile phone system*
2G	*Second generation digital mobile phone system*
3D	*Three Dimensional*
3G	*Third generation digital multimedia mobile phone system*
3GPP	*3rd Generation Partnership Project*
3.5G	*Digital multimedia mobile phone system between 3G and 4G systems*
4G	*Fourth generation digital multimedia mobile phone system*
ACA	*Auto-Complementary Antenna*
AoA	*Angle of Arrival*
AMC	*Artificial Magnetic Conductor*
AMG	*Artificial Magnetic Ground plane*
CCE	*Capacitive Coupling Element*
CST	*Computer Simulation Technology*
DASY	*Dosimetric Assessment SYstem*
DCS	*Digital Cellular System*
DGS	*Defected Ground Structures*
DVB-H	*Digital Video Broadcast Handset*
DUT	*Device Under Test*
EBG	*Electromagnetic Band Gap*
EDG	*Effective Diversity Gain*
E-GSM	*Extended Global System for Mobile communications*
EMC	*Electromagnetic Compatibility*
EurAAP	*European Association on Antennas and Propagation*
FCC	*Federal Communications Commission*
FRC	*Federal Radio Commission*
GNSS	*Global Navigation Satellite System*
GSM	*Global System for Mobile communications*
HFSS	*High Frequency Structure Simulator*
HPF	*High Pass Filter*
IEEE	*Institute of Electrical and Electronics Engineers*
IFA	*Inverted F-Antenna*

i.i.d.	*Identically distributed*
ILA	*Inverted L-Antenna*
LC	*Inductor (L) Capacitor (C)*
LPF	*Low Pass Filter*
LTE	*Long Term Evolution*
LOS	*Line Of Sight*
MB	*Metal Bezel antenna structure*
MIMO	*Multiple Input Multiple Output*
MISO	*Multiple Input Single Output*
MSA	*Microstrip Antenna*
NFC	*Near-Field Communication system*
OQCA	*Optimized Quasi-Complementary Antenna*
OQCAS	*Optimized Quasi-Complementary Antenna with Switch*
OTA	*Over The Air*
PAS	*Power Angular Spectrum*
PBG	*Photonic BandGap*
PCB	*Printed Circuit Board*
PCS	*Personal Communications Service*
PDA	*Personal Digital Assistant*
PIFA	*Planar Inverted F-Antenna*
QCA	*Quasi-Complementary Antenna*
RF	*Radio Frequency*
RFID	*Radio Frequency IDentification*
SAR	*Specific Absorption Rate*
SCM	*Spatial Channel Model*
SCME	*Extended Spatial Channel Model*
SFD	*Symmetrical Folded Dipole*
SIMO	*Single Input Multiple Output*
SMA	*SubMiniature version A*
SNR	*Signal to Noise Ratio*
TCM	*Theory of Characteristic Modes*
TE	*Transverse Electric wave*
TM	*Transverse Magnetic wave*
UMTS	*Universal Mobile Telecommunications System*
UWB	*Ultra Wideband*

VNA	*Vector Network Analyzer*
WLAN	*Wireless Local Area Network*

ε	*Characteristic angle*
ε	*Permittivity*
η	*Wave impedance*
η_0	*Free-space wave impedance*
$\eta_{rad,n}$	*Radiation efficiency of nth antenna element*
η_{MIMO}	*MIMO efficiency*
θ	*Elevation angle*
λ_n	*Eigenvalues*
μ	*Permeability*
ρ	*Complex cross correlation coefficient*
ρ_e	*Envelope correlation*
ϕ	*Azimuth angle*
ψ	*Complex scalar wave function*
ω	*Angular frequency*
Ω	*Solid angle, characteristic impedance*
∇	*Nabla*

A_r	*Magnetic field component*
$\vec{A}$	*Magnetic vector potential*
$b_n(kr)$	*Spherical Bessel function of n^{th} order*
$B_n(kr)$	*Ordinary Bessel function of n^{th} order*
$\hat{B}_n(kr)$	*Spherical vector Bessel function of n^{th} order*
$C_{n,m}$	*Constant in a spherical wave functions, magnetic vector potential*
C_{tr}	*Mutual coupling*
d	*Slot separation, antenna separation*
$D_{n,m}$	*Constant in a spherical wave functions, electric vector potential*
E^i	*Incident field*
E_r	*r component of the electric field*
E_ϕ	*ϕ component of the electric field*
E_θ	*θ component of the electric field*
F_r	*Electric field component*
$\vec{F}$	*Electric vector potential*

$\vec{F}(\theta,\phi)$	*Radiated field of the ith excited antenna element*
$h(m\phi)$	*Spherical harmonics of m^{th} degree*
$h_n^{(1)}(kr)$	*Hankel function of 1nd kind*
$h_n^{(2)}(kr)$	*Hankel function of 2nd kind*
H_r	*r component of the magnetic field*
H_ϕ	*ϕ component of the magnetic field*
H_θ	*θ component of the magnetic field*
$j_n(kr)$	*Bessel function of 1st kind*
J	*Total current of Characteristic modes*
J_n	*Characteristic modes*
$\vec{J}_n$	*Eigenfunctions, Eigencurrents*
k	*Wave number*
L	*Length of the ground plane*
$L_n^m(\cos\theta)$	*Legendre function*
m	*Degree of a spherical mode, integer*
n	*Order of a spherical mode, integer*
$n_n(kr)$	*Bessel function of 2nd kind*
N	*Number of spherical modes*
P_D	*Power radiated by the excited antenna*
P_L	*Power delivered to the load of the unexcited antenna*
Q	*Quality factor*
r_0	*Radius of a minimum sphere over an antenna*
r	*Radius from the origin*
$\vec{r}$	*Radius vector from the origin*
$P_n^m(\cos\theta)$	*Associated Legendre function of the first kind*
$Q_n^m(\cos\theta)$	*Associated Legendre function of the second kind*
R	*Real part of impedance operator*
s	*Slot width*
S_{ii}	*Reflection coefficient*
S_{ij}	*Transmission coefficient*
V_n^i	*Modal excitation coefficient*
w	*Antenna spacing*
W	*Width of the ground plane*
X	*Imaginary part of impedance operator*
Z	*Impedance operator*

Z_0	*Input impedance*
Z_{slot}	*Input impedance of areal slot*
Z_{metal}	*Input impedance of metal conductor*

List of original articles

This dissertation is based on the following 10 articles, which are cited in the text by their Roman numerals (I–X):

I Sonkki M, Antonino-Daviu E, Ferrando-Bataller M, Salonen E (2011) Small Radiating Ground Plane with Higher Order Modes, In: IEEE 5th European Conference on Antennas and Propagation (EuCAP2011): 1243–1247.

II Sonkki M, Ferrando-Bataller M, Antonino-Daviu E, Salonen E (2010) Optimized Dimensions of Ultra Wideband Quasi-Complementary Antenna with Switching Capability, In: 4th European Conference on Antennas and Propagation (EuCAP2010): 1–4.

III Sonkki M, Antonino-Daviu E, Ferrando-Bataller M, Salonen E (2011) Wideband Planar Slotted Radiating Ground Plane Antenna for Portable Devices, In: Wiley's Microwave and Optical Technology Letters 53(12): 2854–2858.

IV Sonkki M, Salonen E (2010) Low Mutual Coupling Between Monopole Antennas by Using Two $\lambda/2$ Slots, In: IEEE Antennas and Wireless Propagation Letters 9: 138–141.

V Sonkki M, Antonino-Daviu E, Ferrando-Bataller M, Salonen E (2009) Optimal Dimensions of Two Microstrip Patch Antennas for Low Mutual Coupling at 5.8 GHz, In: 3th European Conference on Antennas and Propagation (EuCAP2009), 23th–27th March 2009, Berlin, Germany, VDE VERLAG GMBH · Berlin · Offenbach, Germany, 2009: 3515–518.

VI Sonkki M, Cabedo-Fabrés M, Antonino-Daviu E, Ferrando-Bataller M, Salonen E (2011) Creation of a Magnetic Boundary Condition in a Radiating Ground Plane to Excite Antenna Modes, In: IEEE Transactions on Antennas and Propagation 59(10): 3579–3587.

VII Sonkki M, Antonino-Daviu E, Ferrando-Bataller M, Salonen E, (2012) Performance Comparison of a Symmetrical Folded Dipole Antenna for Mobile Terminals and Its Metal Bezel Extension, In: IEEE 6th European Conference on Antennas and Propagation (EuCAP2012): 1913–1916.

VIII Sonkki M, Antonino-Daviu E, Ferrando-Bataller M, Salonen E (2010) Wideband Multi-element Antenna with Symmetrical Chassis Coupling, In: 4th European Conference on Antennas and Propagation (EuCAP2010): 1–3.

IX Sonkki M, Antonino-Daviu E, Ferrando-Bataller M, Salonen E (2011) Planar Wideband Polarization Diversity Antenna for Mobile Terminals, In: IEEE Antennas and Wireless Propagation Letters 10: 939–942.

X Sonkki M, Antonino-Daviu E, Cabedo-Fabrés M, Ferrando-Bataller M, Salonen E, (2012) Improved Planar Wideband Antenna Element and Its Usage in a Mobile MIMO System, In: IEEE Antennas and Wireless Propagation Letters 11: 826–829.

The papers [I]-[III] and [VI]-[X] were supervised by Dr. Erkki Salonen and Prof. Miguel Ferrando Bataller, except papers [IV]-[V], which were supervised by Dr. Erkki Salonen. Dr. Eva Antonino Daviu has been the instructor in papers [I]-[III] and [V]-[X].

The idea for papers [I]-[III], [VI]-[VII], and [IX]-[X] were invented together by the author and Prof. Miguel Ferrando Bataller. The idea for paper [VIII] was invented

together by the author and Dr. Eva Antonino Daviu, whereas the idea for papers [IV]-[V] was invented by the author.

The idea of the metal bezel structure for paper [VII] was invented together by the author, Prof. Miguel Ferrando Bataller, and Dr. Zlatoljub Milosavljevic from Pulse Finland.

The author has conducted all the electromagnetic simulations for papers [I]-[X]. The parametric optimization of the antenna structures, antenna feeding mechanisms, impedance matching, LC- and tapered microstrip line baluns, and the prototype antenna designs for papers [III]-[X] are conducted by the author.

The calculations and analysis of the Characteristic Modes Theory in paper [VI] were conducted by Dr. Marta Cabedo Fabrés and Dr. Eva Antonio Daviu.

The author has performed the prototype antenna measurements for papers [IV]-[X]. The antenna measurements for paper [III], and the SAR-measurements for paper [VII], were performed at Pulse Finland by B.Sc. Tuomas Jääskö and B.Sc. Mikko Heikkinen.

The author has performed all the postprocessing related to the antenna measurements in papers [III]-[X]. The envelope correlations, diversity and MIMO performance calculations for papers [I] and [IX]-[X] are performed by the author.

The author has the main responsibility of analyzing the measurement results in papers [III]-[X]. The main responsibility for analyzing the simulation results in papers [I]-[II] was done together by the author and Prof. Miguel Ferrando Bataller.

The author had the leading role in the preparation of the papers [I]-[X]. Dr. Eva Antonino Daviu participated in the preparation of the papers [I]-[III] and [V]-[X]. Dr. Marta Cabedo Fabrés participated in the preparation of the papers [VI] and [X].

The work for publications [I], [II], [III], [VI], [VII], and [VIII] were done during the Tekes funded project AATE (Adaptation of Antennas to Usage Environments). The industrial companies involved in the project to share technology transfers were Elektrobit, Nokia Devices Oulu, and Pulse Finland.

The research related to the original publications [IV] and [V] was done during the Tekes funded project TAMTAM (Future Active Multi-Frequency Antennas). The industrial companies involved in the project to share technology transfers were Elektrobit, Nokia Devices Oulu, and Pulse Finland.

The final two publications [IX] and [X] were developed during the Tekes funded project MIMOTA (MIMO Terminal Testing Over-the-Air). The industrial companies involved in the project to share technology transfers were Elektrobit, ETS-Lindgren, Nokia Devices Oulu, and Pulse Finland.

Contents

1 Introduction

1.1 Background of the research

Consumers are more and more demanding of the services that their mobile phones are offering. They are used to getting a data connection or making phone calls with their smartphones, and to use applications which require high data rates almost everywhere. An exponential growth in using social networks and audio and video streams is increasing the traffic – advanced smartphones are pushing wireless networks to their limits. Today and in the future, there is and will be a need for multiple radio interfaces for several wireless standards in mobile devices [1].

Multiple radio interfaces and wide bandwidths are required when, at the same time, the data rates are increased. One possibility to increase data rates in mobile applications is to use diversity techniques [2] or an MIMO-system (Multiple-Input-Multiple-Output) [3]. Roughly, diversity techniques improve the reliability of radio links, and can be employed in the MIMO-system as well, whereas MIMO multiplexing is used to improve spectrum efficiency.

A cognitive radio is also under investigation and has shown great interest in scientific communities and commercial companies. In the cognitive radio system, the frequency spectrum resources are shared dynamically and efficiently over a wide frequency range by covering multiple wireless standards [4] such as DVB-H (Digital Video Broadcast Handset), mobile standards, WLANs (Wireless Local Area Network), and UWB (Ultra WideBand). When multiple radio interfaces are required to sense different frequencies simultaneously, wideband antenna characteristics become very attractive.

For all of the wireless communication systems, such as LTE (Long Term Evolution) and LTE Advanced [5], efficient antenna solutions are needed. In addition, the RF (Radio Frequency) front-end design will also have to respond with these challenges. To connect a smartphone to the outer world with a mobile or wireless connection, an antenna is needed to transfer and receive a data stream efficiently [6]. Without this crucial part, making a connection becomes impractical or even impossible.

So, what are these so called antennas? Antennas are devices which convert an alternative current in a guided waveguide into a radiating electromagnetic wave in an unguided medium [7]. This is a technique when the antenna is in a transmitting

mode. The phenomenon is opposite when the antenna is in a receiving mode; an electromagnetic wave is converted to an alternative current.

Nowadays, antennas are needed in almost every application related to radio engineering. A high growth in applications at different radio frequencies or radio interfaces is providing strict demands on antennas; the shape and size are strongly dependent on the frequency and the purpose of use. Antennas can be divided in different groups, e.g., by the way they are radiating; current element, aperture, antenna array, and so on. They can also be divided by the system in which antennas are used, e.g., mobile communications, body-wear, radars, satellites, amateur purposes, etc [7–9].

One important part of antenna design is antenna measurements [7, 10]. When talking about mobile applications, impedance bandwidth, real or complex radiation patters, polarization and radiation or total efficiencies are the most important parameters to investigate the antenna performance. As the impedance bandwidth is easy to measure, e.g., with a Vector Network Analyzer (VNA), to measure radiation patterns, more complicated systems are required. In general, the radiation pattern measurement systems can be separated in four different ways, which are: (1) conventional far-field range, (2) compact range, (3) array of probes, and (4) scanning with a single probe [11]. The first two are far-field measurement systems, whereas, the last two are categorized as near-field measurement systems. Far-field measurement systems are implemented in an anechoic chamber (indoor) or in an outdoor range which is not protected from environmental conditions. Nowadays, a number of near-field antenna measurement systems are also commercially available (e.g. Satimo, EMScan, Nearfield Systems Inc.). The near-field antenna measurement systems offer a quick way to measure antennas in an indoor environment.

Since the space in mobile devices is limited, instead of using an individual antenna for every communication system, one way is to use multi-resonance antennas with frequency tuning/switching, or antennas with wideband characteristics. To further extend the wideband antenna perspective, which is the topic of this dissertation, to a closely packed multi-element antenna solution in a mobile device, interaction between the individual antenna elements arise as a problem in terms of mutual coupling [12, 13]. Mutual coupling affects the correlation between multiple antenna elements, and, thus, to the system data transmission capacity. To overcome the aforementioned challenges, methods to compensate for mutual coupling need to be found.

Also, an investigation of wideband multi-element antenna solutions with a MIMO or diversity characteristics must be considered to enable higher date rates. The vicinity of a

user also cannot be neglected nowadays in a mobile terminal antenna designing. When the effect of a user is counted in the design procedure, it enables a better link budget and improved coverage of a telecommunication system by saving battery energy at the same time [14].

When investigating antenna characteristics, the modal theory is a well known method that is used in physics and electromagnetism. In general, the modal theory is studying dynamic properties of structures under oscillating excitation. In this dissertation, the spherical mode theory [15] and the characteristics mode theory [16] are considered and discussed. As the most common coordinate systems used in antenna studies are cartesian, cylindrical, and spherical coordinate systems [15], only the spherical system is considered in this dissertation.

By using the spherical mode theory, the physical limitations of the omnidirectional antennas can be calculated [17]. On the other hand, when measuring antennas in a near-field, the spherical mode theory also plays an important role [18]. It determinate the number of measurement points on a sphere to achieve an appropriate far-field antenna radiation pattern. On the other hand, by using the characteristic modes theory [16], the current modes of arbitrary shaped conducting bodies can be computed. These theories are used here to study the limited number of modes in a planar mobile ground plane, and how current modes in these ground planes can be excited to gain corresponding radiating modes.

1.2 State of the art and motivation

Remarkable progress in mobile communications systems has been occurred in the last decade. Mobile phone systems have evolved from first generation (1G) analogue systems to digital second generation (2G) systems, and further to third generation (3G) multimedia systems. Now, the 3G systems are being advanced to fourth generation (4G) systems (LTE Advanced) through 3.5G systems, which stand between 3G and 4G systems, in order to transition to 4G systems smoothly from 3G systems [8].

In addition, various wireless mobile systems other than mobile phone systems have been deployed and service areas rather narrow territories, ranging from very short distances to intermediate distances, whereas mobile phone systems provide nation-wide services. The systems not only provide communication services but also perform control, data transmission, identification, and sensing, either through their network or their own structure. Typical systems are e.g. multi-band Global Navigation Satellite

System (GNSS), UWB, Radio Frequency IDentification (RFID), Bluetooth, Near-Field Communications (NFC) systems, WLAN (2.4 and 5.2 GHz) and 60 GHz, TV, FM radio, and mobile WiMAX (Worldwide Interoperability for Microwave Access). Among them, some broadband systems feature capabilities of very high data-rate transmission, even while in motion at very high speed [19].

Another significant possibility with these newly developed wireless systems is to achieve seamless communication links by connection these systems to each other, including mobile phone systems. The operating frequencies used by these systems range from kilohertz region to as high as gigahertz region, depending on the system performance, complexity, transmitting media, data, and so forth. Various antenna solutions to use in these systems have been developed, and accordingly the antenna technology has made progress along with the development of these systems [8].

Antennas used in wireless mobile systems, including mobile phones, must be small in size, compact, built-in, light in weight, multi-band, and yet functional. Increased use of multimedia services has sped deployment of high speed, high data-rate transmission systems, for which advanced antenna systems like adaptive arrays and MIMO arrays have been developed. For example, a smartphone needs to support more than ten 4G and 3.5G networks and all 2G and 3G networks for global coverage and roaming, which means dozens of cellular radio frequency bands plus multi-antenna systems in some of the bands. For MIMO and diversity applications in WLAN, 3.5G, and 4G systems, the multi-antenna systems require low mutual coupling and radiation pattern correlation between antennas in order to realize good diversity and MIMO performance [19].

Before 1998, most of the mobile phone antennas were external, which are simple and easy to reuse. Nowadays, the antennas are internal and it has followed the trend of the mobile phone to become a multimedia handset. The main types of internal antennas are the PIFA [20], the folded monopole antenna [21], loop antenna [22], and dielectric resonator antenna (DRA) [23]. The first systematic analysis work about bandwidth enhancement by using the mobile chassis mode of the mobile chassis was done by Prof. Pertti Vainikainen's group [24], where theoretical maximum relative -6 dB impedance bandwidth of a mobile chassis was simulated to be 95%. In most of the published papers the mobile chassis exploit to excite the fundamental mode (the 1st order mode) [25–27], whereas only few papers present excitation of higher order modes [28]. A survey of internal mobile phone antennas in the last decade can be found in [29].

In a mobile chassis, there exists not only a single resonant mode but several ones, which can be computed in terms of the Theory of Characteristic Modes (TCM) [16].

Prof. Miguel Ferrando's group has developed a simulation tool to compute these modes on planar arbitrary shaped antenna at wide frequency range [30, 31]. These characteristic modes can be used to improve a handset radiating properties by choosing the excitation so that a particular mode is excited without disturbance of other modes. As each resonant mode represents a different resonant frequency and bandwidth properties, the information provided by each mode is very helpful in the antenna design process [32].

Since characteristic modes form a set of orthogonal functions, they can be used to excite a set of orthogonal higher order modes on a single antenna element. For example, on a mobile chassis, by using multiple excitation elements, orthogonal radiation patterns can achieved at a single frequency [28]. In [33], a study of a loop shaped MIMO antenna with four excitation sources is presented to obtain orthogonal radiating modes. The paper presents a design procedure of a multimode MIMO antenna based on the TCM. By properly choosing the excitation mechanism for each mode, a simple and compact antenna for MIMO applications can be designed.

Nowadays there are multiple radio interfaces in mobile and wireless devices to cover different wireless applications. Moreover, the trend for mobile devices is to increase the number of operating frequency bands. In such devices, the space might become a limiting criterion for multiple antenna configurations. One way to reduce the number of antenna elements to cover multiple radio interfaces at wide frequency range is usage of frequency-tunable [34–37], or multi-band antennas [38–41]. In addition, one option is to use wideband antennas [42–45]. These wideband antennas have a relative -6 dB impedance bandwidth between 30–87%, depending on the structure. Among the others, UWB antennas are also studied for mobile applications [46–49].

In [50], a wideband antenna is determined as one which is matched over 10% of a relative frequency band or more with respect to the center frequency, whereas narrow band antenna is matched over less than couple per cent of the relative bandwidth. Still, the required bandwidth of the antenna can depend on the application in question, and the term wideband can mean a different frequency range for different applications [51].

Under normal operating conditions, a mobile terminal will be in interaction with human body and its immediate surroundings, like a head and hand [52, 53]. The effect of the hand is more difficult to quantify as every user holds a terminal differently. This problem is especially important in case of internal antenna, since certain cases the antenna may totally be masked and, thus, affecting dramatically to the link budget [14]. On the other hand, when considering requirements of the radiation absorbed to a human body, the Specific Absorption Rate (SAR) is measured [54].

Lately, the new challenges for the near-field issue in a mobile phone handset were born from the RF multi-transmitters in MIMO, such as how to arrange and control the antenna elements, and how to design a slim handset while still meeting safety limits [19]. MIMO, such as LTE and WLAN will introduce multi-radio transmitter and multiple antennas in a compact terminal. The body tissue property such as the conductivity and permittivity are frequency dependent, which increases the complexity of the SAR problem. The research on minimizing SAR such as the antenna types, the antenna arrangement, and smart adaptive control RF architecture in the mobile terminal is on-going [55]. To shorten the SAR evaluation for the handset with multiple transmitters and antennas, Federal Communication Commission (FCC) has proposed a simplified test method [56].

Recently, the mobile systems have been deployed worldwide to support high-speed data communication in the cellular system. The compact MIMO and diversity antenna design is essential to such terminals with multi-band [57]. Other option is antennas with wideband characteristics [58–60]. These wideband antennas have relative -6 dB impedance bandwidths between 60–81%, depending on structure. Also correlation coefficient between antenna elements is an important parameter to describe behaviour between radiation patterns. The parameter can be calculated from 3D complex radiation pattern of the antennas [2] or by using scattering parameters [61]. Using scattering parameters is practical when correlation is needed to investigated at wide frequency range.

The effectiveness of diversity antenna system is usually presented in terms of diversity gain (DG). The DG can be defined as the improvement in time-averaged signal-to-noise ratio (SNR) of a combined signal from diversity antenna system, relative to the SNR from a single antenna system [62]. An effective diversity gain (EDG) is defined to include the total antenna efficiency, which includes reflection losses, ohmic losses, mutual coupling losses, and correlation between the antenna elements [62]. Thus, the isotropic random environment seems to be a good simplified scenario to evaluate the diversity performance [63].

What comes to the MIMO systems, the parameter to describe MIMO performance is called multiplexing efficiency. The multiplexing efficiency in 2x2 MIMO case includes the same parameters as the EDG, except now the total antenna efficiency of both antennas are counted [64]. As the EDG and MIMO efficiency dependents on correlation, e.g. when maximum ratio combining is used for the received signal, the correlation between antenna elements should be less than 0.5 [2].

A good mobile terminal antenna radiates roughly 50% (-3 dB) of the power available from the transmitter [65]. This value is including different components in a mobile terminal like battery, display etc., and, thus, it can be considered good. However, if the antenna is studied only as an antenna, a higher value for total efficiency can be considered by keeping 50% efficiency as a minimum requirement. If -1 dB (80%) total efficiency for an individual antenna element is accepted [66] with 0.5 maximum correlation between two antennas, and these values are added to formulas 27 and 28, a comparable minimum EDG and MIMO efficiency is defined equal to 7.0 and 0.7, respectively.

To realize a compact MIMO antenna, the antenna system also needs low mutual coupling between the antenna elements. One option to achieve low coupling between the antenna ports is to realize orthogonal radiating modes by combining electric dipole and magnetic dipole such as loop or slot antennas [67, 68]. Another way to reduce mutual coupling is to use parasitic scatterer, which can be used to modify ground plane by notches and slots [69–71], where better than 19 dB isolation can be achieved within relatively narrow frequency range. In [72, 73], compact MIMO antenna structures with isolation better than 18 dB over wide frequency range are presented.

As closed space antennas have strong mutual coupling, by reducing it, low correlation between antenna radiation patterns with good radiation efficiencies can be achieved according to achieve good multiplexing efficiency. For example, in [69, 74] the achieved isolation between the antenna elements in a mobile terminal is better 18 dB, the antenna efficiency 80%, and the correlation smaller than 0.2. In MIMO systems, the minimum physical separation between antenna elements for an appropriate limit in correlation between the multitude of received signals is commonly referred to be $\lambda/2$. However, there is no minimum distance condition but rather a definition of the acceptable correlation level to insure the effectiveness of the MIMO system [54].

For mobile phone case, MIMO and diversity performance can be also obtained by using radiation pattern diversity. To achieve radiation pattern diversity, multiple antenna elements can be used to excite orthogonal radiation patterns on a small mobile terminal chassis at the same frequency [28, 75, 76]. The radiation pattern diversity with orthogonal modes can be amount to polarization diversity, where two orthogonal dipoles represents two orthogonal radiating modes, or to space diversity, where two antenna elements represents two separate modes.

In the future, there is a huge need for practical solutions in portable devices to find efficient antennas for wireless communication systems. Multiple radio interfaces and

wide bandwidths are required when, at the same time the data rates are increased leading to multiple-antenna MIMO/diversity systems. Because of the space in a portable device is limited, instead of using individual antennas for different radio interfaces, alternative approach is to use single or multi-element antennas with frequency tuning/switching or with wideband characteristics. Alternatively, when multiple antennas are closely packed, problems with interaction between the individual antenna elements arise in terms of mutual coupling.

The motivation of the work is to study novel small planar antenna structures for mobile terminals from wideband and multi-element perspective. It is shown how, by exciting only one antenna mode, a wideband impedance bandwidth can be achieved when, at the same time, the antenna structures satisfy good radiation efficiency. Also, a structure to excite orthogonal higher order modes by using one small antenna with multiple excitation elements is presented. These orthogonal radiating modes can be used in MIMO/diversity applications where one mode represents one antenna element in a multi-element system. Also methods to reduce mutual coupling between closely spaced antenna elements is presented.

1.3 Objectives of the dissertation

This section presents topics related to the state-of-art discussed in the previous section in terms of general and specific objectives. The presented results in the dissertation can be divided into three main topics, which are excitation of higher order modes on a mobile chassis by using multiple excitation elements, wideband antennas by exciting only one mode to avoid the excitation of higher order modes, and wideband multi-antenna structures implemented on the same ground plane with low mutual coupling and correlation between the antenna elements.

As the space is limited in a mobile terminal, the idea is to design planar, simple, small, and robust antenna structures at wide impedance bandwidth to cover multiple wireless standards. The antenna structures also need good radiation efficiency over the bandwidth with omni-directional radiation patterns to satisfy a mobile environment challenges.

The section is divided into two separate parts, which are general and specific objectives. The general part describes the challenges related to wideband and multi-element antenna designing in a mobile application, whereas the specific part defines targeted parameters related to the general part, and also to the state of art.

1.3.1 General objectives

According to the spherical mode theory, it is possible to excite higher order spherical modes when using larger antenna aperture size [18]. Mostly small antennas in mobile terminal are used without excitation of a mobile ground plane. On the other hand, if mobile ground plane is used as an antenna, only one or fundamental mode is usually excited, which are based on studies presented in [24]. However, the excitation of the higher order modes is not widely studied in the literature.

The second objective of the dissertation considers wideband antennas. This is an important issue as there is no space in mobile devices for separate antennas for different wireless standards. In such a case, where an antenna element is closely spaced to an electric conductor, an electric boundary condition is valid, and, thus, the currents in the antenna element and the electric conductor propagate into different directions by canceling the radiation.

The third objective of the dissertation is focusing on wideband multi-element antennas. To guarantee good impedance matching and isolation between closely spaced antenna elements in a mobile terminal, interaction between the antenna elements is need to be taken in to account in terms of mutual coupling. This is important to ensure low correlation between antenna elements, and, thus, to achieve good MIMO and diversity performance of the multi-element system.

1.3.2 Specific objectives

As discussed in the Section 1.2, there are several wireless standards in small mobile devices operating at different frequency bands. To come up with these challenges and cover multiple radio interfaces, antenna research will play an important role as they offer a wireless connection to the other devices and mobile services. To cover multiple wireless standards, a mobile antenna designing can be separated into three subareas: frequency-tuneable antennas, multi-frequency antennas, and wideband antennas. This dissertation concentrates on the last one.

As previously mentioned, in most of the published papers the fundamental mode or one mode of a mobile ground plane is excited. Only few published papers present the excitation of higher order modes [28, 75]. It is shown, from theoretical point of view, numerically by electromagnetic simulations, and by using multiple excitation elements, that excitation of more than four orthogonal higher order modes on a planar mobile

ground plane is possible. This is one of the objectives of the dissertation how to obtain more than four orthogonal higher order modes on a small mobile ground plane.

How to place wideband multiple antenna elements into a small multi-standard mobile device with limited space is an important issue. The question is can an antenna element be excited in a close vicinity of an electric conductor without spoiling impedance matching and radiation properties of the antenna, and how to exploit this at wide frequency range.

As discussed the Section 1.2, an antenna has wideband characteristics if its relative impedance bandwidth is greater than 10% [50]. The dissertation is focusing on finding wideband antenna structures with a relative -6 dB bandwidth better than 30% [44]. The objective is to find methods to excite a single current mode within a wide frequency range by avoiding the excitation of higher order current modes of a mobile ground plane, and, thus, extend the antenna frequency bandwidth.

When a wideband antenna element is combined to a multi-element structure, it is possible to obtain a wideband two element antenna system for mobile diversity and/or MIMO application. How to integrate multiple wideband antenna elements into a small multi-standard mobile device without disturbing the antenna impedance matching and radiation properties is another objective of the dissertation.

As discussed previously, for MIMO/diversity system the relative -6 dB impedance bandwidth should be better than 30% when, at the same time the measured total efficiency of an individual antenna is at most -1 dB ($\leq 80\%$) [66] but better than -3 dB ($\geq 50\%$) [65]. On the other hand, the isolation between the antenna elements must be better than 18 dB [69] with correlation smaller than 0.5 [50]. In addition, the EDG was defined to be better than 7.0, and MIMO efficiency better than 0.7. The objective of this dissertation is to show that it is possible to obtain correlation smaller that 0.2 [74] between two antenna elements. By using formulas 27 and 28, this leads to a minimum requirement for EDG and MIMO efficiency, which are 7.8 and 0.78, respectively.

Notice, that the total efficiency of antenna structures in this dissertation are also presented in terms of an average total efficiency over the operating bandwidth. This is because the total efficiency is usually poor at both ends of the frequency bandwidth, and otherwise variation is very small within the operating bandwidth. Thus, the averaged value is easier to compare to the defined total efficiency of the antenna structures ($-3\ldots-1$ dB), as it varies over a wide frequency range.

The Table 1 lists the specific objectives to obtain in the dissertation compared to the values in the literature. Values for EDG and MIMO efficiency are calculated from limits defined by correlation and total efficiency.

Table 1. Objectives of the dissertation compared to the literature.

	Literature / Reference	Specific objectives
Number of modes	4 / [28]	6
Relative -6 dB BW [%]	> 10 / [50]	> 30
Mutual coupling [dB]	< -18 / [72]	< -18
Average total efficiency [dB]	≥ -3 / [65]	$-3 \ldots -1$
Measured correlation	< 0.5 / [50]	< 0.2
EDG	> 7.0 / Calculated	> 7.8
MIMO efficiency [%]	> 0.70 / Calculated	> 0.78

1.4 Structure of the dissertation

The first chapter of this dissertation, Chapter 1, provides a general perspective to the area of the work. In this section, the structure of the dissertation is presented chapter by chapter to better understand the concept.

Chapter 2 will combine together the theory later needed to compare and understand the discussions done in Chapters 3 and 4. In Chapter 2, the modal theory related to spherical and characteristic modes will be presented. First, the theory related to the spherical scalar function will be presented with numerical results and corresponding point sources on a sphere. Second, the spherical vector function will be presented with numerical results and be compared to the scalar case. Both TM- and TE-modes are studied in vector form with corresponding surface currents on a sphere. Finally, the characteristic modes theory will be discussed, and some of the higher order characteristic current modes on a mobile ground plane will be presented. These current modes are compared to the previously studied spherical vector modes, and it will be shown how to obtain these same radiating modes on a planar structure, rather than on a sphere.

Chapter 3 will discuss basic antenna elements, ultra-wide bands and complementary antennas. The wideband antenna structures in mobile terminals found in literature will be compared to the novel antennas that are presented in this dissertation [II, III, IX, X]. The chapter will also discuss different antenna feeding techniques, baluns and basic

narrow band antennas to better understand the presented results of the novel antenna structures.

Chapter 4 will present wideband multi-element antennas for mobile applications [VI, VII, VIII, IX, X]. The image theory and boundary conditions will be discussed and it is shown how they are used to create magnetic boundary conditions on a mobile ground plane [VI], and manufacture a prototype antenna [VI]. The diversity and MIMO techniques will also be discussed and how, by decreasing mutual coupling [IV, V], a space diversity can be achieved. The wideband antennas presented in Section 3.4.1 will be combined here as multi-element structures to gain space and polarization diversity [IX, X]. Radiation pattern diversity will be presented with multiple dipoles as excitation elements to gain orthogonal radiation patterns [I]. Also, the parameters to study diversity and MIMO performances will be presented in terms of envelope correlation, effective diversity gain, and MIMO efficiency.

Chapter 5 will summarize the results of the original papers that are presented in this dissertation. Results are also compared to the values defined in the objectives.

Chapter 6 will discuss and compare the results presented in the dissertation to the previously published results. Also, how commercial companies can exploit the results will be discussed and recommendations for future work will be presented.

Chapter 7 will summarize the most important findings of the dissertation, whereas, the Chapter 8, will conclude the results related to the state-of-art defined in the Section 1.2.

2 Theory of spherical and characteristic modes

This chapter presents the basic theory related to the spherical and characteristic modes. The theoretical examination starts from spherical scalar modes as a background to the spherical vector modes. In both cases, a few radiating modes are presented with corresponding point sources in scalar cases, and with surface currents on a sphere in vector cases. Only a few modes are presented, because when considering the size of a mobile ground plane, it can only support a few higher order modes [28, 75].

It is also shown how the same modes excited on a sphere can be found on a planar radiating ground plane. Numerical results are presented in every case and the results are compared to find the correlation between the modes. The theoretical results presented in this chapter are later compared in Chapters 3 and 4 to the antenna structures presented in the original papers [I] - [X].

2.1 Theory of spherical modes

As a background, the first modal approach to antennas was taken by Chu in 1948 [17], and later, in 1960, Harrington was able to determine the fundamental limitations of antennas [77]. They assumed that any radiating field of an antenna can be written as a sum of spherical vector waves, enclosed by a sphere. The radiated power of an antenna is then calculated from the propagating modes within the sphere, while all the modes contribute reactive power.

When the sphere enclosing the antenna is very small, there are no propagating modes in the spherical waveguide, as all modes are evanescent (below the cut-off). However, if the sphere containing the antenna is large enough, several propagating modes will be supported. This is a well known property in the spherical antenna measurement theory. When the size of the antenna is limited, only a reduced number of radiating modes can be measured [18]. The minimum sphere for an antenna is defined by the smallest radius completely bounding the antenna. The number of resonating modes is given by $N = kr_0$, where k is the wave number and r_0 is a radius of the minimum sphere enclosing the antenna.

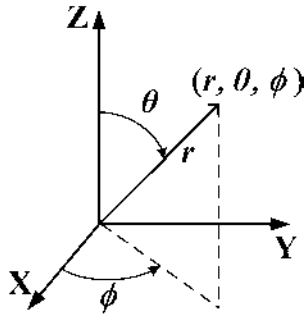

Fig 1. Spherical coordinate system.

The theoretical part of the spherical modes are presented here, first with scalar modes (charges) and then with vector modes (currents) on a sphere. The sphere is used to study the modes because it is a simple canonical surface and easy to analyze. Additionally, the spherical case is general and any planar surface is possible to find by decreasing the radius of a sphere [31]. In the vector case, the purpose is to show the relationship between the currents in a sphere and how they correspond to the radiated field. And as it will be shown later with the characteristic modes theory, the radiating modes in a planar structure are very similar to those with the spherical ones. The spherical modes connect together the theory, and how they can be used to analyze the limited number of excited modes of small antennas. In [31], spherical modes have been studied on a conventional sphere, but these modes have never been compared exactly to the modes excited on a planar mobile ground plane.

The spherical coordinate system is presented in Fig. 1. It can be considered as a geocentric system, the origin of which is the mass center of the Earth. The Z-axis is orientated to the North as a direction of the Earth's axis of revolution, and the plane determined by the XY-axis is considered to be the equatorial line of the Earth.

2.1.1 Spherical scalar wave function

This section introduces the theory of spherical scalar wave function based on Harrington's book [15]. Spherical modes are presented in a spherical coordinate system, the definition of which is shown in Fig. 1, where ϕ (Phi) is an azimuth angle and θ (Theta) is an elevation angle.

To solve the wave equation, the source-free scalar Helmholtz equation in the spherical coordinate system to construct the electromagnetic field is needed. The general form of the Helmholtz equation is

$$\nabla^2\psi + k^2\psi = 0, \tag{1}$$

where ψ is a complex scalar wave function, $\nabla^2\psi$ represents a scalar Laplace scalar operator, and k is a wave number. In the spherical coordinates, the Helmholtz equation gets the form

$$\frac{1}{r^2}\frac{\partial}{\partial r}\left(r^2\frac{\partial\psi}{\partial r}\right) + \frac{1}{r^2\sin\theta}\frac{\partial}{\partial\theta}\left(\sin\theta\frac{\partial\psi}{\partial\theta}\right) + \frac{1}{r^2\sin^2\theta}\frac{\partial^2\psi}{\partial\phi^2} + k^2\psi = 0. \tag{2}$$

The equation (2) is separated into three different functions. The r dependence is closely related to Bessel's equation and it is called *spherical Bessel functions* (Appendix 1), denoted as $b_n(kr)$. These functions are related to the ordinary Bessel functions by

$$b_n(kr) = \sqrt{\frac{\pi}{2kr}}B_{n+1/2}(kr). \tag{3}$$

The second dependence of θ is related to Legendre's functions (Appendix 2) and it is called *associated Legendre function*. Commonly used solutions are

$$L_n^m(\cos\theta) \sim P_n^m(\cos\theta),\ \ Q_n^m(\cos\theta), \tag{4}$$

where $P_n^m(\cos\theta)$ are the associated Legendre functions of the first kind and $Q_n^m(\cos\theta)$ are the associated Legendre functions of the second kind. In this dissertation, the Legendre function of the first kind is used in the calculations.

The third dependence of ϕ is a harmonic function, giving the solution $h(m\phi)$. Commonly used harmonic functions are

$$\sin(m\phi),\ \ \cos(m\phi),\ \ e^{jm\phi},\ \ e^{-jm\phi} \tag{5}$$

with m as an integer.

Forming the product solutions (3) - (5) to the Helmholtz equation, the elementary wave functions for the spherical coordinate system is

$$\psi_{m,n} = b_n(kr)L_n^m(\cos\theta)h(m\phi). \tag{6}$$

By forming linear combinations of the elementary wave functions, a more general solution to the Helmholtz can be constructed

$$\begin{aligned}\psi &= \sum_m\sum_n C_{m,n}\psi_{m,n}\\ \psi &= \sum_m\sum_n C_{m,n}b_n(kr)L_n^m(\cos\theta)h(m\phi),\end{aligned} \tag{7}$$

where $C_{m,n}$ are constants. The solutions to the associated Legendre equation have singularities at $\theta = 0$ or $\theta = \pi$, except the $P_n^m(\cos\theta)$ with n an integer.

The behaviour of the spherical Bessel functions is different depending on the studied case. For k real, $j_n(kr)$ (Bessel function of the 1st kind) and $n_n(kr)$ (Bessel function of the 2nd kind) represent standing waves, when $h_n^{(1)}(kr)$ (Hankel function of the 1st kind) represents an inward-travelling wave, and $h_n^{(2)}(kr)$ (Hankel function of 2nd kind) represents an outward-travelling wave. The zero-order Bessel functions can be found in Appendix 1, based on [18].

To represent a finite field outside of a sphere, which is more interesting from an antenna radiation point of view, outward-travelling waves are

$$\psi_{m,n} = h_n^{(2)}(kr)P_n^m(\cos\theta)e^{jm\phi} \tag{8}$$

with m and n integers are the wanted elementary wave functions.

2.1.2 Numerical results of spherical scalar modes

This section presents the numerical results related to the theory that were presented in the previous section (2.1.1). The fundamental solutions for spherical modes can be calculated by using (6), where index m is related to the degree of the azimuthal variation, while the index n denotes (order) the number of total variation in the elevation and azimuth.

The special case of the spherical modes is the case with symmetry in the azimuth plane or revolution in symmetry, when $m = 0$. These modes are presented in Fig. 2. The coordinate system which is used to study the modes is the same as shown in Fig. 1. The sphere under the mode represents a polarization of the point sources used to excite the corresponding scalar mode. The red corresponds to a positive charge and blue as a negative charge. These previously presented modal solutions can be associated to a fixed number of sources located on the surface of a sphere.

In Fig. 3, some of the fundamental modes proportional to the harmonics function $\cos(m\phi)$ are presented. The modes of harmonics $\sin(m\phi)$ are the same after applying a 90 degree rotation in the azimuth plane. The presented modes can be seen as a radiation of a set of different signal sources. Notice that the index $m \leq n$. The coordinate system which is used to study the modes is the same as shown in Fig. 1.

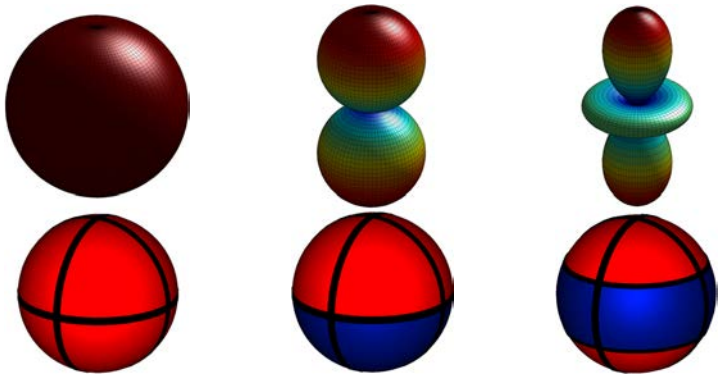

(a) m = 0, n = 0 (b) m = 0, n = 1 (c) m = 0, n = 2

Fig 2. Special cases of spherical scalar modes with no azimuthal variation (degree m = 0).

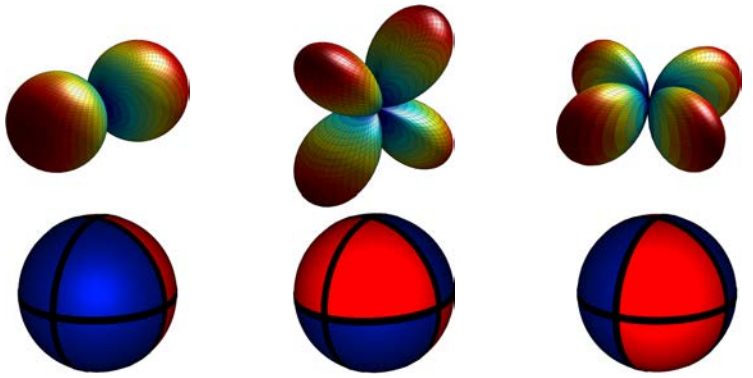

(a) m = 1, n = 1 (b) m = 1, n = 2 (c) m = 2, n = 2

Fig 3. Some fundamental higher order spherical scalar modes.

2.1.3 Spherical vector wave function

This section introduces the theory of spherical vector wave function based on Harrington [15]. The wave function ψ can be represented in terms of electromagnetic fields as vector potentials. To do so, a presentation of an arbitrary electromagnetic field in spherical coordinates is possible by constructing the field as a superposition of two parts;

one TM mode (Transverse Magnetic) to r and the other TE mode (Transverse Electric) to r. For this, magnetic vector potential $\vec{A} = A_r\hat{r}$ and electric vector potential $\vec{F} = F_r\hat{r}$ are presented, where $\hat{r}$ represent a radius vector from the origin. The field components A_r and F_r, with respect to r, are not solutions to the scalar Helmholtz equation $\nabla^2 A_r \neq (\nabla^2\vec{A})_r$ (see Appendix 3) [15]. The vector form for A_r is

$$\left(\nabla^2 + k^2\right)\frac{A_r}{r} = 0, \tag{9}$$

where A_r/r is a solution to the scalar Helmholtz equation (ψ).

A dual development applies to the electric vector potential $\vec{F} = F_r\hat{r}$, as

$$\left(\nabla^2 + k^2\right)\frac{F_r}{r} = 0. \tag{10}$$

The ψ's in (9) and (10) have r dependence, and, thus, it is convenient to introduce another spherical vector Bessel function, defined as

$$\hat{B}_n(kr) = krb_n(kr) = \sqrt{\frac{\pi kr}{2}}B_{n+1/2}(kr). \tag{11}$$

And then, the general form to represent A_r and F_r in terms of the spherical Bessel function, is

$$\sum_{m,n} C_{m,n}\hat{B}_n(kr)L_n^m(\cos\theta)h(m\phi), \tag{12}$$

where $C_{m,n}$ are constants.

The explicit formulas for the field components to satisfy the vector Helmholtz equation $\nabla^2\vec{\psi} + k^2\vec{\psi} = 0$ in spherical coordinate system can be presented in terms of A_r and F_r as follows

$$\begin{aligned}
E_r &= \frac{1}{j\omega\varepsilon}\left(\frac{\partial^2}{\partial r^2} + k^2\right)A_r \\
E_\theta &= -\frac{1}{r\sin\theta}\frac{\partial F_r}{\partial\phi} + \frac{1}{j\omega\varepsilon r}\frac{\partial^2 A_r}{\partial r\partial\theta} \\
E_\phi &= \frac{1}{r}\frac{\partial F_r}{\partial\theta} + \frac{1}{j\omega\varepsilon r\sin\theta}\frac{\partial^2 A_r}{\partial r\partial\phi} \\
H_r &= \frac{1}{j\omega\mu}\left(\frac{\partial^2}{\partial r^2} + k^2\right)F_r \\
H_\theta &= \frac{1}{r\sin\theta}\frac{\partial A_r}{\partial\phi} + \frac{1}{j\omega\mu r}\frac{\partial^2 F_r}{\partial r\partial\theta} \\
H_\phi &= -\frac{1}{r}\frac{\partial A_r}{\partial\theta} + \frac{1}{j\omega\mu r\sin\theta}\frac{\partial^2 F_r}{\partial r\partial\phi}.
\end{aligned} \tag{13}$$

When $F_r = 0$, which means only A_r exists, we have field TM to r. Similarly, when $A_r = 0$, the equations represent a field of TE-mode to r.

2.1.4 Numerical results of spherical vector modes

This section presents the numerical results of the spherical vector modes presented in 2.1.3. The coordinate system which is used in the study is the same as shown in Fig. 1.

The formulation starts from (13). First, by studying TM-modes against the Z-axis, the electric field component F_r is set to 0. By adding (12) to (13), the components of the electric field in the TM-mode get the following form

$$\begin{aligned} E_r &= \frac{1}{j\omega\varepsilon}\left(\frac{\partial^2}{\partial r^2}+k^2\right)\sum_{m,n} C_{m,n}\hat{B}_n(kr)L_n^m(\cos\theta)h(m\phi) \\ E_\theta &= \frac{1}{j\omega\varepsilon r}\frac{\partial^2}{\partial r\partial\theta}\sum_{m,n} C_{m,n}\hat{B}_n(kr)L_n^m(\cos\theta)h(m\phi) \\ E_\phi &= \frac{1}{j\omega\varepsilon r\sin\theta}\frac{\partial^2}{\partial r\partial\phi}\sum_{m,n} C_{m,n}\hat{B}_n(kr)L_n^m(\cos\theta)h(m\phi), \end{aligned} \tag{14}$$

where $C_{m,n}$ corresponds to a magnetic vector potential. Mark $h(m\phi) = \cos(m\phi)$ as done in the scalar case. The low-order normalized Legendre polynomials, to calculate the electric field, can be found in Appendix 2, based on [18].

To gain TE-modes, the magnetic field component A_r is set to 0. Now, the components of the TE-mode get the following form

$$\begin{aligned} E_\theta &= -\frac{1}{r\sin\theta}\frac{\partial}{\partial\phi}\sum_{m,n} D_{m,n}\hat{B}_n(kr)L_n^m(\cos\theta)h(m\phi) \\ E_\phi &= \frac{1}{r}\frac{\partial}{\partial\theta}\sum_{m,n} D_{m,n}\hat{B}_n(kr)L_n^m(\cos\theta)h(m\phi), \end{aligned} \tag{15}$$

where $D_{m,n}$ represents an electric vector potential. As it can be notice the radial component of the field vanish in TE case.

As mentioned in Section 2.1.2, the special case of the spherical modes is the symmetry in the azimuth plane, when $m = 0$. Figure 4 presents the vector TM-mode equivalent for scalar modes presented in Fig. 2. Below the corresponding mode, the excitation of the vector modes is marked as surface currents on a sphere. The coordinate system which is used to study the modes is the same as shown in Fig. 1.

Figure 5 presents the vector TE-mode, which is equivalent to TM-modes in Fig. 4. Notice how the total field of the both modes are exactly the same. The only difference

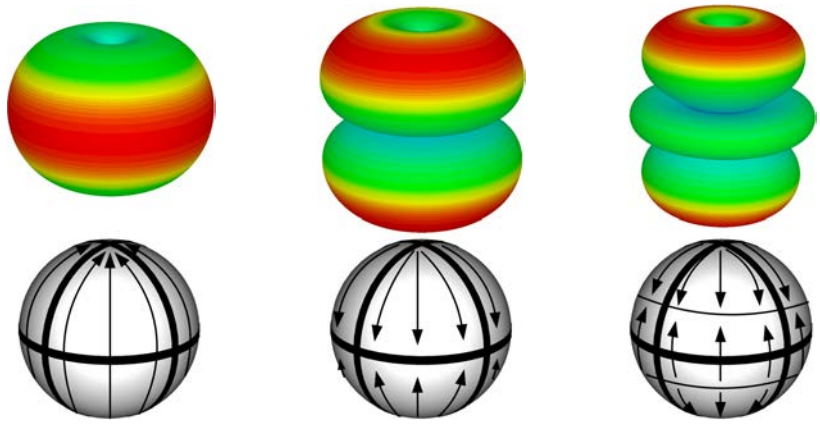

(a) m = 0, n = 0 (b) m = 0, n = 1 (c) m = 0, n = 2

Fig 4. Special cases of spherical vector TM-modes with no azimuthal variation (order m = 0) against Z-axis. Below the spherical mode, the surface currents on a sphere are presented, related to the corresponding mode.

appears in the surface currents; The TM-mode has a vertical current in every mode, since the TE-mode has horizontal (loop) currents.

Figures 6 and 7 presents a number of higher order vector modes which have the same form as in the scalar case. The mode ($m = 0$, $n = 0$) can be considered to be a fundamental mode. The mode represents a dipole kind of radiation. Other modes are higher order modes, with a variation in θ and a ϕ component.

It is good to notice that the mode ($m = 0$, $n = 0$) should be a sphere as in the scalar case. But, as it is well known, an isotropic radiator is physically not possible, and, thus, zeros appear in $\theta = 0$ and $\theta = \pi$, as can be seen in the radiation pattern. This is due to the fact that the direction of the electric field vectors propagating towards the same pole are cancelling each other. Thus, the vector mode $m = 0$, $n = 0$ can be seen as a scalar mode, multiplied by the radiation pattern of a dipole.

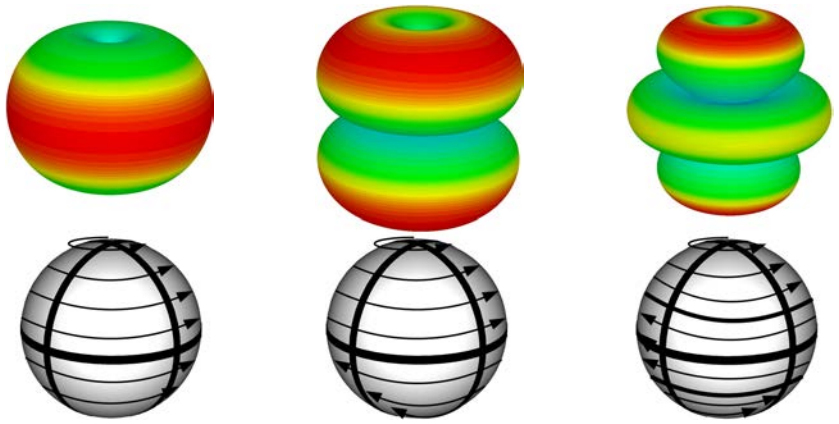

(a) m = 0, n = 0 (b) m = 0, n = 1 (c) m = 0, n = 2

Fig 5. Special cases of spherical vector TE-modes with no azimuthal variation (order m = 0) against a Z-axis. Below the spherical mode, the surface currents on a sphere are presented related to the corresponding mode.

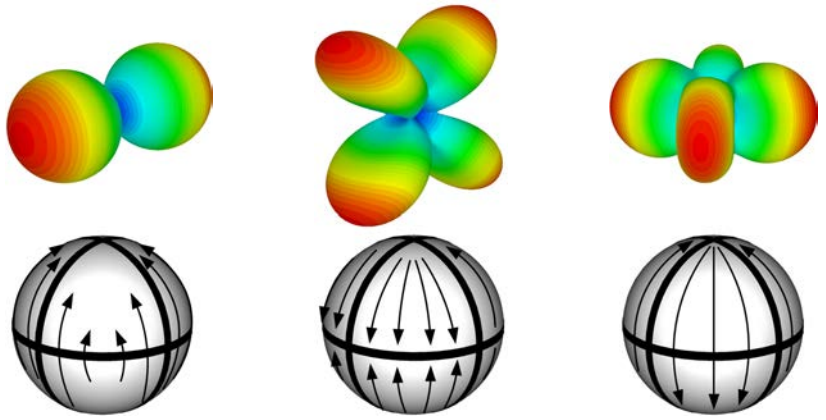

(a) m = 1, n = 1 (b) m = 1, n = 2 (c) m = 2, n = 2

Fig 6. Some fundamental higher order spherical vector TM modes against the Z-axis. Below the spherical mode, the surface currents on a sphere are presented, related to the corresponding mode.

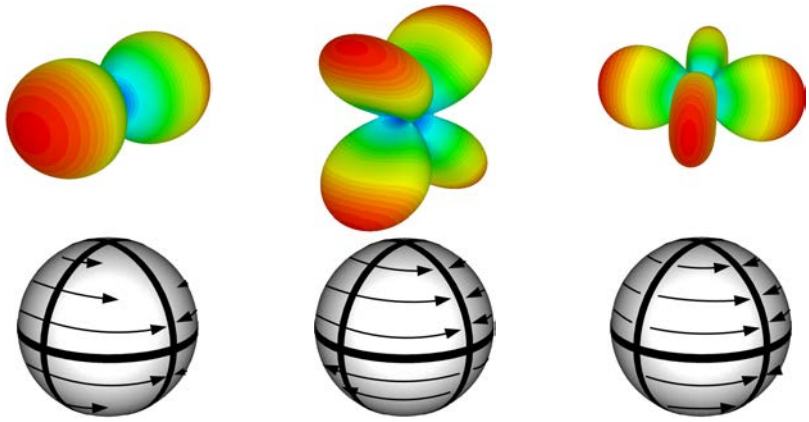

(a) m = 1, n = 1 (b) m = 1, n = 2 (c) m = 2, n = 2

Fig 7. Some fundamental higher order spherical vector TE modes against the Z-axis. Below the spherical mode, the surface currents on a sphere are presented related to the corresponding mode.

2.2 Introduction to characteristic modes theory

This chapter shortly introduces the Theory of Characteristic Modes (TCM), which was first developed by Garbacz [78] and later refined by Harrington and Mautz during the seventies [16]. It can be used to obtain the radiating modes of any arbitrarily-shaped metallic structure. These radiating modes, known as characteristic modes, not only present really attractive orthogonality properties, but also bring physical insight into the radiating phenomena that is taking place on the antenna. Because of these advantages, TCM is extremely useful for systematic analysis and the design of an antenna. Recently, TCM has been used for the design of diverse wire and planar antennas in [30–32, 75] and [VI]. A commercial 3D electromagnetic simulations software, called FEKO (FEldberechnung für Körper mit beliebiger Oberfläche, Field Calculations for Bodies with Arbitrary Surface), includes an option to analyze characteristic modes, and brings the characteristic modes analysis to the commercial field. The software uses the antenna structure, published in [33], to demonstrate the characteristic modes of a metallic ring. The antenna is designed in Universitat Politècnica de València, by the researches in the Group of Electromagnetic Radiation.

As explained in [16], characteristic modes or characteristic currents can be obtained as the eigenfunctions of the following particular weighted eigenvalue equation

$$X(\vec{J}_n) = \lambda_n R(\vec{J}_n), \tag{16}$$

where λ_n are the eigenvalues, $\vec{J}_n$ are the eigenfunctions or eigencurrents, and R and X are the real and imaginary parts of the impedance operator

$$Z = R + jX. \tag{17}$$

Characteristic modes can be defined as a set of orthogonal real surface currents associated to any conducting object, which depend on its shape and size, and are independent of any excitation source. As characteristic modes form a set of orthogonal functions, they can be used to expand the total current J on the surface of the antenna, as follows:

$$J = \sum_n \frac{V_n^i J_n}{1 + j\lambda_n}, \tag{18}$$

where J_n are the eigencurrents or characteristic modes, λ_n are the eigenvalues, and V_n^i is the modal excitation coefficient. The modal excitation coefficient can be obtained as

$$V_n^i = \langle J_n, E^i \rangle = \oiint J_n \cdot E^i ds. \tag{19}$$

The product $V_n^i J_n$ in (18) models coupling between the excitation and n^{th} mode, and determines which mode will be excited by the antenna feed or incident field (E^i). Note that the total current in (18) also depends on λ_n, which is the eigenvalue associated to the n^{th} characteristic current mode.

The variation of the eigenvalues as a function frequency provides information about the resonance frequency and radiating bandwidth of the different current modes. In general, eigenvalues range from -∞ to +∞. Considering that a mode is at resonance when its associated eigenvalue is zero, it is inferred that the smaller the magnitude of the eigenvalue is, the more efficiently the mode radiates when excited. Additionally, the sign of the eigenvalue determines whether the mode contributes stored magnetic energy ($\lambda_n > 0$) or electric energy ($\lambda_n < 0$).

The resonance frequency of the current modes can be determined, using the information provided by its associated characteristic angles (α_n). Characteristic angles can be defined as

$$\alpha_n = 180^\circ - \tan^{-1}(\lambda_n), \tag{20}$$

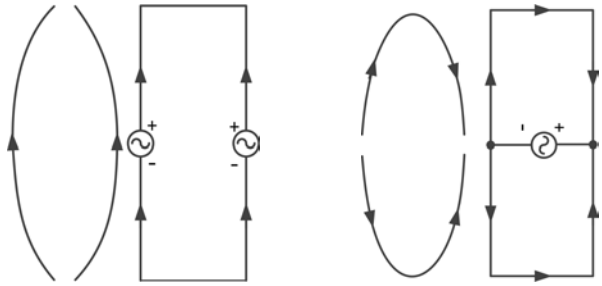

(a) Antenna mode (b) Transmission line mode

Fig 8. Analogy between an elliptical loop and a folded dipole.

where λ_n are the eigenvalues associated to each characteristic mode. From a physical point of view, the characteristic angle models the phase angle between a characteristic current J_n and the associated characteristic field E_n. Hence, a mode is at resonance when its characteristic angle α_n is 180°. The closer the characteristic angle is to 180°, the better radiating behaviour the mode presents.

Related to the behaviour of the characteristic angle, the characteristic modes can be separated into two different modes, depending on their behaviour: *antenna mode* in Fig. 8(a) and *transmission line mode* in Fig. 8(b) [11]. Whereas the antenna modes are efficient radiators representing the gentle slope of the characteristic angle, the transmission line modes are characterized by a poor radiating performance with the steep slope of the characteristic angle. As in the antenna mode, the currents propagate in phase (Fig. 8(a)), it is considered to be an efficient radiator. In contrast, currents in the transmission line mode (Fig. 8(b)) propagate in the opposite phase, so the radiation of the mode is weak. As a result, from the antenna design point of view, it is suitable to excite antenna modes to gain a good performance.

2.2.1 Characteristic modes in a small radiating ground plane with corresponding spherical modes

The section shows that it is possible to obtain higher order modes with a planar structure, which are all orthogonal to each other. The section studies surface current distributions on a planar radiating ground plane, and shows how the radiation corresponds to the spherical vector modes presented in Section 2.1.4.

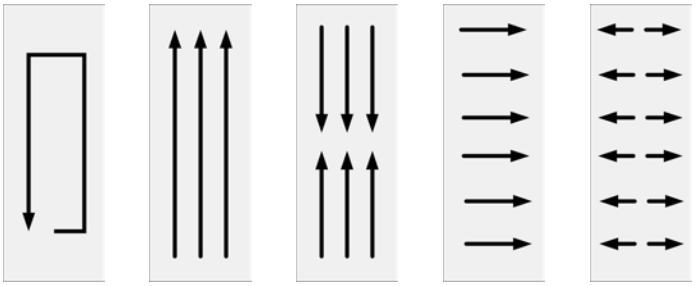

(a) Mode 0 (b) Mode 1 (c) Mode 2 (d) Mode 3 (e) Mode 4

Fig 9. The first five characteristic current modes appearing in a conducting ground plane (I, published by permission of EurAAP).

Surface current distribution shows the total current over the surface of the antenna. This total current is a combination of different current modes, and can be expressed as the sum of the characteristic modes. If one mode is very dominant at a certain frequency, the total current distribution is practically the modal current. And so, the total current distribution will be the same as the mode in question. In practise, at some frequencies, the behaviour of the antenna is due to the combination of two or more modes, and, therefore, the total current is not only one modal current, but a combination of current modes.

Figure 9 presents the first five characteristic current modes appearing in a planar rectangle shaped conducting ground plane. Notice that the Mode 0 (TE mode) is a special case by representing a non-radiating current loop contributing a magnetic energy. The excitation of this mode is avoided due to its poor radiating properties. The radiation pattern of this mode is similar to an electrically small loop antenna. Mode 1 is considered to be a fundamental mode, whereas modes 2–4 are higher order modes that appear at higher frequencies.

Mode 1 is characterized with vertical currents (TM mode) and it is the first radiating mode awaking in a rectangular ground plane. The current zeros are at both ends of the ground plane, corresponding to dipole like radiation.

Mode 2 is a higher order mode with a vertical current distribution (TM mode). Current zeros appear at both ends and in the middle of the ground plane as an equatorial cut. This corresponds to a radiation pattern, where two maximums appear at both ends of the ground plane with a zero in the middle.

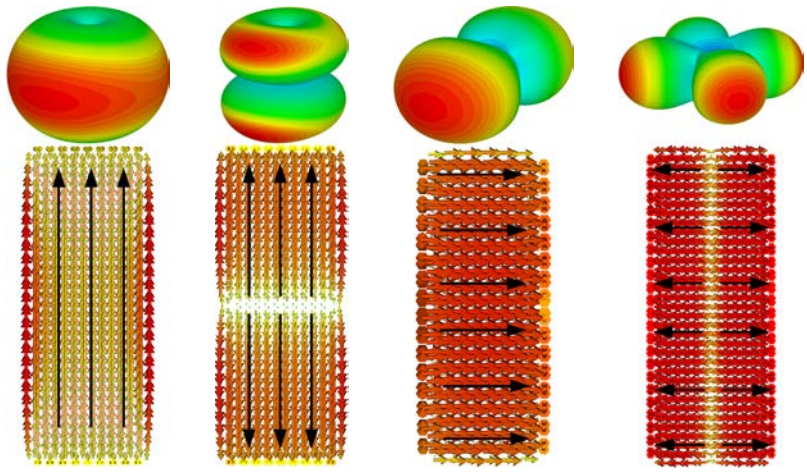

(a) Mode 1 (b) Mode 2 (c) Mode 3 (d) Mode 4

Fig 10. The first four surface current modes appearing in a conducting ground plane with corresponding radiating mode. The modes in (a) and (b) correspond to a TM mode, whereas (c) and (d) to the TE mode.

Mode 3 is characterized with horizontal currents (TE mode). Currents of this mode are orthogonal to Mode 1. The mode generates current zeros on the every edge of the ground plane and, thus, the radiation pattern has two spheres on both sides of the ground plane.

As the previous mode, Mode 4 is orthogonal to Mode 2 with horizontal currents (TE mode). This mode has current zeros on every edge of the ground plane, just like Mode 3, but one vertical zero appears in the middle of the ground plane, creating a clover kind of radiation pattern.

In Fig. 10, the surface currents on the conducting ground plane and their corresponding spherical vector modes are shown, as previously studied in 2.1.4. Spherical modes of the corresponding characteristic modes can be categorized in two groups related to the propagation direction of the surface current, as was discussed in 2.1.4. These are TE or TM modes. As can be clearly seen, modes 1 and 2 belong to the TM mode, whereas modes 3 and 4 to the TE mode.

As the modes in Fig. 10 (a) and (b) are corresponding to a TM mode, they characteristic currents are flowing vertically in a mobile ground plane. The equivalent spherical vector mode for the characteristic current Mode 1 is TM mode m = 0, n = 0.

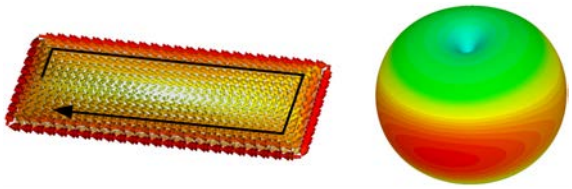

Fig 11. The special case of the non-radiating characteristic loop mode, Mode 0. The mode is corresponding to a TE mode m = 0, n = 0.

This is the fundamental mode and corresponds to a dipole kind of radiation. Mode 2 is a higher order vertical current mode whose radiation pattern corresponds to the TM mode m = 0, n = 1, respectively. The mode is generating a zero in the middle of the ground plane and that can be seen in the spherical vector mode as an equatorial zero in the radiation pattern.

The modes in Fig. 10 (c) and (d) are corresponding to a TE vector mode with horizontally propagating characteristic currents. The similarity of the characteristic current Mode 3 can be seen with TE mode m = 1, n = 1. The mode is generating a zero around a radiated sphere from the North to the South. In proportion, the characteristic current Mode 4 is equivalent to the vector TE mode m = 2, n = 2. The radiation pattern is clearly creating a clover kind of radiation pattern.

Notice that the radiating modes are slightly different compared to the theoretical spherical vector modes. This is due to the fact that the ground plane has an asymmetrical shape. When exciting a square shaped ground plane instead of a rectangular one, the generated modes would be similar to those with the theoretical ones.

Mode 0 of Fig. 11 is corresponding to a spherical vector TE mode m = 0, n = 0. This can be easily seen when pushing the North and South poles of the sphere in Fig. 5 (a) down against the Z-axis, so that the structure becomes flat. The surface currents then propagate on both sides of the ground plane, rather than on a sphere.

2.3 Summary

The chapter briefly discussed the theory related to the spherical and characteristic modes. The first section presented scalar spherical modes as a base for the spherical vector modes presentation in the second section. In both sections, numerical results were presented and the modes were compared.

In the scalar case, the point sources were presented with corresponding numerical results, whereas in the vector case, the corresponding surface currents were presented on a sphere. In the third section, characteristic modes were discussed and current modes on a planar mobile ground plane were presented with corresponding radiation patterns.

The surface currents on a planar ground plane was studied with respect to the characteristic mode theory and compared to the obtained spherical vector modes. With different excitation configurations, the surface currents of a planar antenna can be forced to higher order forms to obtain orthogonal radiation patterns. The results obtained in the theoretical foundation will be compared to the simulated and measured results in later chapters.

As a conclusion, it was shown that it is possible to excite the same radiating modes on a planar rectangular ground plane as on a conventional sphere with corresponding surface current distributions.

3 Wideband antennas

The chapter presents wideband antennas for mobile applications. The chapter starts with a discussion on impedance matching and baluns related to the antenna feeding mechanisms used in the prototype antennas presented in original papers [III] - [X]. The electrically small antennas are discussed with general principles, and in the terms of designing a mobile antenna.

Ultra-wideband antennas and complementary antennas are discussed, and an ultra-wideband quasi-complementary bowtie antenna for a mobile application with switching capability is presented in [II].

The final section presents planar quasi-complementary antenna structures, created by using an electric conductor and a magnetic notch or a magnetic square slot. The structures use monopole excitation, as presented in [III], or dipole excitations as presented in [IX] and [X]. By using a properly designed magnetic slot, the monopole and dipoles can be closely spaced to a conducting ground plane, and, thus, the antenna performance can be enhanced compared to a reference case without the magnetic slot. The enhancement in the antenna performance is achieved in terms of input impedance, bandwidth, and radiation efficiency as the currents in the ground plane can be reinforced.

The quasi-complementary antenna elements presented in this chapter with a dipole excitation ([IX] and [X]) are combined to multi-element antenna structures in Chapter 4 to create mobile diversity and MIMO systems.

By designing an efficient feeding network, it is possible to excite a radiating current mode on a planar ground plane in such a way that it remains over a wide frequency range without the disturbance of higher order modes. The chapter focuses on finding novel and simple wideband antenna structures which relative -6 dB bandwidth is better than 30%, defined as criteria of a wideband antenna in Section 1.3.2 (Table 1). The antenna structures presented in this chapter utilize a ground plane of a mobile chassis as a radiating element.

3.1 Antenna feeding

Most antennas are connected to radio modules using three different methods. The first one, and maybe the most common way, is to use coaxial cable where an antenna

is connected to the inner connector and the outer connector to the antenna ground plane. Typically, quarter-wave monopoles, helical antennas, and some planar antennas (microstrip antennas) use coaxial feeds in wireless applications.

Coaxial connections can be made over a range of characteristic impedance to simplify matching between antenna and radio, although most standard coaxial connectors have a 50 Ω characteristic impedance. Coaxial connections are unbalanced and require a balun to feed balanced antennas, such as a dipole [79]. Coaxial feeding mechanism has been used in the prototype antennas presented in original papers [III] - [X]. 50 Ω coaxial feed without a separate impedance matching network is used in original papers [III] - [V].

The second connection option is the use of a microstrip feed between radio and antenna. The connection is suitable for cases where the radio module and antenna are on the same circuit board. This type of connection can directly incorporate impedance matching circuitry and be fabricated along with the using common printed circuit techniques [79]. A microstrip feed has been used in the antenna structure presented in [VIII].

The third connection is electromagnetic coupling that is also common in portable wireless devices. It relies on the transmission of signals between the radio and the antenna without a direct connection. Much of its popularity results from its decreased cost relative to other fixed connections that require moulded, machined, or complex feed structures. This kind of connection can take on a variety of forms depending on the antenna and space available in the package to establish the coupling.

The electromagnetic coupling of a microstrip or planar antenna via a slot in a ground plane (aperture coupling) or via a buried microstrip line (proximity coupling) often eliminates the need for a matching network and can broaden the bandwidth of the antenna [79]. The electromagnetic coupling to a mobile chassis was first presented by Vainikainen [24].

In the original papers, a monopole [III] or a dipole ([IX] and [X]) is used as a coupling element. Also in [VIII], presented in Section 4.3.2, symmetrically excited patch elements are used to couple energy to the mobile ground plane.

3.1.1 Impedance matching

Impedance matching is a control of impedance for the purpose of obtaining a maximum power transfer or minimum reflection. Usually, the radio module and the antenna for wireless applications are designed for standard characteristic impedance, so that no

impedance matching network is necessary. However, if the antenna impedance does not match with the radio input impedance, an impedance matching network is required.

In the case of resonant antennas, an impedance match can be established using quarter-wave transformers, transmission line tubes, or lumped elements. These solutions provide relatively narrow bandwidths, but usually meet system requirements since the antenna has narrow bandwidth. Cascading multiple quarter-wave transformers or the use of tapered transmission lines can provide broader impedance bandwidths [79]. One way to change the input impedance of a dipole is to use asymmetrical feeding by displacing the feed point off-centre [9].

Lumped elements have been used to carry out impedance matching in the original papers [VI] and [VII], where the matching network functions as a part of a balun. Tapered transmission lines to perform impedance matching have been used in papers [IX] and [X], where the matching is also carried out as part of a balun. It is good to notice that in papers [III] - [V] and [VIII] - [X], the antenna structure itself can be modified to gain impedance matching in certain limitations. In [III], [IV], [IX], and [X], the input impedance can be modified by changing the slot dimensions related to the excitation element(s), whereas in [V] and [VIII], by varying patch dimensions and patch feeding points, different input impedances can be achieved.

3.1.2 Baluns

When connecting an antenna to a transmission line, it is important to deliver all the available power from the transmitter or to the receiver. There are two primary conditions to satisfy a good feed: the impedance matching between the antenna and transmission line, and the excitation of the current distribution of the antenna. The former needs, in certain cases, the balancing of the currents. Some of the antennas have a symmetrical nature (half-wave dipole or loop antenna), thus, the currents should also be symmetrical (or balanced).

In the balanced case, the currents on the transmission line are equal in magnitude and opposite in direction, which yields a small radiation from the transmission line for a closely spaced conductor (Fig. 12(a)). For unbalanced operations, the currents in a transmission line are non-equal and there is a net current flow on the transmission line leading to uncontrolled radiation towards the desired direction or of the desired polarization (Fig. 12(b)) [9].

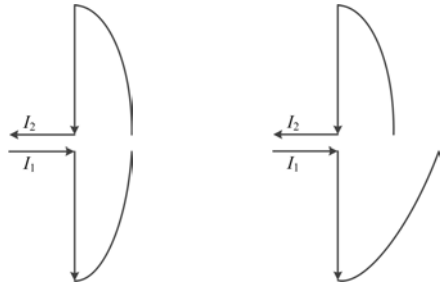

(a) Balanced currents, $I_1 = I_2$

(b) Unbalanced currents, $I_1 > I_2$

Fig 12. Balanced and unbalanced signals of a centre-fed dipole.

Parallel wire lines are naturally balanced in that if an incident wave is launched down the line, it will excite balanced currents on a symmetrical antenna. On the other hand, a coaxial transmission line is not balanced. A wave travelling down the coax may have a balanced current mode, that is, the currents on the inner conductor and the inside of the outer conductor are equal in magnitude and opposite in direction. However, when this wave reaches the symmetrical antenna, the current may flow back on the outside of the outer conductor, which unbalances the antenna and transmission line. To suppress this outside surface current, a balun (balanced to unbalanced transformer) is used [9].

Antennas, if not driven properly, may interact in undesirable and unpredictable ways with their environment. Frequently, this interaction can be minimized by enforcing a balanced operation, e.g., the currents in the two arms of a symmetric dipole should be equal. A balun is a 3-port network, designed to couple an unbalanced transmission line at one port to a balanced transmission line at the other two ports. A balun may be a current balun, which forces the currents at the balanced ports to be equal and opposite, or a voltage balun which does the same for the voltages at the balanced ports. Though many types of different baluns, many of them also possess an impedance transformation properties [10].

A common balun structure is a reciprocal element, and, thus, it is possible to change an input port with an output port and maintain the same functionality. So, if a signal from an unbalanced port is the input signal, the balun structure has to transform it into a signal on a balanced port. Therefore, the input signal must be turned into two non-ground signals. This can be done by using a low pass branch generating a +90°

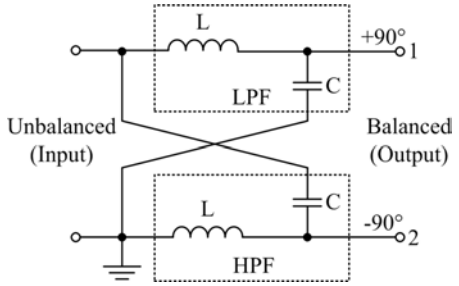

Fig 13. The principal of an LC-balun structure.

signal, and a high pass branch generating a -90° signal. Using this as a balanced signal fulfils the desired needs for a balun transformer [10].

In the next sections, two different wideband baluns are presented. Both are used in the antenna prototypes that are presented in the original papers.

LC-balun

In LC-balun, the incoming unbalanced wave energy is divided equally between two channels, one providing a 90° lead, the other, a 90° lag. The output voltage is balanced with respect to the ground, and it is in quadrature with the input voltage. The lattice may be proportioned to match any two (input and output) resistance values as shown in Fig. 13. The LC-balun consists of a high-pass filter (HPF), and a low-pass filter (LPF) to generate a phase difference with a balanced signal [80]. While the inductor is passing signal at lower frequencies, the capacitor does the same at higher frequencies. An LC-balun design is a compromise for an intersection point between LPF and HPF.

The lumped-element reactances may also be replaced by transmission line stubs, which are particularly suitable for printed-circuit applications [10].

The lattice balun may be generalized to a higher-order circuit to improve bandwidth [10]. Fig. 14 shows a cascaded LC-balun to feed the symmetrical folded dipole published in [VI] and [VII]. The cascaded LC-balun in the figure only presents the feed of a one port, as the other port is symmetrical. Symmetrical feeding is discussed later in Section 4.3.

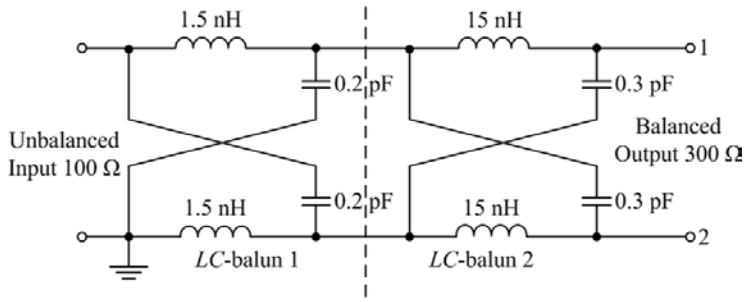

Fig 14. A cascaded LC-balun structure used to feed a symmetrical folded dipole (VI, published by permission of IEEE).

Tapered microstrip line balun

A tapered microstrip line balun is a transmission line that converts from an unbalanced line (coaxial or stripline) to a balanced two conductor line. The tapered microstrip balun has an advantage that the impedance can be matched by tapering the width of the strips. It can be designed for bandwidths that are several octaves wide [10]. Fig. 15(a) shows the principal of the tapered microstrip line balun.

When a microstrip line is joined to a balanced stripline, a step discontinuity between the ground plane of the microstrip line and the bottom conductor of the balanced stripline exists. A step discontinuity also exists between the top strip conductors of these two lines. But the step discontinuity in the former case is larger than in the later case [81]. Transmission line tapers are generally employed to achieve a good match between the two lines [82]. The tapered microstrip line balun presented in Fig. 15(b) is used to feed prototype antennas in original publications [IX] and [X].

3.2 Basic narrow band antennas

This section discusses the principles and needs for designing mobile antennas. As there are many types of antennas used, they are only shortly discussed and the principles are presented.

Mobile antennas are subjected to a wide range of variations in the environment that they encounter. The propagation conditions vary from wideband multipath arrival of angle (AoA) to very strong Line-of-Sight (LOS) component. The orientation of the

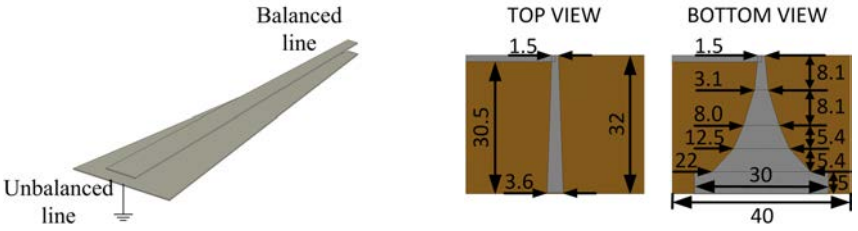

(a) the principal of a tapered microstrip line balun.

(b) Tapered microstrip line balun to feed quasi-complementary antenna.

Fig 15. Tapered microstrip line balun (b, IX, published by permission of IEEE).

mobile phone is mostly random, they need to operate in close proximity of a user, and are suitable for manufacturing in very large volumes. Users also prefer antenna to be fully integrated to the terminal [83].

In general, antenna design can be classically separated in different requirements, which are radiation pattern, input impedance, bandwidth, operating frequency, polarization, size, and radiation efficiency [79]. Still, as the future lies in small, internally mounted antennas that are able to work well over a wide frequency range, additional factors need to be taken into account, like small physical size, mechanical robustness, and cost. On the other hand, the interaction between the antenna and the user (e.g. SAR) is an important design parameter as well [54].

Various antenna elements have been used for mobile applications. There is no single specific type of antenna element, but designs that differ depending on the practical mobile systems. The most typical linear structures are dipole, monopole, loop, inverted-L antenna (ILA), inverted-F antenna (IFA), normal mode helix (omni-directional), and meander line antenna. When it comes to planar antennas, the most common are microstrip antenna (MSA), planar inverted F-antenna (PIFA), parallel plate antenna, and slot antenna. Small ceramic ships are also commonly used [8].

Mobile antennas can often be classified as electrically small antennas [17, 84, 85], defined as those whose radiating structure can be obtained within a sphere of radius r_0, such that $kr_0 < 1$, where $r_0 = \lambda_0/2\pi$. Electrically small antennas with a limited aperture size cannot achieve high directivity [86].

Similarly, the bandwidth and directivity cannot both be increased if the antenna is kept small. For a losses antenna, the effects are a high Q factor (quality factor) and,

hence, small bandwidth, a small radiation resistance resulting in a low efficiency, and a likely greater antenna sensitivity to mechanical and electrical tolerances. When the antenna has intrinsic losses, the bandwidth is less narrow. The smallest Q within a given size of enclosed sphere is obtained from a dipole-type field, operating at a fundamental mode of the antenna [87] (Mode 1 in Fig. 9).

The excitation of higher order modes should be avoided as they disturb the performance of the fundamental mode. Unless the mode in issue is wanted to be excited e.g. in case of radiation pattern diversity, as presented in Section 4.7.1. Assuming a resistive matched load, for a first order mode, weather electric or magnetic, the Q is related to the electric size of the antenna by [87]

$$Q = \frac{1}{(kr)^3} + \frac{1}{kr}. \tag{21}$$

3.3 Ultra-wideband antennas in mobile applications

This section is shortly discussion a basics of the Ultra-wideband (UWB) antennas based on [10]. The UWB is a technology for short-range high-data-rate wireless communications, high-accuracy image radar, and localization systems. UWB antenna design is challenging due to the extreme broad bandwidth and carrier-free features. UWB antenna is an antenna which is capable of producing similar radiation (pattern and gain) over a very wire frequency range. Notice that defining an antenna bandwidth which is based on a return loss (S_{11}) being lower than -10 dB does not guarantee strong radiation. When an antenna contains absorptive materials, a low return loss indicates a low return, and nothing about the radiation.

UWB antenna radiation can be separated by three different approaches. In the first one (i), a perturbing electromagnetic resonance is broadening a resonance peak. These kinds of UWB antennas achieve a wide bandwidth by introducing incoherent resonance and effectively lowering the quality factor of the electromagnetic resonance. Common antenna types in this category are dipoles [88–92] and monopoles [93–97]. On the other hand, to avoid an excitation of the 2nd or higher modes, exciting only the fundamental 1st order mode also offers wideband antenna characteristics.

The second one (ii) only allows one dominant radiation region that is physically small compared with wavelengths. These UWB antennas achieve wide bandwidth by controlling diffraction on the antenna structures via careful geometry design or the proper utilization of absorptive loading [98–100]. Antennas in this category often

produce some degree of frequency-dependent gain and patterns because of the fraction and absorption as functions of frequency. For instance, a curved section of an antenna may appear to be smooth for short wavelengths and produce less diffraction, but may suddenly bend for long wavelengths (e.g. tapered slot antenna [101–103]). Similarly, a section of tapered resistive loading could be long and have smooth tapering for short wavelengths, but would be short and sudden for long wavelengths [104].

The third one (iii) is maintaining a similar radiation/scattering geometry (shape and dimension) in terms of wavelengths. This group of UWB antenna are probably the most widely used. This type of antenna adopts frequency-independent or frequency-scaled geometries. Among them, angle defined geometry, complementary antenna with an electric conductor and a magnetic slot [105–107], where the imaginary part of the electric conductor cancels the imaginary part of the magnetic slot (presented in the next section), and log-periodic geometry are the best known [108, 109].

Several UWB antennas for mobile devices have been proposed in [47, 110–116]. Also, a wide variety of different UWB antennas for portable devices can be found in [117, 118].

3.3.1 Complementary antenna

Consider a metal antenna with an input impedance Z_{metal}. A dual structure can be formed by replacing the metal with air. The resulting complementary antenna has input impedance Z_{slot}. Babinet's principal in (22) can be used to find the impedance of a complementary antenna, where η_0 is the wave impedance in free space. This assumes that no dielectric or magnetic materials are present. If so, the proper η must be used.

$$Z_{metal} Z_{slot} = \frac{\eta_0^2}{4}. \tag{22}$$

The product of the impedance (22) of two complementary antennas is constant. If the antenna is its own complement, frequency-independent impedance behaviour is achieved. This is so called self-complementary property, in which the antenna and its complement are identical. A self-complementary structure can be made to exactly overlay its complement through translation or rotation [9].

The value of the impedance for self-complementary antennas is $Z_{metal} = Z_{slot} = \eta_0/2$ [119]. The origin of the complementary antennas comes from Babinet's principal in optics, which Booker extended to vector electromagnetic fields [120].

3.3.2 Complementary antenna for mobile terminal with switching capability

The section presents an optimization of auto-complementary antenna to a quasi-complementary monopole antenna with switching capability, originally studied in [II]. The purpose is to find an antenna structure for mobile terminals, which covers UWB-standard (3.1–10.6 GHz) [121] and some lower frequencies. In the studies, three different antennas are simulated and compared: Auto-Complementary Antenna (ACA), Quasi- Complementary Antenna (QCA), and Optimized Quasi- Complementary Antenna (OQCA). The QCA is a scaled folded bow-tie antenna, presented in [122].

The optimized antenna structures are presented in Fig. 16. For comparison, the initial relationship of the dimensions W and H_1 of the ACA and the OQCA were calculated, so that the area of the antenna in all cases is 1600 mm^2.

After finding the optimized dimensions for the OQCA, the structure is split in half as a monopole and integrated to a ground plane of a portable device as mentioned previously. The optimization is performed with the monopole as well. The width of the monopole is fixed to $W = 40$ mm, which is the width of a ground plane. The length of the ground plane is 90 mm, respectively. The ratio of the width and height (W/H_2) of the monopole antenna is calculated by using the ratio of the optimized cases. This is because the area of the antenna cannot be the same in this case, as it is fixed to the ground plane.

In Fig. 16(b), the switches are added to the end of the folded elements. The structure is called Optimized Quasi-Complementary Antenna with Switching capability (OQCAS). This simulates a capability of switching the antenna to cover other wireless standards at lower frequencies.

In Fig. 17(a), the simulated frequency responses of the ACA, QCA, and OQCA are presented. One can notice with the optimized structure that the -10 dB lower frequency limit can be reached related to the QCA; the difference is only 120 MHz. The benefit is that the whole -10 dB impedance bandwidth can be covered without an upward peak at 6.5 GHz. The lower frequency of the QCA is 2.1 GHz against the 2.22 GHz frequency of the optimized structure. With the ACA, the -10 dB lower frequency is 2.42 GHz.

Figure 17(b) presents the frequency responses of the monopole structure with the ground plane. It can be seen that the difference between the antennas is getting relatively smaller. The -10 dB lower frequency is 3.2 GHz with QCA against 3.3 GHz with OQCA. At the same time, the -10 dB lower frequency with the ACA is 3.45 GHz. The

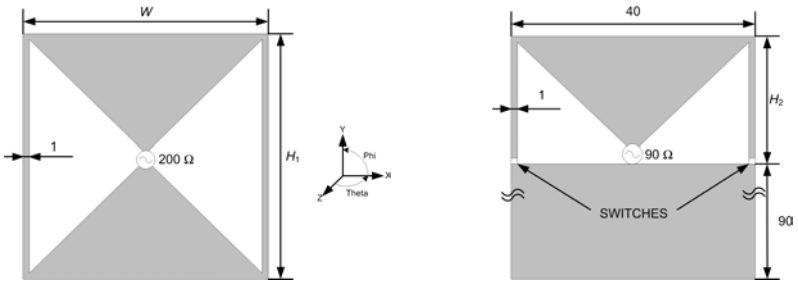

(a) (b)

Fig 16. (a) ACA (*W* = 40 mm, H_1 = 40mm) to be optimized to QCA (*W* = 34.6 mm, H_1 = 46.2 mm. (b) OQC monopole antenna (*W* = 40 mm, H_2 = 23.6 mm) with a ground plane and switching capability (II, published by permission of EurAAP).

return loss of more than −10 dB around 5.5 GHz is avoided in this case as well. The OQCAS, the switched case is also presented in Fig. 17(b). By using the switches, the −6 dB frequency band can be covered up from 0.94 GHz with a band-notch behaviour between 1.44 GHz and 3.72 GHz.

As comparing the results to the UWB-standard, it can be observed that the lower frequency limit (3.1 GHz) is not exactly achieved. This is due to the fact that the antenna width is limited to 40 mm. This can be easily corrected by increasing the ground plane width by few millimeters. The 40 mm width is used here as a reference as done in the original papers [I], [VI]-[X].

In Fig. 18, the simulated 3D-radiation patterns and the corresponding surface current distributions at 1.2, 3.45, 7.5, and 10 GHz center frequencies are presented. Figure 18(a) represents the monopole with a switching capability, whereas, in Figures 18(b), 18(c), and 18(d) the optimized monopole with a ground plane is presented. The radiation patterns are omni-directional, even at the 3.45 GHz, the antenna is slightly directive to the direction of -Y. This is caused by the surface currents on the ground plane.

In Fig. 18(a), it can be observed that the radiating surface currents are concentrated on the longitudinal sides of the ground plane. This corresponds to a fundamental characteristic mode, Mode 1. When using an open circuit, the currents are coupled to the ground plane causing the radiation pattern similar to a dipole (TM vector mode m = 0, n = 0) at the 1.2 GHz center frequency. The strong surface currents around the triangular slots are in transmission line mode, and thus not radiating.

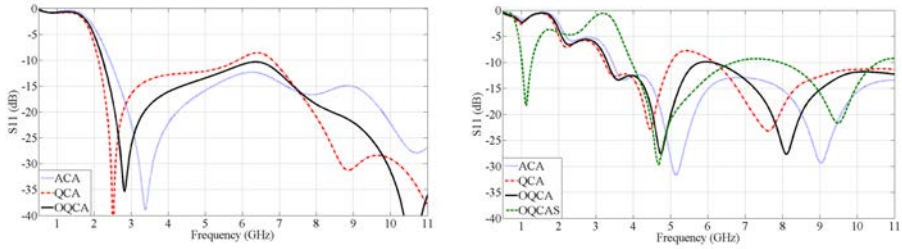

(a) (b)

Fig 17. Simulated frequency responses of studied antenna structures (a) and with a mobile ground plane (b). OQCAS presents the switching to lower frequencies (II, published by permission of EurAAP).

When it comes to the surface currents at 3.45 GHz in Fig. 18(b), the radiating currents are on both sides of the monopole structure. This time, the currents are partly on the ground plane as well, which corresponds to the 44 mm half-wave length at 3.45 GHz. The radiating mode is very close to the higher order TM vector mode (m = 0, n = 2). One can also notice at 7.5 GHz and 10 GHz in Figures 18(c) and 18(d), the surface currents are concentrated around the monopole structure. This can be seen well in the corresponding radiation patterns.

When comparing the results to UWB antennas for mobile applications presented in [48, 49, 113, 114, 116], it can be notice the results remain very similar what comes to the frequency range. This is natural as the standard [121] defines the -10 dB impedance bandwidth.

The major difference compared to the references is that the OQCAS antenna structure has a switching capability, which allows the structure exploit the fundamental mode (Mode 1) of the mobile chassis at low frequencies. In this case the center frequency is around 1.2 GHz, with 42% relative impedance bandwidth (0.94–1.44 GHz), and still allowing the usage of the wireless standards at higher frequencies up from 3.72 GHz. It can be concluded, that the relative -6 dB impedance bandwidth better that 30% (Table 1), was achieved.

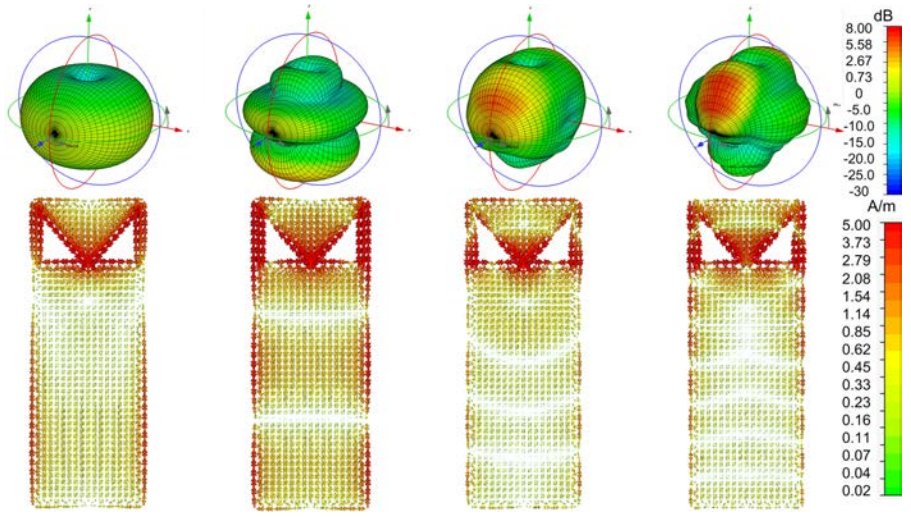

Fig 18. Simulated surface current distribution and radiation patterns of OQCA with ground plane (a) at 1.2 GHz with 2.1 dB realized gain, (b) at 3.45 GHz with 4.9 dB realized gain, (c) at 7.5 GHz with 6.4 dB realized gain, and (d) at 10 GHz with 7.3 dB realized gain. The scale of the presented surface current distribution is between 0...5 A/m, and the radiation patterns between -30...8 dB (II, published by permission of EurAAP).

3.4 Wideband antennas for mobile applications

In many applications, an antenna must operate efficiently over a wide frequency range. Wideband antennas refer to a category of antennas with a relatively constant performance over a wide frequency band. However, this is a general statement as an antenna has several electrical parameters, including bandwidth, input impedance, gain, polarization, losses, and radiation efficiency. This is due to the fact that an antenna can have very diverse applications and its desirable parameters can vary significantly. The bandwidth can depend on the application and the term wideband can mean a different frequency range for different applications [8, 51].

Wideband antenna characteristics can be achieved in different ways. One possibility to address this problem is to use the ground plane of the device as a radiating element [24, 123–126]. A large radiating ground plane is usually available in devices with

big screens, for example, mini-laptops. By adding a slot to the ground plane, the antenna operating frequencies and bandwidth can be modified [127, 128]. The other approach to cover a wide frequency range is to use frequency-tuneable antennas instead of wideband antennas [129–132]. One way to achieve wideband characteristics is to combine multiple resonances to one antenna [133–140] or wideband antennas [42–45].

In this section, slotted ground planes are used as a radiating element and the antenna feeding is designed to avoid the excitation of higher order modes at wide frequency range.

3.4.1 Quasi-complementary antennas with dipole feed

This section presents wideband quasi-complementary antenna structures. Two different slot structures are presented: a notch presented in [IX], and a square slot presented in [X]. By the antenna structure, a sort of magnetic boundary condition can be created with a combination of an electric dipole and a conducting ground plane. In order to establish this condition, the electric dipole is used as an excitation element, closely spaced (0.5 mm) to the conducting ground plane including a magnetic slot. As shown in [X] by simulations, the QCA element is easy to scale to other frequency ranges. By scaling the antenna structure by 3, the size corresponds to a modern smartphone (120 mm $\times$ 70 mm), covering the 0.7–2.1 GHz frequency band.

Figure 19(a) shows three different antenna structures that are compared in terms of the input impedance (real and imaginary parts separately), reflection coefficient, and surface current distribution. The compared antennas are a simple electric dipole, a magnetic slot cut into an electric conductor, and a combination of both as the QCA. Additionally, Fig. 19(b) presents an electric dipole with a magnetic square shaped quasi-complementary slot cut into a conducting ground plane. The antenna is considered to be an improved structure compared to the notch in Fig. 19(a). The distance of the electric dipole from the conducting ground plane is 0.5 mm as in the notch case. This Quasi-Complementary Antenna (QCA) structure is compared by the same terms as the notch structure: to a dipole, to a dipole closely-spaced to an electric conductor, and to a symmetrically excited square slot. Symmetrical excitation means that both sources have the same amplitude and phase. It can be noticed how the electric length of the slot is half of the length of the dipole for both structures.

In Figures 20(a) and 20(b), the antennas are compared in terms of the real and imaginary parts of the input impedance. Notice, that Active Z is determined here

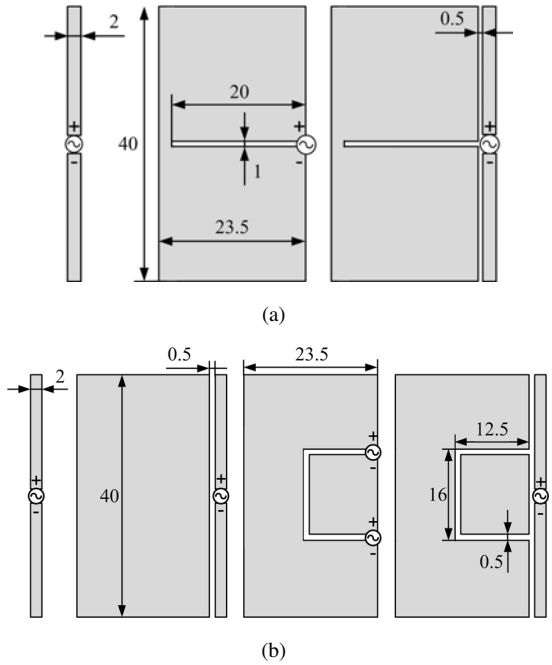

Fig 19. Quasi-complementary antennas with (a) a notch and (b) a square shape slot. Antenna structures to be compared with the QCA structures, are presented in the same figure (IX and X, published by permission of IEEE).

as $(Z_{11} + Z_{21})$, and it represents a symmetrical excitation of both sources (with same amplitude and phase) of the square slot shown in Fig. 19(b), which count the coupling between the sources. The average of the real part of the notch QCA in Fig. 20(a) is approximately 125 Ω, in contrast to the magnetic slot with 250 Ω. Respectively, for the square shape QCA, the same values are approximately 150 Ω and 200 Ω. As observed, all of the structures that include the electric dipole exhibit a common resonance at approximately 3.3 GHz.

As expected, in Fig. 20(a) (square slot), it can be seen that the real part of the input impedance is smaller in the case of the dipole close to the ground plane with a slot rather than the isolated dipole. This means that there is not a good coupling between the dipole and the conducting ground plane, and that the presence of the ground plane close to the dipole does not significantly improve the performance of the isolated electric dipole.

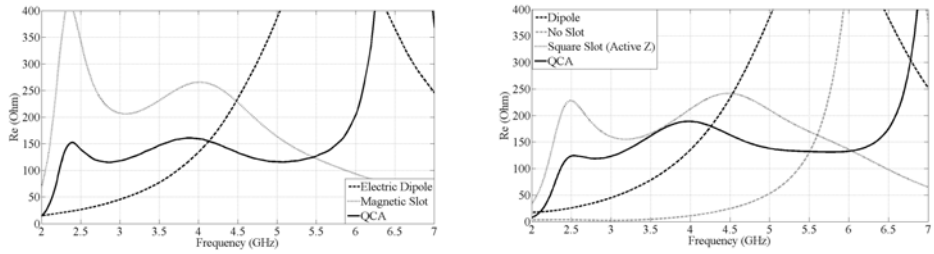

(a) Real part of the input impedance

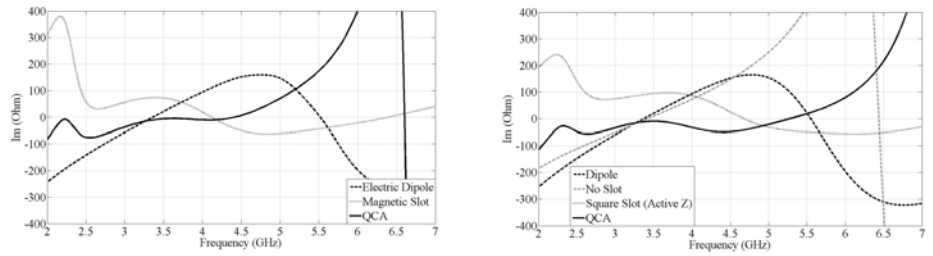

(b) Imaginary part of the input impedance

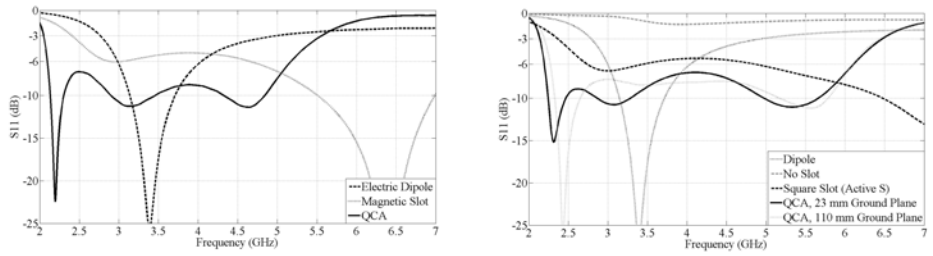

(c) Reflection coefficient

Fig 20. Simulated (a) real part and (b) imaginary part of the input impedance, and (c) reflection coefficient of the QCA antenna elements and the reference structures (modified from IX and X, published by permission of IEEE).

However, this coupling can be enhanced by cutting a magnetic slot into the conducting ground plane.

As can be observed in the imaginary part of both antenna structures in Fig. 20(b), the complementary behaviour of the electric dipole and the magnetic slot are compensating each other in the QCA structure in terms of capacitive and inductive behaviour. This is approximately between 2 and 5 GHz for the notch QCA and between 2 and 6 GHz for

the square shape QCA. As a result, the imaginary part of the input impedance for the QCA structure exhibits a very flat profile that favours the impedance matching. This is the main reason for the wideband characteristics of the QCA.

It should also be highlighted that the imaginary part of the input impedance of the single dipole, and the structure formed by the conducting ground plane and the dipole, is very similar at the lowest frequencies, but rather different above 4.5 GHz.

Figure 20(c) represents the reflection coefficient of the QCA antenna structures. For comparison, the input impedance of a resonant dipole (75 Ω, approximately) is chosen as the reference impedance for all of the analyzed structures. As observed, the −6 dB impedance bandwidth of the notch QCA is from 2.1 to 5.2 GHz, which represents an 85% relative bandwidth. For the square shape QCA, the −6 dB impedance bandwidth is from 2.2 GHz to 6.1 GHz, corresponding to a 94% relative bandwidth, whereas, the −6 dB relative impedance bandwidth of the dipole is limited to 28.5%. The symmetrically excited square slot is presented as the Active S parameter ($S_{11} + S_{21}$) and since it can be seen, it operates at a higher frequency band. As observed, the dipole close to the electric conductor without a slot (Fig. 20(c)) is unmatched over the whole bandwidth.

The effect of a mobile ground plane with the square QCA structure is compared in Fig. 20(c) by the simulations, as well. The length of the compared ground plane is 110 mm, which is the same as the length of the prototype antennas presented in Section 4.6.1 and 4.8.4. It is interesting to notice how the length of the conducting ground plane does not significantly affect the −6 dB impedance bandwidth of the antenna. This is due to the fact that the radiating currents in the ground plane are concentrated around or close to the slot.

In Fig. 21, a simulation result of the scaled QCA structure in Fig. 19(b) is presented. The scaling factor is 3, and, thus, the antenna size has become $(120 \times 70)\text{mm}^2$, which corresponds with the size of a modern smartphone. With the scaled structure, a −6 dB impedance bandwidth from 700 MHz to 2.1 GHz is achieved, corresponding to 100% relative frequency bandwidth. In the simulation, the slot width and dipole distance from the ground plane are the same as shown in Fig. 19(b), which is 0.5 mm. The slot dimensions are L = 43 mm and W = 37 mm, whereas in Fig. 19(b), L = 12.5 mm and W = 16 mm, and thus, slightly modified after scaling the antenna.

The simulated surface current distributions at 2, 3, 4, and 5 GHz are presented in Fig. 22 for the QCA structures, and for a reference structure without a slot. Black arrows represent the propagating direction of the surface currents in the electric conductor with

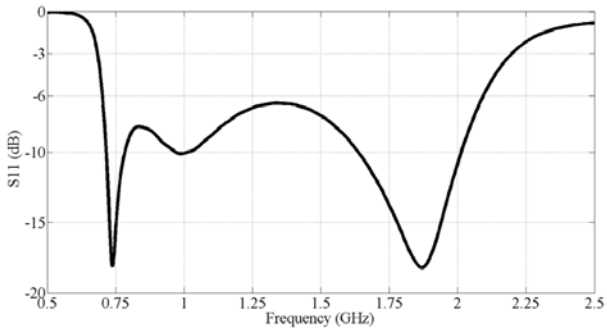

Fig 21. Simulated frequency response of a square shaped slot QCA structure, scaled by factor 3. (X, published by permission of IEEE).

a magnetic slot, whereas, the white arrows show the direction of the propagated surface currents in the electric dipole.

Figure 22(a) presents the surface currents at 2 GHz. As can be observed, these current modes correspond with the vertical current mode (Mode 1) of a rectangular ground plane [32]. As observed, the presence of the magnetic slot disturbs the vertical current flow, forcing the currents to meander. This meandering creates a horizontal current component that reduces the theoretical resonance frequency of the rectangular ground plane.

It is good to notice that the currents appearing around the slot are very strong. Also note that the electric dipole couples to the ground plane in an electric way. As a result, the vertical currents in the dipole flow in the opposite phase to the currents in the ground plane, so there is a current cancellation and the contribution to the radiation of the dipole itself is very small in this mode. The same phenomenon can be seen at the higher frequencies, with the reference structure without a slot.

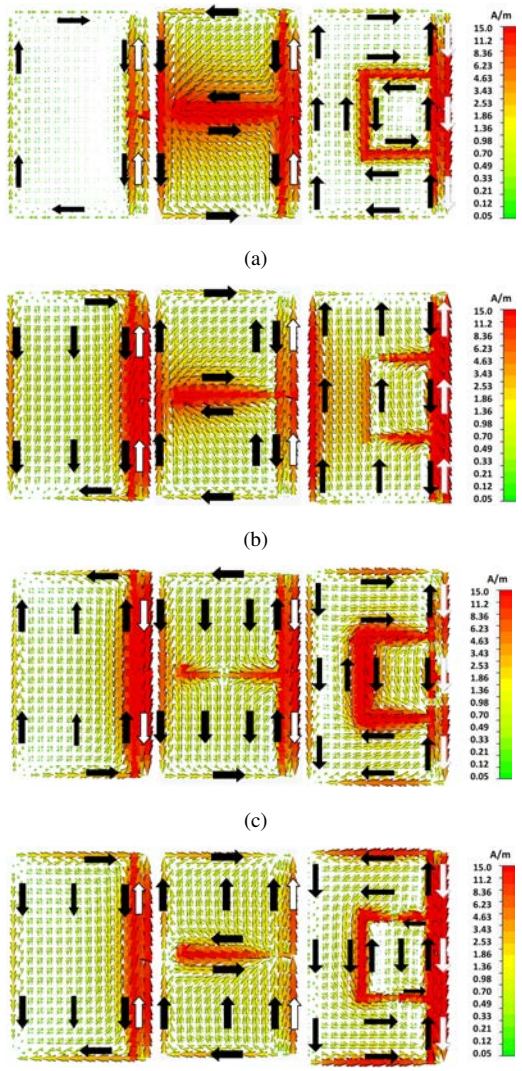

Fig 22. Simulated surface currents distribution of reference dipole and the QCA structures at (a) 2 GHz (b) 3 GHz, (c) 4 GHz, and (d) 5 GHz. On the left, the reference dipole is close to a conducting ground plane without a slot, in the middle QCA with a notch, and on the right, QCA with a square slot (modified from IX and X, published by permission of IEEE).

Figure 22(b) shows the surface current distributions at 3 GHz. This current is a result of the simultaneous excitation of mode in Fig. 22(a) and a dipole mode. The contribution of the mode appearing at 2 GHz can be seen in the left part of the ground plane which presents vertical currents (Mode 1). The resonance frequency of this mode is close to the electric length of the dipole, approximately $\lambda/2$, and, thus, the dipole can be seen as a main radiator.

The surface current distribution at 4 GHz is presented in Fig. 22(c). This current results in a linear combination of the previous modes. The currents around the slot can be connected to mode at 2 GHz, the currents along the dipole to mode at 3 GHz, and the currents flowing in an upper and low part of the ground plane are considered as higher order modes.

The surface current distribution at 5 GHz is shown in Fig. 22(d). Again, these currents are a combination of the same modes as shown at 4 GHz. The currents at the left border of the ground are now quite weak, while the currents around the slots and at the dipole are the dominant ones. Notice, that with the notch, QCA creates currents which flow in the same direction in the dipole and the ground plane. At 5 GHz, the electrical length of the external perimeter of the slots is close to 1λ, and, therefore, the slots are at their first resonance.

The surface currents of the QCAs can be considered as a linear combination of different current modes, as discussed previously. As observed in all cases, the presence of the magnetic slot in the ground plane and the excitation by means of the electric dipole, forces a strong vertical current distribution in the ground plane, which has the same propagation direction as the dipole, and thus, they can be seen to reinforce each other.

An electric boundary condition is present at the interface between the electric dipole and the conducting ground plane in all the studied cases, except the notch at 5 GHz. The vertical current mode in the ground plane represents the fundamental mode (Mode 1), and exhibits very wideband radiating properties. It is then responsible for the improved behaviour of the proposed structure [141], compared to the studied references.

The presented QCA antenna structures are planar, and they can be also considered as a mobile chassis size as the simulated frequency response shows in Fig. 21. When comparing the -6 dB impedance bandwidth to the results presented in [24], where theoretical maximum relative bandwidth of a mobile chassis was simulated to be 95%, the corresponding values for QCA elements are 85, 94, and 100%, and, thus, well

correlates with the theory. It can be concluded, that the relative -6 dB impedance bandwidth better that 30% (Table 1), was achieved.

However, in [24] two resonances appear over the simulated frequency band as the QCA structures have three resonances; this is due to the magnetic slot as discussed previously. Still, it can be clearly seen from the surface current distributions in Fig. 22 how horizontal currents are canceling each other. Thus, only vertical currents remain by offering good radiation properties as they propagate to the same direction with the excitation dipole, and corresponds with the fundamental mode (Mode 1).

3.4.2 Quasi-complementary antenna with monopole feed

Nowadays, many countries offer a digital video broadcasting handheld (DVB-H) service to mobile phones. The DVB-H system operates at a lower frequency than other mobile phone communication bands and requires a broad impedance bandwidth 474...858 MHz (58% relative bandwidth), satisfying an antenna gain greater than -10 to -5 dBi over the frequency range [142].

When considering the size of an antenna at DVB-H frequencies, the limited space available in a portable device becomes critical. One possibility to address this problem in low frequencies is to use the ground plane of the device as a radiating element. A large radiating ground plane is usually available in devices with big screens, for example, mini-laptops.

This section studies a planar radiating ground plane, originally presented in [III], and shows how it can be excited over a very wide bandwidth by using a narrow complementary slot. A complementary slot serves as a matching element for a monopole to couple energy to a radiating ground plane. The resulting structure is very simple and easy to implement in practical applications.

Figure 23 presents the structure and dimensions of the planar radiating ground plane. The dimensions of the ground plane are designed to correspond approximately to those of a mini-laptop, large PDA (Personal Digital Assistant), or a tablet. The prototype of the fabricated antenna is shown in Fig. 23(b), where both monopoles are supported by a small piece of white foam ($\varepsilon = 1$). As shown, the slot which is associated with Monopole 2 is hidden by one of the pieces.

The radiating ground plane is excited by two monopoles, 34 and 90 mm in length, which act as coupling elements. Moreover, two complementary slots (26 and 90 mm in length) are implemented orthogonally to the corresponding monopoles into the radiating

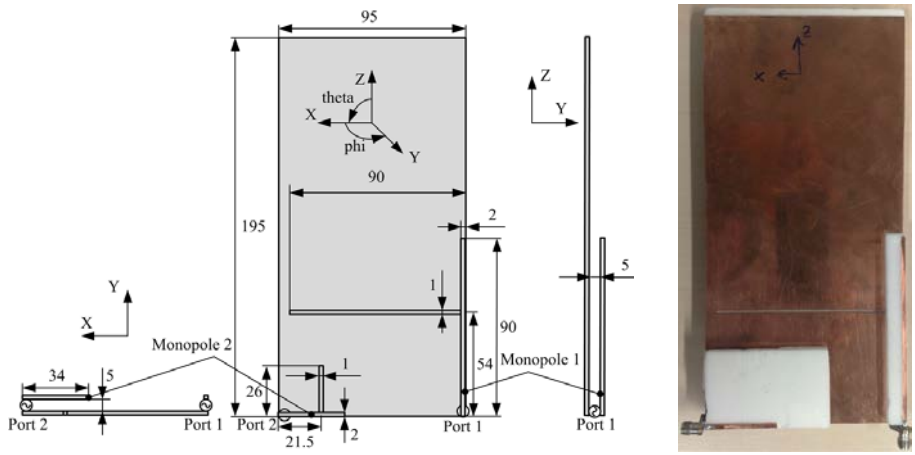

Fig 23. Quasi-complementary antenna for portable device. In figure (a) a planar radiating ground plane, and in (b), a prototype antenna are presented (III, published by permission of John Wiley and Sons).

ground plane. The positions of the slots in the ground plane were optimized using CST Microwave Studio.

Monopole 2 and its corresponding slot have relatively different dimensions compared with Monopole 1, because both monopoles see the ground plane as a different size. Furthermore, the ground plane for Monopole 2 can be seen scaled from the main ground plane, limited by the 90 mm slot.

By optimizing the slot position and length, it is possible to find an optimum value of a 50 Ω input impedance of the excited monopole. Using the slot, the monopole antenna can be located very close to the ground plane, providing good coupling to the ground plane, and by offering good antenna performance.

The measured and simulated reflection coefficient and measured maximum gain of Monopole 1 are presented in Fig. 25(a). The measured total gain in the DVB-H band is approximately -5 dBi at 474 MHz and 4 dBi at 858 MHz. The maximum gain is 5–10 dB higher than the minimum requirements of the DVB-H standard [142] and, thus, exceedingly satisfies the standard, as presented in the same figure. The impedance matching at 474 MHz is -1.8 dB, which, in turn, satisfies the standard, based on studies presented in [143].

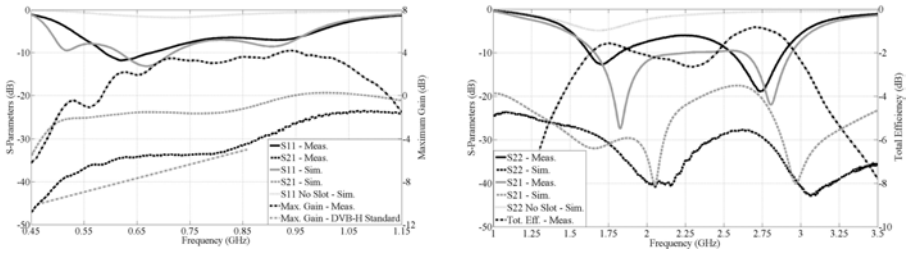

(a) (b)

Fig 24. Measured and simulated S-parameters (a) for Monopole 1, with a measured maximum gain and (b) for Monopole 2, with a measured total efficiency. Simulated S parameters are compared with the case without a slot (III, published by permission of John Wiley and Sons).

Separated from the DVB-H standard (474–858 MHz), the GSM850 and GSM900 bands can be covered within the −6 dB impedance bandwidth with the Monopole 1. The relative −6 dB bandwidth of the Monopole 1 is 57%. Additionally, the measured isolation between Monopoles 1 and 2 is higher than 25 dB over the whole operating bandwidth. For comparison, to demonstrate the effectiveness of the slot, the simulated frequency response without the slot is also presented in Fig. 25(a). It can be noticed that by properly optimizing the slot, matching can be improved significantly over a very wide bandwidth.

Figure 24(b) presents the measured and simulated reflection coefficient for Monopole 2. The measured −6 dB impedance bandwidth ranges from 1.53 to 3.0 GHz and the simulations predicted the same bandwidth with a slightly better matching. The measured relative bandwidth, in the case of Monopole 2, is 65%. The measured isolation over the operating bandwidth is once again over 25 dB, as in the lower frequency band.

As previously, the case with the slot in the ground plane is compared with the case without the slot. As shown, matching is dramatically improved in this case as well. Fig. 24(b) also presents the measured total efficiency of Monopole 2. The total efficiency is defined as the relation between the radiated power (P_{rad}) of the antenna and the power delivered to the antenna port (P_{del}). In a logarithmic scale, the total efficiency is presented as $10\log_{10}(P_{rad}/P_{del})$. It can be observed that the total efficiency is more than −3 dB over the operating impedance bandwidth, and the average is −1.81 dB.

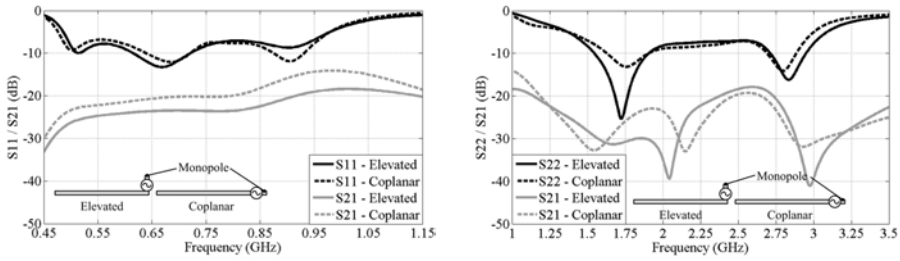

(a) (b)

Fig 25. Performance of simulated S-parameters for structures with elevated and coplanar monopole: (a) Monopole 1 and (b) Monopole 2 (III, published by permission of John Wiley and Sons).

The monopole can be implemented to the side of the ground plane to make the structure coplanar. Fig. 25 shows a comparison of the simulated S-parameters obtained with the coplanar monopole and the elevated monopole. In both cases, the distance of the monopole from the ground plane is 5 mm. As observed, the behaviour of the antenna is very similar in both cases.

The measured radiation patterns of Monopole 1 at 500 and 900 MHz are presented in Figures 26(a) and 26(b), respectively. As one can notice, the radiation patterns at the measured frequencies do not show very deep nulls, so the propagated signal can be easily received from all directions. The maximum gain at 500 MHz is -2.3 dBi, which is approximately the same in every cut. The radiation pattern can be observed as being dipole-like. The maximum 3.2 dBi gain at 900 MHz can be found in the YZ plane. It is also notable that the radiation pattern at 900 MHz corresponds well with the radiation of a monopole on a ground plane.

Figures 26(c) and 26(d) depict the measured radiation patterns of Monopole 2 at 1.70 and 2.75 GHz. A 3.9 dBi maximum gain at 1.7 GHz can be observed at the intersection of the XY and YZ planes, while a 4.1 dBi maximum at 2.75 GHz can be found in the XY plane. It is also notable that the radiation patterns at both measured frequencies have no deep nulls. The same was observed with Monopole 1 in the lower frequency band.

In Fig. 27(a), two separate current paths on both sides of the ground plane can be observed in the structure with the slot at 500 MHz. Strong vertical currents in the ground plane are corresponding to the fundamental mode, Mode 1. This is the main reason for the radiation of the antenna, with no deep nulls at the lower frequencies. Notice that the

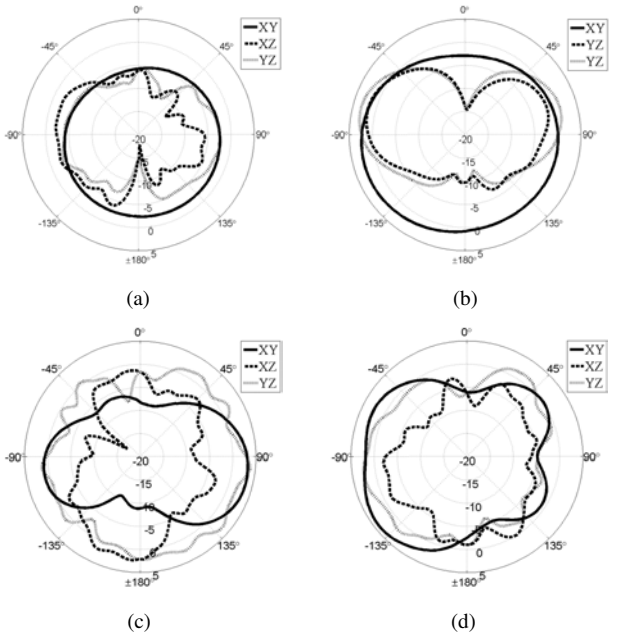

Fig 26. Measured radiation patterns in total gain at (a) 500 MHz, (b) 900 MHz, (c) 1.70 GHz, and (d) 2.75 GHz (III, published by permission of John Wiley and Sons).

slot itself also reinforces the symmetrical vertical currents on the left side of the ground plane.

At 900 MHz in Fig. 27(b), it can be seen that the presence of the slot keeps the surface currents propagating vertically in the ground plane (Mode 1), as observed at the previous frequency. These currents above the slot create a monopole on a ground plane kind of radiation, which can be seen in Fig. 26(b), whereas the currents below the slot represent low radiation.

The surface current distributions at 1.70 GHz are presented in Fig. 27(c). In this case, the main mechanism of radiation is the currents that are propagating horizontally in the bottom part of the ground plane, which correlates with a higher order mode, Mode 3.

Figure 27(d) depicts the surface currents of Monopole 2 at 2.75 GHz. As the frequency increases, nulls start to appear in the horizontal and vertical current distribution, as a combination of two or more higher order current modes. At 2.75 GHz, currents around the slot are in resonance with vertical currents on both sides of the ground plane

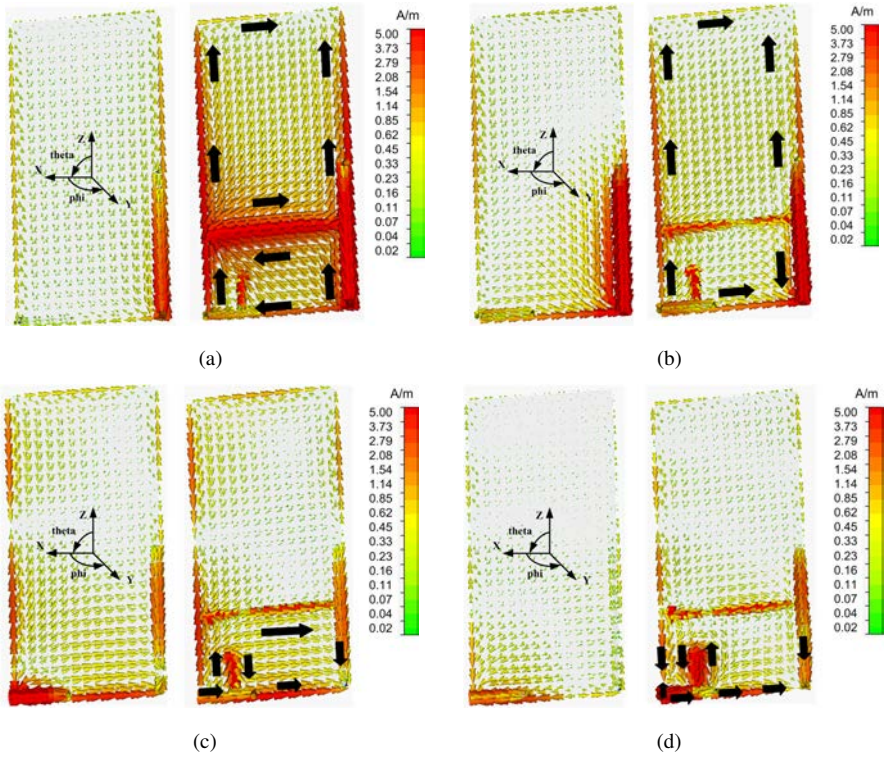

Fig 27. Simulated surface current distributions at (a) 500 MHz, (b) 900 MHz, (c) 1.70 GHz, and (d) 2.75 GHz. On the left side, the structure without the slot is presented. The scale is normalized to 5 A/m. Black arrows are included to facilitate visualization of the current flow (III, published by permission of John Wiley and Sons).

limited by the 90 mm slot. These vertical currents are responsible for the radiating behavior that is exhibited by the antenna at this frequency (54 mm wavelength).

It can be observed that the presence of the slot reinforces the coupling of the field to the radiating ground plane at the studied frequencies within both operating bandwidths. When comparing the results to [143], clear difference is that, instead of awakening 3 resonances, the studied antenna structure represents only fundamental mode over the DVB-H band. This can be seen in the surface currents in Figures 27(a) and 27(b). On the other hand, both structures satisfy the DVB-H standard in terms of maximum gain.

The antenna structure presented in section has higher maximum gain, which is explained with larger antenna size and better impedance matching.

As in [143], a matching circuitry is used to broaden the impedance bandwidth of the capacitive coupling element (CCE) for the DVB-H bandwidth, which increases the total losses of the antenna structures. The structure presented in this section has very simple feeding mechanism, and, thus, the losses are also very low.

As only maximum gain is measured at the low band, the measured total efficiency at the higher band is predicting good total efficiency at the lower band as well because the structures are scaled. On the other hand, by using monopole excitation, a narrow notch is needed to cut into the ground plane. This may decrease the mechanical strength of the antenna structure, whereas by using CCE kind of an excitation this can be avoided.

The objective of the wideband antenna structures is to gain relative -6 dB impedance bandwidth better than 30% (Table 1). As the antennas are supporting 57% and 65% relative -6 dB impedance bandwidths at lower and higher bands, respectively, they satisfy the criteria of a wideband antenna.

With the proposed antenna structure, the DVB-H standard, GSM standards, UMTS standards, 2.45 GHz WLAN, and future LTE bands can be covered.

3.5 Summary

This chapter presented wideband antennas for mobile terminals. It also discussed the required impedance matching techniques and balun structures when designing wideband antennas, or antennas in general.

The presented novel and simple antenna structures were based on an idea of a complementary antenna, with an electric conductor (inductive behaviour) close to a conducting ground plane slot cut into it (capacitive behaviour). These two opposite components were canceling each other in terms of the imaginary part of the input impedance at wide frequency range. The structures supported the idea of a single current mode excitation.

To gain a wide frequency bandwidth, the structures were modified by simulations to find a quasi-complementary shape, meaning that the electric conductor and the magnetic slot are not exactly complementary. The antenna structures utilize a ground plane of a portable device as a radiating element.

In conclusion, it was shown that by designing an antenna feeding properly, a fundamental radiating antenna mode can be excited at a wide frequency bandwidth. By

proper antenna feeding, the excitation of higher order modes was avoided, and, thus, the disturbance of unwanted modes can be neglected. It was shown that the radiating and current modes of the antenna structures presented in the original papers correlates well with the modes presented in the theory part of the dissertation.

4 Wideband multi-element antennas

This chapter presents the wideband multi-element antennas related to mobile and wireless applications. The two first sections of this chapter will discuss the electric and magnetic boundary conditions, as well as the image theory. It is shown, by using characteristic modes theory and symmetrical feeding, how a magnetic boundary condition can be created to a conducting mobile ground plane [VI].

The image theory is used to implement a prototype antenna in [VI]. The image theory and characteristic mode theory are compared to show the similarities in both theories. It is shown how the magnetic boundary condition in the image theory corresponds to the antenna modes in the characteristic mode theory, and that the electric boundary condition corresponds to transmission line modes, respectively.

Next, wideband multi-element antennas with symmetrical feeding are discussed, based on [VI], [VII] and [VIII]. In [VII], a metal bezel extension of a symmetrical folded dipole is presented with measurement results, and these results are compared. To study the vicinity of a head phantom close to the antenna structures, the measured SAR-values and S_{11}-parameters are compared.

Then, diversity in mobile applications is discussed in general matter. The space diversity technique is first presented and it is shown how, by reducing mutual coupling between closely spaced antennas in [IV] and [V], good isolation can be achieved at a wide frequency bandwidth. Then, polarization diversity and radiation pattern diversity methods are presented with corresponding examples related to the original papers [IX] and [I], respectively.

The final part of the chapter briefly discusses MIMO systems with diversity and multiplexing approaches. An implementation of a multi-element antenna for a mobile MIMO application is presented, based on [X]. And finally, parameters to study MIMO and diversity performances are presented with practical examples based on [I], [IX], and [X].

For MIMO/diversity systems, the relative -6 dB impedance bandwidth should be better than 30%, when at the same time the measured maximum total efficiency of an individual antenna is at most -1 dB ($\leq 80\%$) but better than -3 dB (50%). On the other hand, the isolation between the antenna elements must be better than 18 dB with correlation smaller than 0.2. With these values, the limit for effective diversity

gain (EDG) is better than 7.8 and for MIMO efficiency better than 0.78, as defined in objectives (Table 1).

It is good to mention that the quasi-complementary antennas presented in Section 3.4.1, are combined in this Chapter to two different multi-element antennas to obtain diversity with a low correlation between the antenna elements presented in [IX] and [X].

4.1 Electric and magnetic boundary conditions

Magnetic and electric conductors are well known basic concepts in literature. They are useful tools when studying boundary conditions in electromagnetic problems. Boundary conditions specify how the tangential and normal components of the electromagnetic field in one medium are related to the components of the field across the boundary in another medium.

An electric boundary condition may be a boundary of an electric conductor and a dielectric material. In such a condition, the lines of the electric field point away from the conducting surface, where the charge density is positive and directly toward the conducting surface where the charge density is negative. In other words, the electric field is always normal to the surface at the conducting boundary [144]. When a unit vector is pointing normally away from the conducting surface, the tangential component of the electric field vanishes; a metal conductor is shorting the tangential component by forcing it to zero. This is important when considering antennas that are close to the conducting material, since such an antenna has a negative image current and it radiates almost nothing.

In a magnetic condition, respectively, the normal component of a magnetic flux is continuous across the boundary between two adjacent media. The tangential component of the electric field is continuous across the boundary, whereas the tangential component of the magnetic field has vanished [144]. This condition is important from the antenna radiation point of view. Still, such a condition does not physically exist. The magnetic condition is used more as a tool in electromagnetic analysis.

One possibility to physically create a magnetic condition is to use periodical structures such as high-impedance electromagnetic surfaces or photonic bandgaps (PBG) [145, 146]. They are also called artificial magnetic conductors (AMC) or artificial magnetic ground planes (AMG). By using these materials, an antenna can be laid very close to such a surface without disturbing its radiation properties [147, 148].

A magnetic conductor can be seen as a medium with a high permeability, when a good electric conductor can be seen as a highly conductive metal or dielectric with very high permittivity. When the reflection coefficient of the electric conductor is -1, for the magnetic conductor it is +1. This means that the phase difference of the reflected wave is 0° for a magnetic conductor representing an open circuit, and the electric conductor shows a 180° phase shift representing a short circuit. This is an important definition when considering antenna radiation properties [149].

Figure 28 presents the basic mechanism for creating an artificial magnetic boundary condition in a radiating mobile ground plane by using the symmetrical excitation presented in [VI]. The black line in the middle of the ground plane represents the line of symmetry of the ground plane where the magnetic condition is created. The dashed lines represent the lines of symmetry of the two separate planes, dividing them both into halves. When the ground plane is separated into two parts that are uniform in width, the surface impedance of the separate parts is equal, thus, leading to good antenna performance.

As depicted in Fig. 28, having sources at the longer edges of the ground plane provokes a vertical current distribution at the centre of the radiating ground plane, i.e., a magnetic boundary condition is imposed along the central line of symmetry. To create the magnetic boundary condition, both sources need to be excited symmetrically, so that the symmetrical excitation introduces simultaneous amplitudes and phases in both sources. The arrows pointing upward correspond to the directions of the currents when the magnetic boundary condition is valid.

In order to physically implement the magnetic boundary condition in a radiating ground plane, the structure in Fig. 29(a) is presented. It consists of a slotted ground plane, where two symmetrical excitations are used to create the magnetic condition along the line of symmetry. As observed, the structure is the result of a combination of two symmetrical planar folded dipoles with the overall dimensions of a typical mobile handset. The symmetry criterion for dividing the ground plane is the same as presented in Fig. 29(a). The slot length is 106 mm and the input impedance of Source 1 and 2 is 300 Ω.

Figure 29(b) shows the normalized current distribution at resonance for the characteristic mode (Mode 1) of the symmetrical folded dipole at 1.3 GHz, originally presented in [VI]. The antenna mode exhibits a magnetic boundary condition at the axis of symmetry of the radiating ground plane, so all the currents over the structure are in phase at the resonance frequency representing excellent radiation properties.

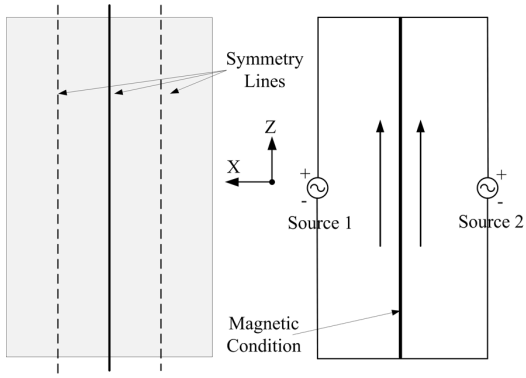

Fig 28. On the left side, a ground plane is divided into symmetrical planes, where a magnetic boundary condition is applied along the central line of symmetry. On the right side, a magnetic boundary condition is imposed by applying double symmetrical feeding at the longer edges of the ground plane (VI, published by permission of IEEE).

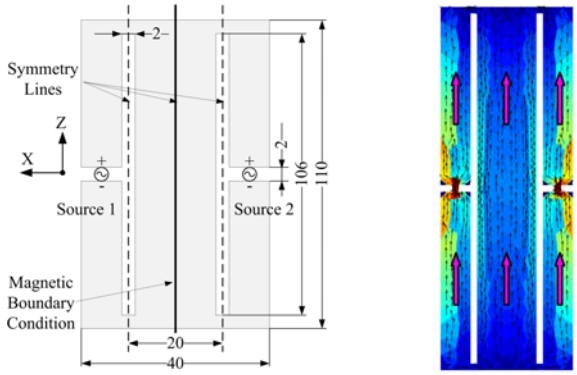

Fig 29. (a) Two symmetrical folded planar dipoles are combined to create an artificial magnetic boundary condition between the dipoles. (b) The result is a symmetrical folded dipole, which creates symmetrical currents to the ground plane (VI, published by permission of IEEE).

It can clearly be seen from the characteristics mode how the currents are strong at the points where symmetrical feeding is correctly implemented. The characteristic modes analysis of the antenna structure is presented and discussed in the next section.

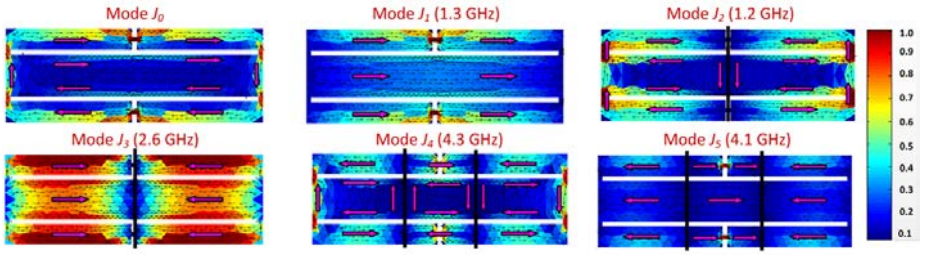

Fig 30. Characteristic modes analysis of the symmetrical folded dipole (VI, published by permission of IEEE).

4.1.1 Modal analysis of symmetrical folded dipole to demonstrate magnetic boundary condition

A modal analysis of the symmetrical folded dipole is performed by means of the Theory of Characteristic Modes to illustrate the interest of creating a magnetic boundary condition in a slotted radiating ground plane. The analysis is based on the original paper [VI].

This analysis reveals that two kinds of modes can be excited in the slotted ground plane: Antenna modes and transmission line modes presented in Section (2.2). The creation of a magnetic boundary condition in the plane of the symmetry of the structure is necessary to force an excitation of antenna modes that exhibit a broader radiation band and enhanced radiating efficiency. Moreover, the excitation of some higher order modes, which disturb the radiating behaviour of the antenna, is avoided by means of this feeding technique.

A modal study of the symmetrical folded dipole described in Fig. 29(a) is presented in Fig. 30. The figure shows the normalized current distributions at resonance for the first six characteristic modes of the symmetrical folded dipole. Antenna modes J_1, J_3, and J_5 exhibit a magnetic boundary condition at the axis of symmetry of the radiating ground plane, so all of the currents over the structure are in phase at the resonance frequency. On the contrary, transmission line modes J_0, J_2, and J_4 present currents flowing in the opposite phase, generating poor radiation.

Figure 31 depicts the characteristic angles curves for the first six characteristic modes of the symmetrical folded dipole shown in Fig. 30. Again, there is a special non-resonant inductive mode, whose currents form a closed loop around the structure.

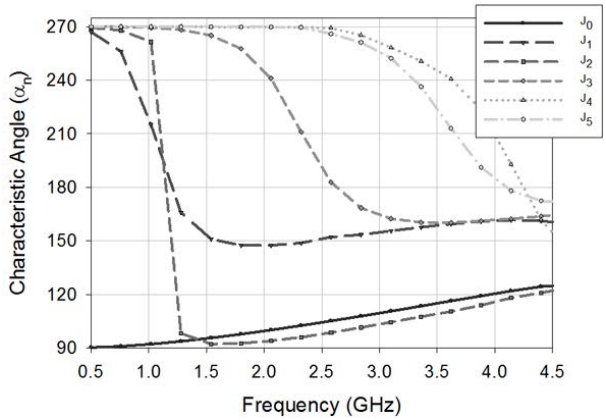

Fig 31. Variation of the characteristic angles as a function of frequency associated to the first six characteristic modes of the symmetrical folded dipole (VI, published by permission of IEEE).

The antenna modes J_1, J_3, and J_5 present the softest slope at 180°, and hence, the largest radiation bandwidth.

Figure 32 illustrates the contribution of each mode to the total power radiated by the antenna when it is fed symmetrically. As observed, the symmetrical feeding only favours the excitation of those modes that exhibit a magnetic condition in the symmetry plane of the ground plane. As confirmed by Fig. 32, the modes J_1 and J_5 are precisely the ones that present the widest radiating bandwidth (together with mode J_3, which is not excited, as it presents zero current at the feeding points). Once more, the mode J_1 plays an essential role in the structure. It dominates at the lowest frequencies and it keeps its contribution to the total radiated power long after the resonance. This mode combines with mode J_5 to create the radiation maximum observed at 4 GHz.

Figure 33 shows the Active S-parameter computed with different reference impedances, when the symmetrical folded dipole is symmetrically fed. Again, the best matching for the excited antenna modes J_1 and J_5 is obtained for the reference impedance of 300 Ω.

The modal analysis of the symmetrical folded dipole demonstrated that it is possible to only excite those modes whose currents flow symmetrically with respect to the symmetry plane of the ground plane (i.e., they exhibit a magnetic condition in the symmetry plane). By using symmetrical feeding, the appearance of some transmission line modes, whose excitation would ruin the matching bandwidth, can be avoided.

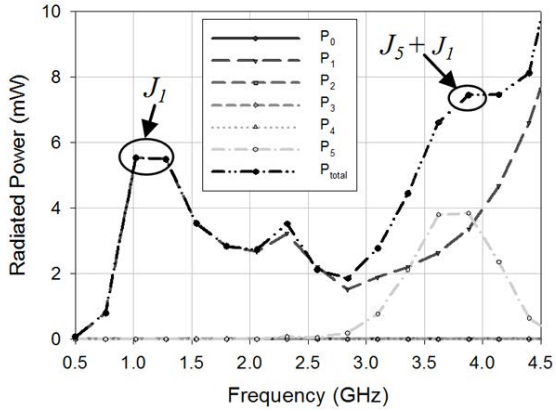

Fig 32. Contribution of each mode to the total radiated power of the symmetrical folded dipole, when it is fed simultaneously at the centre of the upper and lower dipoles (VI, published by permission of IEEE).

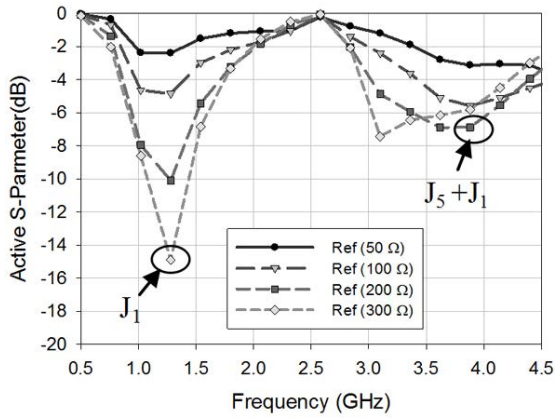

Fig 33. Active S-parameter calculated for different reference impedances of the symmetrical folded dipole excited with symmetry (VI, published by permission of IEEE).

Therefore, since the excitation of transmission line J_4 mode is avoided by means of the magnetic condition imposed by the symmetrical feeding, an increment in the impedance bandwidth can be obtained if a smooth transition between the mode J_1 and mode J_5 is achieved. This can be accomplished if the length of the slot is decreased.

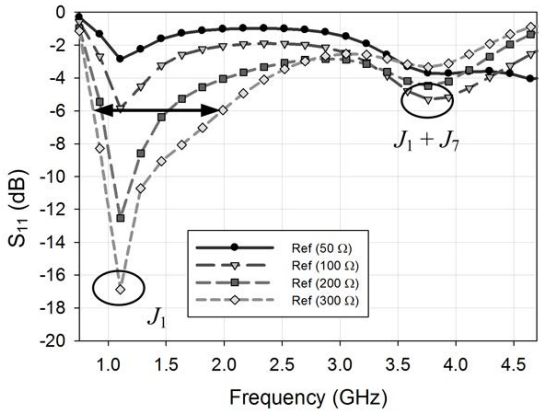

Fig 34. Active S-parameter calculated for different reference impedances of the symmetrical folded dipole excited with symmetry (VI, published by permission of IEEE).

In this case, the modes excited in the antenna are the same as in the case of a 106 mm slot length, so neither the resonance frequency nor the radiating bandwidth of these modes is altered by the length of the slots. However, the transition from mode J_1 to mode J_5 can be improved by increasing the impedance bandwidth of the antenna.

The length value required to obtain the maximum impedance bandwidth is 50 mm, and the results obtained for the Active S-parameter, computed for different reference impedances, are plotted in Fig. 34. As observed, a larger -6 dB relative impedance bandwidth is obtained (80%) with the 50 mm slot length than with the 106 mm slot length, where a relative impedance bandwidth of 53% was achieved. This increment of the operating bandwidth favours the antenna to cover different mobile standards.

4.2 Image theory

An important method to simplify electromagnetic problems is image theory. To analyze the performance of an antenna near an infinite plane conductor, virtual sources or images can be introduced, as presented in Fig. 35(a). For analysis purposes only, the equivalent charge gives the same radiated field on and above the conductor as the actual charge itself [11].

(a) (b)

Fig 35. (a) Electric source above and its image below electric conductor (electric boundary condition). (b) Electric source above and it image below magnetic conductor (magnetic boundary condition).

The image theory states that any given charge above an infinite perfectly conducting plane, is electrically equivalent to the charge and its image with the conducting plane removed [144]. From an antenna point of view, a virtual source or image can be placed below the ground plane to represent the reflections from the ground plane. The electromagnetic field above the ground plane can be considered as a sum of the electromagnetic fields due to the real source and the image source with ground plane removed.

Figure 36 shows the relationship between the characteristic modes theory, presented in Section 2.2, and the image theory. As the image theory states that the ground plane should be infinite, the characteristic modes can be used to analyze a finite or limited size conducting ground plane. The relationship between these methods is that when the characteristic modes state that the mode is an antenna mode shown in Fig. 36(b), it is equivalent to the magnetic boundary condition in the image theory, shown in Fig. 35(b). Respectively, the transmission line mode in Fig. 36(a) in the characteristic modes theory corresponds to an electric boundary condition in the image theory in Fig. 35(b).

A monopole antenna results from applying image theory to a dipole. If the conducting ground plane is placed below a single element of length $L/2$ carrying a current in Fig. 37(a), then, the combined system acts identically to a dipole of length L. Except that the radiation only takes place above the conducting plane so that the directivity is doubled and radiation resistance is halved. The quarter-wave length monopole, thus, approximates the half-wave length dipole [83].

The image theory was successfully used in original paper [VI] for making a symmetrical folded dipole prototype antenna. The prototype is presented in Fig. 37(b) with a large ground plane size 300 mm $\times$ 300 mm.

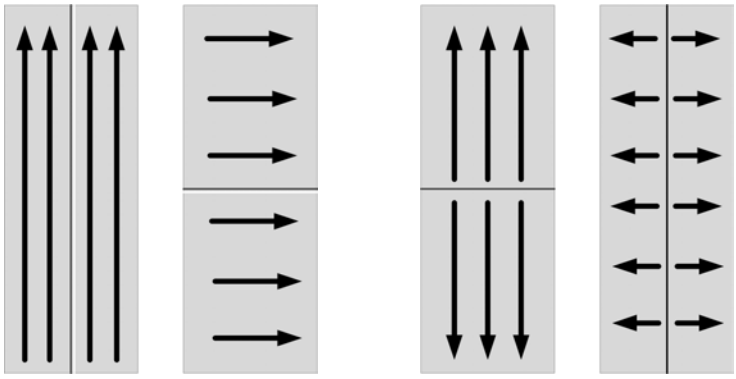

(a) (b)

Fig 36. (a) An antenna mode in the characteristic theory corresponds to a magnetic boundary condition in the image theory. (b) A transmission line mode in the characteristic theory corresponds to an electric boundary condition in the image theory.

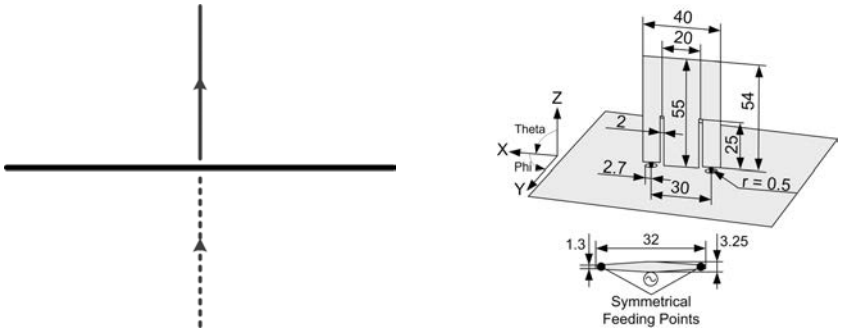

(a) (b)

Fig 37. (a) Image theory applied to a monopole antenna. (b) Symmetrical folded dipole prototype antenna implemented by using image theory with a ground plane size 300 mm x 300 mm (b, VI, published by permission of IEEE).

4.3 Wideband multi-element antennas with symmetrical feeding

The use of a radiating ground plane as part of the antenna in mobile devices was proposed about 10 years ago to increase antenna radiation efficiency and bandwidth

[24]. But, using a symmetrical feeding to excite currents on a mobile ground plane is not a commonly used principal. The idea of using symmetrical feeding is to modify surface currents to behave in a certain way.

Some compact antenna structures with symmetrical feeding are presented in [150–153]. Also, a multiport MIMO antenna with symmetrical feeding to gain orthogonal radiation patterns is proposed in [154]. A monopole antenna with symmetrical feeding is used to avoid the excitation of higher order modes in [155]. In addition, some studies to excite orthogonal current modes have been presented in [30, 31].

In this section, two antenna structures to couple energy a mobile ground plane are presented based on [VI] and [VIII].

4.3.1 Symmetrical folded dipole and its metal bezel extension

This section presents a comparison of antenna structures which supports the excitation of a single current mode within a wide frequency range, and avoids the excitation of higher order current modes of a mobile ground plane. Avoiding the excitation of these modes, symmetrical feeding studied in Section 4.1.1 is used with the compared antenna structures. The method creates a magnetic boundary condition between two adjacent folded dipoles by favoring an excitation of radiating antenna mode. Objectives to gain with the antenna structure can be found in Table 1.

In [VI], the measurement results of the prototype planar symmetrical folded dipole (SFD) were presented. This section compares SFD to a further investigated metal bezel (MB), published in [VII]. The MB ground plane is widened, compared to SFD, so that the structure is still symmetrical, as presented in Fig. 29. Both antenna structures represent the fundamental mode (Mode 1) shown in Figures 9(b) and 10(a).

In the metal bezel structure, the slots in the ground plane are separated closer to the edge of a mobile chassis, while the antenna is integrated as part of the device. This kind of antenna solution will release space inside the mobile terminal when separate antennas for different operating frequencies are no longer needed. Figure 38(a) presents the compared antennas structures, together with the coordinate system and the dimensions. It can be noticed that the structures are very similar, except the ground plane of the metal bezel is extended in width and bent up to represent a mobile chassis frame.

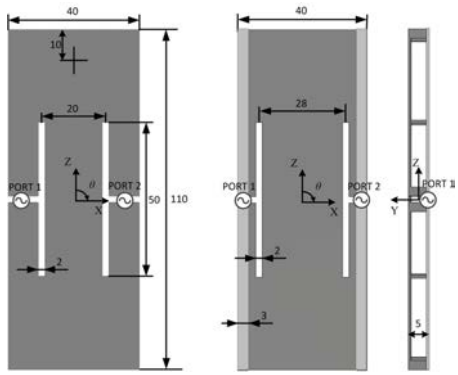

(a)

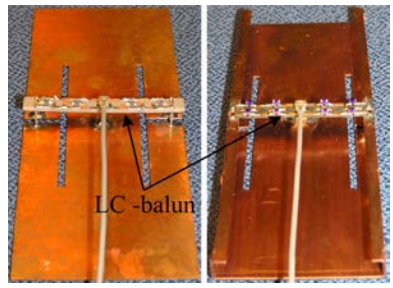

(b)

Fig 38. (a) layout of the symmetrical folded dipole and metal bezel. In (b), the prototype antennas of both structures are presented (VII, published by permission of IEEE).

Figure 39 presents the measured S_{11}-parameter and the total efficiency of the SFD and MB in free space. The -6 dB impedance bandwidth of SFD is from 904 MHz to 1960 MHz, whereas the MB ranges from 908 MHz to 1993 MHz, corresponding to 74% and 75% relative impedance bandwidths, respectively. This is very close to the theoretical impedance bandwidth presented in Fig. 34. The total efficiencies at the aforementioned bands are between $-3.3\ldots-0.7$ dB (average -1.63 dB) and $-3.3\ldots-0.6$ dB (average -1.42 dB), respectively.

Figure 40 presents the radiation patterns of SFD and MB at 950 MHz and 1950 MHz. The radiation patterns and the total efficiency measurements of the antennas are performed with Satimo StarLab. The maximum gain for SFD at 950 MHz is 1.9 dBi,

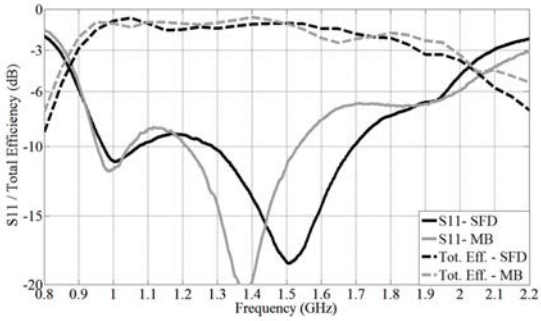

Fig 39. Measured S-parameters of the symmetrical folded dipole and its metal bezel extension (VII, published by permission of IEEE).

and for MB, 0.2 dBi. The higher gain of SFD is due to the slightly directive behaviour of the radiation, approximately in $\pm 75^\circ$ (XZ- and YZ-planes). At 1950 MHz, the values are 1.2 dBi and 1.7 dBi, respectively. The radiated vector mode of both antennas corresponds to the TM mode of order m = 0 and n = 0, as presented in Fig. 5(a).

Therefore, it can be concluded that the impedance bandwidth and total efficiencies are very similar with both antennas. The main difference in the impedance bandwidth is caused by the antenna feeding and the values of the lumped components that are used in the balun. The difference in the radiation patterns is caused by the LC-balun implementation. Also, the improved balun design in the case of MB can be observed in the symmetry of the radiation patterns, especially at 1950 MHz.

When comparing the results to a wideband folded dipole antenna presented in [156], by using symmetrical feeding it is possible to improve the relative -6 dB impedance bandwidth from 63% to 75% (20% improvement). This is reached by using symmetrical feeding by avoiding the excitation of higher order modes, and by creating a magnetic boundary condition between the folded dipoles. The value also shows that the determined -6 dB impedance bandwidth better than 30% was achieved.

On the other hand, when comparing the total efficiencies to the wideband PIFA for mobile terminals presented in [45], the maximum values are very similar: PIFA -0.3 dB, against -0.7 dB and -0.6 dB for the symmetrically fed structures in this section. On the other hand, the minimum total efficiencies are little lower: PIFA -2.22 dB, against -3.3 dB for the symmetrically fed structures. This is explained with losses of the lumped components in the symmetrical feeding network.

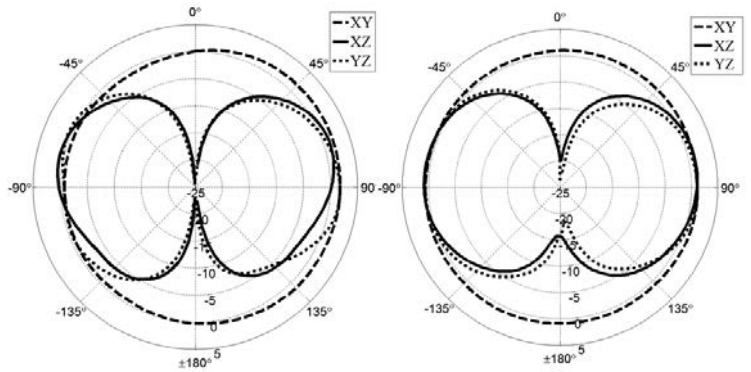

(a)

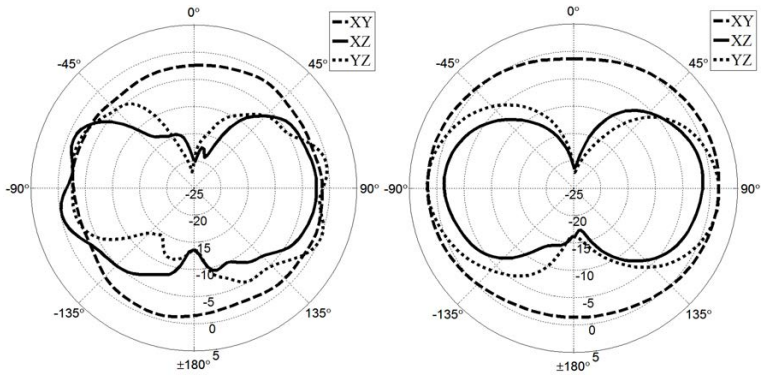

(b)

Fig 40. Radiation patterns of symmetrical folded dipole (on left) and metal bezel (on right) at (a) 950 MHz (b) 1950 MHz. Feeding implemented by using cascaded LC-baluns (VII, published by permission of IEEE).

Still, average total efficiencies are -1.63 dB (69%) for symmetrical folded dipole, and -1.42 dB (72%) for metal bezel. This is slightly lower than -1 dB (80%) but much better than -3 dB (50%), and, thus, well satisfies the goal defined in Table 1.

With the proposed antenna structure, E-GSM (880–960 MHz), GPS, DCS-1800 (1710–1880 MHz), and PCS-1900 (1850–1990 MHz) can be covered.

Effect of a head phantom to the performance of the SFD and the metal bezel in terms of SAR and S_{11}-parameter

The user influence on the mobile terminal antenna performance has been known for a long period. Since the first studies were presented decades ago [157], the effect of the user has been investigated with different user effect scenarios, including calling and browsing modes [158–160].

The amount of user effects depends on the antenna type (internal or external), the operation frequency, and, in particular, the operating environment. PIFA types of antennas are relatively robust against the vicinity of the user. However, with the most harmful hand grips, the performance decreases in both calling and browsing mode usages [158, 161].

Several solutions to mitigate the performance degradation of a mobile terminal, caused by a lossy tissue, have been developed. Appropriate design practices include the shaping of the terminal ground plane [162], optimization of the antenna location [163], and the use of balanced antennas [164]. Also, metal stripes have been proposed between the mobile antenna and the user to reduce radiation towards the head [165]. Moreover, active methods exist which include dynamically switchable antenna structures [166] and control of the antenna impedance matching [167]. The highest drawbacks of actively controlled antennas are increased power consumption due to component losses and the cost of the control system itself.

In order to identify the human head or hand near the antenna, the use of proximity sensors has also been proposed. A capacitive solution to detect human tissue has been developed in [168]. However, the implementation of a sensing system increases the power consumption of actively controllable antennas. Still, CPU processing and communications can be seen as the largest energy consumers in mobile devices. Also, screens nowadays, when they are not in a screensaver mode, are large energy consumers [169].

In this section, an effect of a head phantom to the performance of the symmetrical folded dipole and the metal bezel is shortly discussed in terms of SAR-measurements with corresponding *S*-parameters, presented in [VII]. The passive measurements are carried out with the DASY4 [170] measurement system.

The specific absorption rate (SAR) measures the energy absorbed by the body when it is exposed to an electromagnetic field. The measured SAR-values are compared at 898 MHz (E-GSM), 1747 MHz (DCS-1800), 1880 MHz (PCS-1900), and 1950 MHz

Table 2. Measured SAR-values of the symmetrical folded dipole and the metal bezel (VII, published by permission of IEEE).

	898 MHz	1747 MHz	1880 MHz	1950 MHz
S_{11} (dB)				
SFD	-9.7	-10.6	-7.9	-6.1
MB_1	-6.9	-10.6	-6.2	-5.8
MB_2	-12.5	-6.7	-6.9	-6.2
SAR in W/kg over 10 g of averaged mass				
SFD	1.2	0.17	0.10	0.68
MB_1	1.01	0.15	0.27	0.45
MB_2	0.95	0.16	0.29	0.92
SAR in W/kg over 1 g of averaged mass				
SFD	1.86	0.29	0.19	1.38
MB_1	1.6	0.28	0.59	0.77
MB_2	1.42	0.29	0.61	1.94
TX Power	31.9 dBm	27.8 dBm	27.8 dBm	24.0 dBm
Phantom medium				
	$\sigma = 0.96(\Omega m)^{-1}$	$\sigma = 1.36(\Omega m)^{-1}$	$\sigma = 1.4(\Omega m)^{-1}$	$\sigma = 1.4(\Omega m)^{-1}$
	$\varepsilon = 41.8$	$\varepsilon = 41.1$	$\varepsilon = 40.2$	$\varepsilon = 40.2$
	$\rho = 1000 kg/m^3$	$\rho = 1000 kg/m^3$	$\rho = 1000 kg/m^3$	$\rho = 1000 kg/m^3$

(UMTS) in Table 2 with the corresponding S_{11}. The center frequencies are chosen, so that they are in the middle of the studied mobile standard uplink. The TX-powers presented in Table 2 are digitally modulated continuous powers of the mobile standards transmitted to the antenna under test.

The IEEE C95.1 - 2005 standard [171], which is used in Europe, Japan, and Korea, defines the SAR-limit to be 2 W/kg over 10 g of averaged mass. The 47FRC2.1093 [172] standard limit (Australia, Canada, New Zealand, U.S.) is 1.6 W/kg over 1 g of averaged mass. The lower limit of 47FRC2.1093 is stricter, because it is volume-averaged over a smaller amount of tissue.

The ground plane distance in the measurements from the head phantom is 5 mm as proposed in [171], corresponding to the height of the metal bezel, and the upper edge of the ground plane is 10 mm from the centre of the ear (see a cross in Fig. 38(a)).

MB_1 means that the Y-direction of metal bezel is toward the phantom, and in MB_2, the Y-direction is outwards from the phantom. The measured S_{11} changes, compared to the free space, when the antenna is taken close to the measurement phantom, and, thus, it is also presented in Table 2 for comparison. It can be noticed how, especially at 898 MHz, the matching is improved due to the vicinity of the phantom.

As can be noticed, the measured SAR-values satisfy the IEEE C95.1 - 2005 standard well, whereas the value exceeds the 47FRC2.1093 standard with SFD at 898 MHz and MB_2 at 1950 MHz. This is due to slightly directive radiation patterns, and can be seen in the direction of $+90^\circ$ (SFD) and -90° (MB_2) in the XY- and YZ-planes (towards the head). The SAR-values well correlates with the PIFA results in [173], where the distance of the ground plane from head phantom was also 5 mm.

Since the SAR-values are exceeding the 47FRC2.1093 standard at a few frequencies, this must be taken into account when designing mobile phone terminals for end users to keep the SAR-values within the acceptable limits. With the measured antenna structures, this can be done by implementing the antenna so that the radiation is outwards from the user's head. As the metal bezel antenna structure is closer to a real application, it means that the bezel itself, as a directive element, can be placed outward from the head to reduce radiation towards the head.

Fig. 41 shows the measured *S*-parameters of the studied antenna structures related to the free space measurement. In the figure, a down shift in the frequency can be observed at 1 GHz resonance with both antennas, caused by the capacitive loading of the head phantom. MB_2 is the most sensitive for the head phantom in terms of impedance matching, since the bezel is against the head and, thus, the antenna structure is closer to the head. At the higher frequencies, the matching with the metal bezel gets slightly poorer, when, with SFD, the matching gets better or stays the same. Still, the impedance matching is below -6 dB.

When considering narrow band antennas, the frequency shift might arise as a problem when it decreases the matching and needs a tuning system to get the resonance back at the central frequency [174]. As the results propose, when considering wideband antennas, the frequency shift still remains, but it cannot be seen as harmful as compared to a narrow band antenna.

More about the user effects and its compensation methods can be found in the following dissertations [52, 53].

4.3.2 Chassis coupling with symmetrically excited patches

As discussed in the previous section with symmetrical feeding, the dissertation is focusing on finding wideband antenna structures defined in Table 1.

This section presents a chassis coupling antenna structure with multiple patch elements based on original paper [VIII]. The excitation is carried out by symmetrically

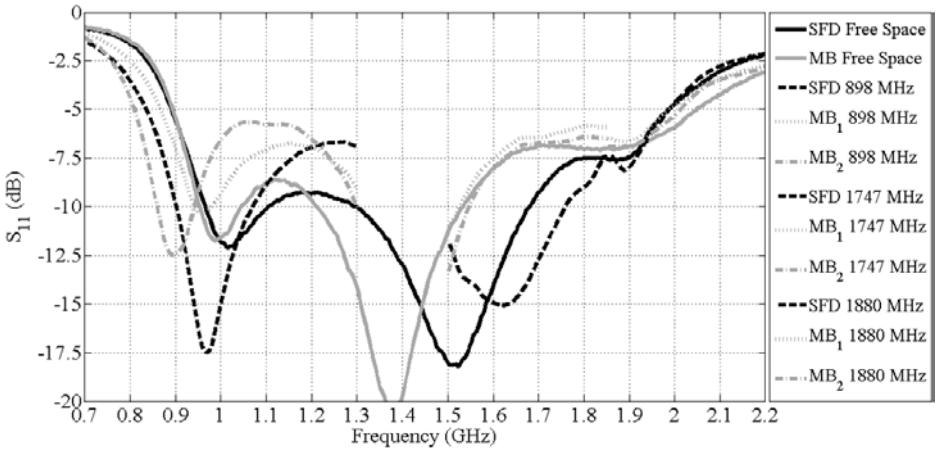

Fig 41. Measured S-parameters of the symmetrical folded dipole and its metal bezel extension in vicinity of head phantom, and in free space.

implemented and excited patch elements. The structure forces the surface currents to propagate along the mobile chassis by offering wide impedance bandwidth and good radiation properties. The excitation method supports the excitation of radiating mode, Mode 2, at wide frequency range.

The antenna structure, with symmetrically implemented patches, is presented in Fig. 42. The structure has a total of four patch elements where, at both ends of the mobile chassis, the pair of patches is excited symmetrically. The elements 1 and 2 have the same source, and the signal of the source is divided to both patches equally. The elements 3 and 4 are excited with the same principal. The symmetrical feeding in this case means that the pair of patch elements is excited with the same amplitude and phase. A 50 Ω transmission line is used to deliver the signal to the pair of patch elements.

Figure 43 presents the measured and simulated reflection coefficient of the patch elements 1 and 2 (S_{11}) with the isolation to the elements 3 and 4 (S_{21}). The measured -6 dB impedance bandwidth from 2.415 GHz to 3.535 GHz offers a 1.12 GHz bandwidth which corresponds to a 37.6% relative bandwidth. At the same time, the measured isolation is less than -14 dB. It can be noticed the simulated *S*-parameters correspond well with the measured ones.

In Fig. 43, the measured total efficiency is also presented. At the -6 dB impedance bandwidth, the total efficiency is better than -3 dB (average -1.86 dB). This proves

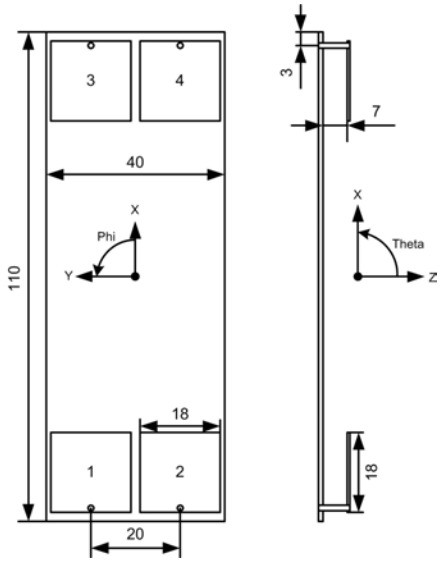

Fig 42. Symmetrically implemented multi-element antenna structure with coordinate system. Dimensions are in mm (VIII, published by permission of EurAAP).

that the antenna is radiating well at the whole bandwidth. To measure the antenna radiation characteristics, the commercial measurement system, Satimo StarLab, is used. The elements 1 and 2 are measured when the transmission line of the elements 3 and 4 is terminated with a 50 Ω load to avoid reflections in an open circuit. The radiation patterns are measured with the same method.

In Fig. 44, the measured radiation patterns at 2.45 GHz and 3.55 GHz are presented. The maximum total gain is 0.6 dBi and 4.0 dBi at the related frequencies. For both frequencies, the maximum can be found in the XZ-plane. One can notice asymmetrical radiation behaviour in the XY- and YZ-planes at both frequencies. This is caused by the absorbing material which is used to cover the 50 Ω termination to avoid reflections. For the very same reason, the total efficiency and radiation patterns are slightly poorer since part of the radiated power is absorbed. The absorbing material is located to the position of $\phi = -90^\circ$ in the XY-plane and $\theta = -90^\circ$ in the YZ-plane.

Surface current distributions of the symmetrically excited patches 1 and 2 are presented in Fig. 45. The frequencies are the same as in Fig. 44, where the radiation patterns are presented. The figures shows how the currents are propagating vertically along the chassis. The direction of the surface currents explains the radiation patterns

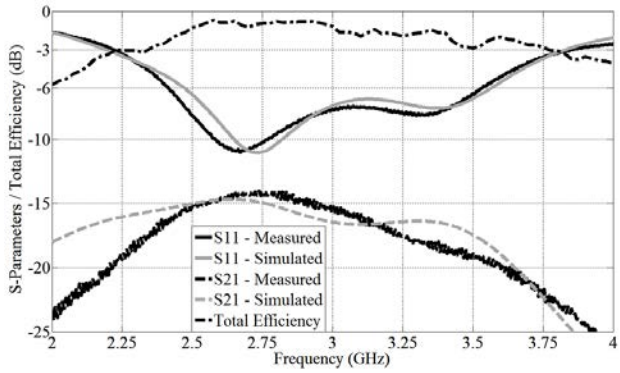

Fig 43. Measured and simulated frequency responses of the studied antenna structure. In the same plot, the measured total efficiency is presented as a function of frequency. S_{11} represents the reflection coefficient of the symmetrical feeding for patches 1 and 2. S_{21} represents the isolation between patches 1 and 2 and patches 3 and 4 (VIII, published by permission of EurAAP).

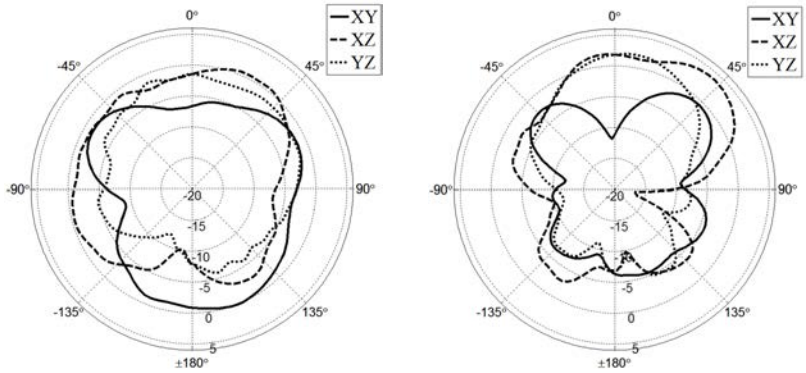

Fig 44. Measured radiation patterns of the symmetrically excited patches 1 and 2 at (a) 2.45 GHz with 0.6 dBi maximum gain, and (b) 3.55 GHz with 4.0 dBi maximum gain. The radiation patterns represent the total gain in dBi (VIII, published by permission of EurAAP).

well. The radiation is symmetrical in the XY- and YZ-planes as expected. Whereas, the directive radiation in the XZ-plane, in angle between 0–45°, is caused by the

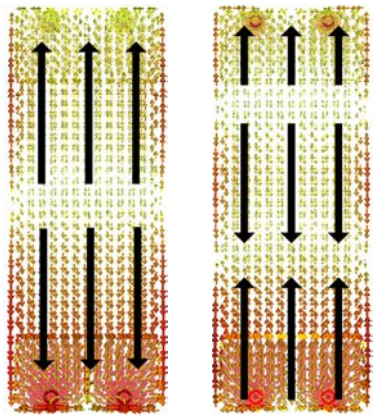

(a) (b)

Fig 45. Simulated surface currents distributions at (a) 2.45 GHz and (b) 3.55 GHz (modified from VIII, published by permission of EurAAP).

asymmetrical placing of the patches related to the ground plane. The current modes at both frequencies correspond well with Mode 2 in Fig. 9(c), even the though second zero appears at 3.55 GHz.

When comparing the results to papers [28, 75, 76], where higher order modes are studied on a mobile ground plane in, it can be concluded it is a difficult task. The simulated relative -6 dB impedance bandwidths of the structures for Mode 2 are 8, 6.5, and 40%, respectively. The antenna structure in this section presents 37.6% relative bandwidth for Mode 2. The relative -6 dB bandwidth (40%) of the excited Mode 2 in [76], corresponds well with the antenna structure presented in this section.

On the other hand, the simulated total efficiency of Mode 2 in [28] is -0.8 dB (83%) at 2.5 GHz. For comparison, the presented antenna structure has a maximum total efficiency of -0.73 (84%) at 2.55 GHz, and minimum -3 dB (50%) at 2.415 GHz, with average -1.86 dB (65.6%).

It can be concluded the antenna structure has slightly lower average total efficiency over the -6 dB bandwidth than defined in objectives, which was -1 dB (80%). The total efficiency can be still considered good because it is much better than the defined minimum total efficiency, which was -3 dB (50%). Results also well correlates with the referred paper. Also, the relative -6 dB impedance bandwidth ($> 30\%$) is exceeded.

With the proposed antenna structure, Bluetooth (2.4 GHz) 2.45 GHz WLAN, 3.5 GHz WiMAX, and LTE band (2496–3600 MHz), can be covered.

4.4 Diversity in mobile applications

This section describes the basics of the diversity used in wireless communications. Wireless system operates via the transmission of electromagnetic waves. Various propagation effects, such as reflections of electromagnetic waves from the wall, occur depending on the environment. Various means by which the wave reaches the receiver are referred to as propagation paths. Usually, the signal arriving at a receiver is a combination of many components arriving from various directions as a result of multipath propagation. Transmission systems suffer from multipath, because the wave coming from different directions at different times interfere, causing the received signal power to fluctuate randomly as a function of distance. This causes signal distortion called fading [10].

In such a condition, any communication scheme will likely suffer from errors. A solution to improve the performance is to ensure that the information symbols pass through multiple independent signal paths. This ensures that a reliable communication is possible for as long as one of the paths is strong. The technique is called diversity and it can dramatically improve the performance over a fading radio channel.

There are many ways to achieve independently fading channels. Diversity over time can be obtained via coding and interleaving. This means that the information is coded and the coded symbols are dispersed over time in different coherent periods, so that different parts of the codewords experience independent fading. Analogously, diversity can be exploited over frequency in so far as the channel is frequency selective. In a channel with multiple transmit or receive antennas that are spaced sufficiently far enough, diversity can also be obtained over space. In general, since diversity is an important resource, a wireless system typically uses several types of diversity [175].

When in a radio channel where 1 transmit antenna and 2 or more receiving antennas are used, the channel is called SIMO (single-input-multiple-output), as shown in Fig. 46(a). The receiver diversity combines independent fading paths associated with multiple receive antennas to obtain resultant signal. The combining process can be done in several ways which vary in complexity and overall performance. Most of the combining techniques are linear, which means that the output of the combiner is a weighted sum of the different fading paths or receiving branches [175–177].

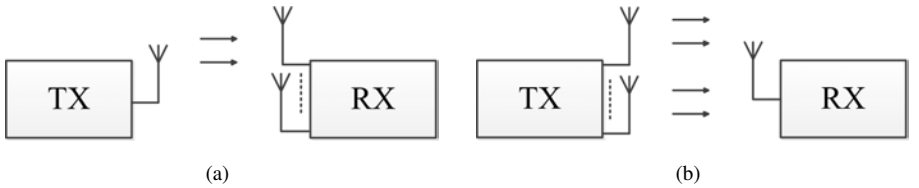

Fig 46. Principal of (a) SIMO and (b) MISO radio channel models.

When considering transmit diversity, multiple antennas are used in the transmitter end of the radio channel and one antenna to receive. The radio channel is called MISO (multiple-input-single-output) and is shown in Fig. 46(b). This is commonly used in the downlink of a cellular system, since it is often easier to have multiple antennas at the base station than in a mobile handset.

It is easy to achieve a diversity gain by simply transmitting the same symbol over different antennas during different symbol times. At any time, only one antenna is turned on when the rest are silent. This is called a repetition code. It only uses one antenna at a time and transmits the coded symbols of the time diversity code successfully over the different antennas by providing coding gain over repeated codes [175].

The diversity performance is measured with diversity gain, and can be shown as a decibels value of equivalent signal-to-noise ratio. The diversity gain depends on the number of branches, the signal combination algorithm, and the mutual statistics of the signals between the branches. In good diversity performance, the mean powers of the branches should be similar and the fading nature of the branches should be mutually uncorrelated. If the branch mean powers are too different, then the more-powerful branch dominates and there is a corresponding decrease in the diversity gain. Similarly, as the branch mutual correlation increases, the diversity gain reduces relative to the uncorrelated case. There is a small reduction in the diversity gain as a long correlation is reasonably low, and uncorrelated branches are often taken to be envelope correlation coefficient values less than 0.7 [50].

In this section, the diversity techniques studied in the original papers are presented. Space, polarization, and radiation pattern diversity techniques are discussed.

4.5 Space diversity

Space diversity, or antenna/spatial diversity, can be obtained by placing multiple antennas at the transmitter and/or the receiver [177]. If the antennas are placed sufficiently far apart, the channel gains between different antenna pairs fade more or less independently, and, thus, independent signal paths are created.

The required antenna separation depends on the local scattering environment, as well as on the carrier frequency. For a mobile which is near to the ground with many scatterers around, the channel de-correlates over shorter spatial distances, and a typical antenna separation d of half to one carrier wavelength is sufficient [178] (Fig. 47(a)). For base stations on high towers, a larger antenna separation of several to 10's of wavelengths may be required.

The use of space transmitting or receiving antennas is a very common way to achieve diversity. In its simplest form, a single transmitting antenna beam radiates a certain amount of the scattering or reflecting medium. Viewed from the receiver side, radiated energy has an angular spread, which is a function of the transmitting beamwidth, the distance from each terminal to the radiated energy, and the direction of scattering or reflection.

The energy carrying rays arriving at the receiving point appear to radiate over some angular spread. The additional stochastic nature of a medium will cause observations at the receiving point to indicate an apparent variation in an angle of arrival for an incident radiation, within this angular spread [177].

4.5.1 Space diversity with closely spaced antennas in low mutual coupling

Mutual coupling is a well known effect in multi-element antennas and antenna arrays, in both receive and transmit modes. The effect becomes more critical when the inter-element spacing of antenna elements is reduced. This kind of situation can occur in mobile communications, especially in mobile phones, where limitations in space become an important variable.

Mutual coupling is a phenomenon that distorts the behaviour of radiating elements by another antenna element(s). Every antenna element affects every other element by radiating through the air or by propagating surface currents through a ground plane.

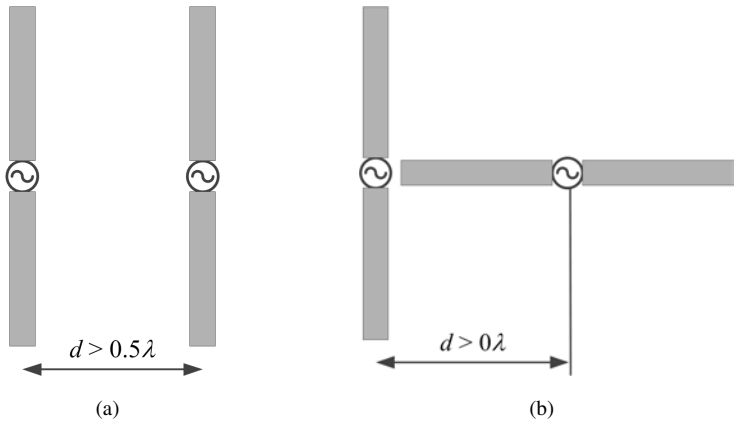

Fig 47. Principal of (a) space diversity and (b) polarization diversity.

Surface currents might cause a larger problem, especially when antenna elements are closely packed.

The calculation of mutual coupling in a two antenna system is presented in [179]. In the calculation of mutual coupling in the transmission mode, an excitation source is placed at the feed of one antenna element, while the other antenna element is terminated to a matched load. Mutual coupling is then calculated by

$$C_{tr} = \frac{P_L}{P_D}, \tag{23}$$

where P_D is the power radiated by the excited antenna, and P_L is the power delivered to the load of the unexcited antenna. The measured S-parameters between the two antennas are related to the transmission mode coupling calculation by

$$C_{tr} = \frac{|S_{21}|^2}{1-|S_{11}|^2}. \tag{24}$$

Mutual coupling modifies the phase and distribution on each antenna element of the included current. As a result, antenna gain, beamwidth, pattern, resonance frequency, and input impedance are affected. Analytical studies with half wavelength dipoles have shown that mutual coupling decrease proportional to $1/d^2$ as the distance d increases in wavelengths between the antenna elements [9]. This implies that mutual coupling will also depend on the frequency.

The effect of mutual coupling on spatial diversity and multiple input-multiple output (MIMO) systems can be desirable, depending upon the antenna configuration and the

environment. For example, in a poor scattering environment, mutual coupling decreases the correlation between individual antennas by generating dissimilar antenna element patterns, which leads to radiation pattern diversity [180]. However, the mutual coupling is an unwanted phenomenon in most of the cases, like in antenna arrays, spatial diversity and MIMO systems.

In [181], a reduction in mutual coupling was studied using a simulated quarter-wavelength slot between two compactly-spaced monopole antennas on a printed circuit board (PCB). By using a 13.5 mm slot between the antennas, the mutual coupling can be reduced by approximately 6 dB at a center frequency of 3.5 GHz, when compared to the reference arrangement without the quarter-wavelength slot. By using the slot, the diversity characteristics could be improved, in terms of total efficiency, by 20% for each antenna element. The correlation coefficient and diversity gain were also improved.

A microstrip filter using defected ground structures (DGS) has slots in a ground plane that are perpendicular to the wave propagation direction, disturbing the current distribution in the ground plane and having a resonant behaviour. DGS is able to provide a bandstop filtering effect due to the combination of inductance and capacitance [182]. In [183], the simulated DGS structure between patch antennas is used to reduce mutual coupling by 18 dB at a 6 GHz center frequency, when compared to a conventional ground plane, and still keep the radiation characteristics of an antenna.

The slotted ground plane in [184, 185] has been used to reduce the mutual coupling effect in closely spaced antenna elements. With this kind of slit arrangement, a very compact structure can be achieved and the antennas will retain good radiation characteristics. The structure is measured with 0.093λ spaced monopole antennas and a 16 dB reduction in mutual coupling is achieved over the reference ground plane at a 2.53 GHz center frequency.

Electromagnetic band gap (EBG), where a periodical structure is placed between the antenna elements, is used to achieve low mutual coupling between antenna elements in [186, 187]. In these two EBG references, the mutual coupling improvement at the resonant frequencies was between 8–13 dB.

As discussed in the objectives, the isolation between the antenna elements must be better than 18 dB for MIMO/diversity systems. At the same time, the relative -6 dB impedance bandwidth should be better than 30%. In next sections, methods to reduce mutual coupling between closely spaced antenna elements are presented with wide frequency band and low mutual coupling.

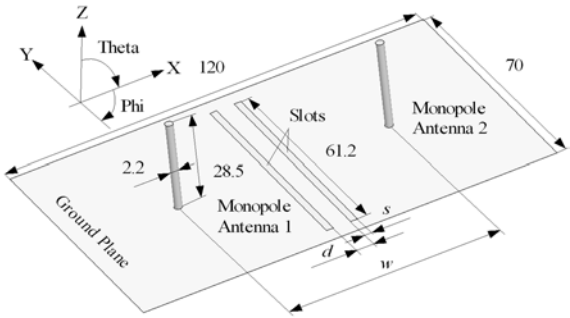

Fig 48. Studied monopole array with two $\lambda/2$ slots to reduce mutual coupling (IV, published by permission of IEEE).

Mutual coupling reduction by using two $\lambda/2$ slots between monopole antennas

This section presents a mutual coupling reduction between monopole antenna by using two $\lambda/2$ slots. The structure was originally presented in [IV]. The studied ground plane structure is shown in Fig. 48. It consists of a pair of slots, each half a wavelength long at 2.45 GHz, of width s and slot separation d. The slots are cut through the ground plane and are air-insulated. The thickness of the ground plane was 1.5 mm. The length and diameter of the monopole antennas used in this study were designed to match a 50Ω transmission line. The antennas were quarter-wavelength monopoles at 2.45 GHz. Different cases were tested in [IV] to understand the phenomenon of mutual coupling and its relationship to radiation characteristics, as only the best results are presented here.

Figure 49(a) shows the measured and simulated S-parameters with measured mutual coupling against frequency for the reference ground plane and ground plane with slots with $w = 0.5\lambda$ antenna spacing at 2.45 GHz. The measured mutual coupling is calculated from S_{11} and S_{21} measurements by using (24). HFSS was used in the simulations.

The measured -10 dB impedance bandwidth is 15% with a 2.45 GHz center frequency, and the mutual coupling across the impedance bandwidth is approximately -15 dB for the reference ground plane. For comparison, in Fig. 49(a), the measured and simulated S-parameters with the measured mutual coupling for a ground plane containing two half-wavelength slots, with $s = 0.8$ mm slot width, and $d = 6.25$ mm slot separation. Mutual coupling between the antenna elements is significantly reduced

within the same impedance bandwidth. At the aforementioned bandwidth, the mutual coupling is between $-42.0 \ldots -15.6$ dB, where the lowest mutual coupling of -42.0 dB is achieved at 2.493 GHz. This is a 27 dB improvement over the reference structure without slots. S_{11} at 2.5 GHz is naturally improved as the mutual coupling is reduced.

Figure 49(b) shows the measured and simulated *S*-parameters with a measured mutual coupling against frequency for the reference ground plane with antenna $w = 0.173\lambda$ spacing at 2.45 GHz. As expected, the measured -10 dB impedance bandwidth is very poor when the antennas are closely packed, only 1.96% of the 2.45 GHz center frequency. This means that the mutual coupling is considerably more than -10 dB across the bandwidth, approximately -7 dB. When comparing the results to the ground plane structure with the same slot dimensions as in the $w = 0.5\lambda$ antenna separation (Fig. 49(a)), the measured mutual coupling against frequency shows a major improvement between the antenna elements. The measured impedance bandwidth improved significantly: 37.8% at the 2.45 GHz center frequency. Mutual coupling within the impedance bandwidth was between $-50 \ldots -13.7$ dB. The lowest -50.0 dB mutual coupling was achieved at 2.55 GHz, which corresponds to a 43 dB improvement, compared with the reference.

The far-field radiation pattern measurements in four different cases are presented in Fig. 50, in terms of total gain. For comparison, the slot dimensions *s* and *d* are the same as in the case to study impedance matching. In the reference with an antenna spacing of $w = 0.5\lambda$ in Fig. 50(a), the radiation pattern is asymmetrical only in the XZ plane. Monopole 2 is asymmetrically implemented related to the ground plane center and, thus, effects the radiation properties in the asymmetric sense. Figure 50(b) also presents radiation patterns of $w = 0.5\lambda$, antenna spacing with the $\lambda/2$ slots. The same kind of behaviour can be observed as in the reference case, except now, the currents in the +X-direction on the ground plane have a directive behaviour in the XZ plane, in the direction of $+45^\circ$. Different current distributions over the slots are creating a deeper null in the direction of -135°.

Figure 50(b) presents the radiation properties of the reference ground plane with an antenna spacing of $w = 0.173\lambda$. One can observe that when the measured Monopole 2 is implemented closer to the centre of the ground plane, the radiation patterns in all of the planes are now more symmetrical compared to the reference case with an antenna spacing of $\lambda/2$.

When it comes to the structure with antenna spacing with the $\lambda/2$ slots in Fig. 50(b), major changes can be seen in the XZ plane. More similar current distributions

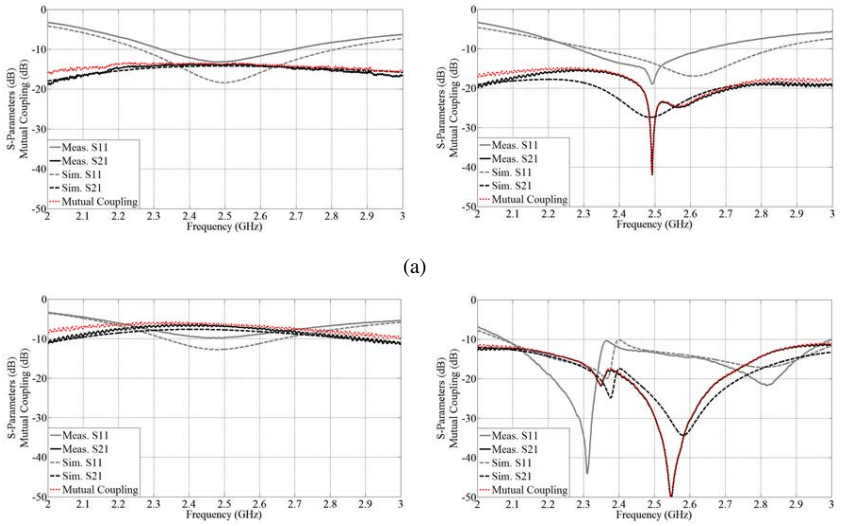

(a)

(b)

Fig 49. Measured and simulated S-parameters with measured mutual coupling of the reference structure (on left) and structure with two $\lambda/2$ slots (on right). Monopole separation *w* (a) 0.5λ, and (b) 0.173λ at 2.45 GHz (IV, published by permission of IEEE).

of the slots create deeper nulls in the directions of -15° and $+120^\circ$. The directive radiation in the direction of $+45^\circ$ is caused by the surface currents in the ground plane, as was presented in $w = 0.5\lambda$ case. Still, in the XZ plane, one can see leakage of the radiating field passing through the slots under the ground plane. This is explained by the asymmetric current distributions over the slots; the slot closer to Monopole 2 has a stronger current than the slot closer to Monopole 1.

In Fig. 51, the simulated surface current distributions at 2.45 GHz over the reference ground plane and the ground plane with two slots with the same s and d, and with antenna spacing 0.5λ in Fig. 51(a), and 0.173λ in Fig. 51(b), are presented. Thus, the figures correspond to the measured radiation patterns.

Comparisons of the figures show that the half-wavelength slot traps a large proportion of the surface currents. The pictures prove how effectively the structure with two slots reduces mutual coupling in the studied case. It is also notable that the currents around the slots represents a transmission line mode shown in Fig. 8(b), and, thus, they do not

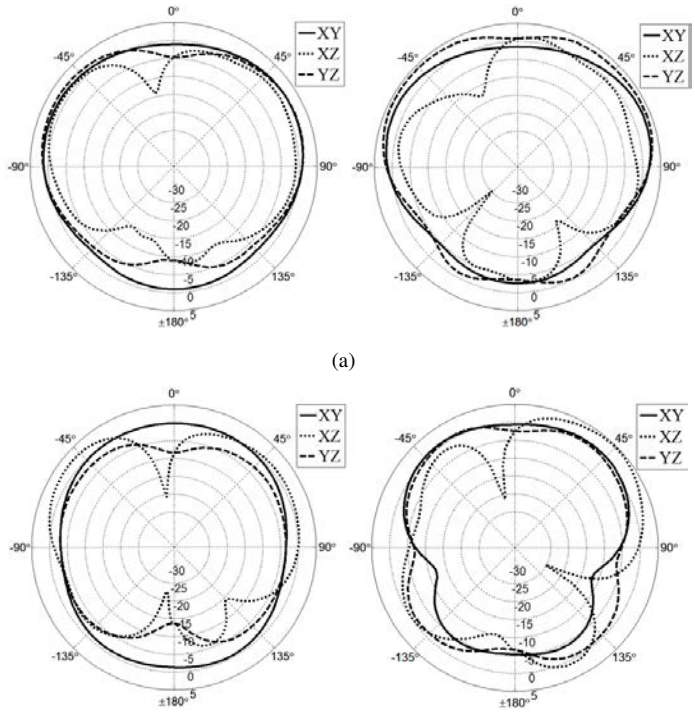

Fig 50. Measured radiation patterns of reference structure (on the left) and structure with two $\lambda/2$ slots (on right) at 2.45 GHz. Monopole separation (a) 0.5λ, and (b) 0.173λ at 2.45 GHz (IV, published by permission of IEEE).

represent significant radiation. CST Microwave Studio was used to simulate the surface current distributions.

The improved characteristics of low mutual coupling can be seen to depend on two different mechanisms that affect the surface currents. First, at both ends of the slots, the surface currents are cancelled because of a half-wavelength phase difference, and this can be seen as a downward peak in mutual coupling. Second, the propagation direction of the surface currents on both sides of the $\lambda/2$ slot is opposite, as can be seen in the vector presentations in Fig. 51. This has the effect of mutually cancelling the electromagnetic fields on both sides of the slots.

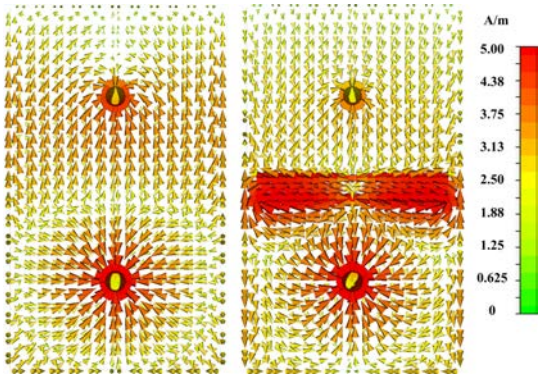

(a)

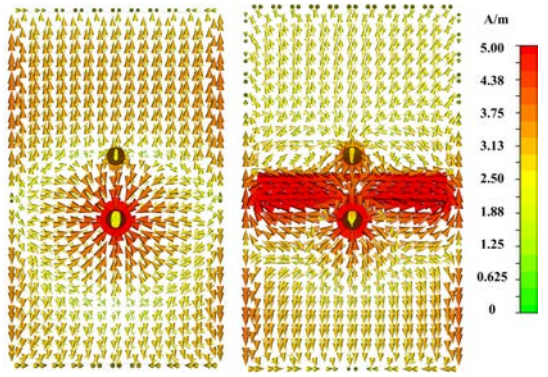

(b)

Fig 51. Simulated surface current distributions of the reference structure (on the left) and a structure with two $\lambda/2$ slots (on the right) at 2.45 GHz. Monopole separation (a) 0.5λ, and (b) 0.173λ at 2.45 GHz.

The results were showing that by using two slots between monopoles, the mutual coupling can be reduced when, at the same time the impedance matching and bandwidth can be improved. When comparing the results in [184], where slits were used to reduce mutual coupling between two monopoles, the relative -6 dB bandwidth of the slitted structure is 41% against 46% achieved with the $\lambda/2$ slot structure. Still, the achieved -10 dB relative impedance bandwidth is much larger with the $\lambda/2$ slot structure, meaning 36% against 27% for slitted structure.

On the other hand, the mutual coupling smaller than −18 dB is achieved with both structures in terms of relative frequency bandwidth, which with both structures are around 2.5 GHz center frequency. For the $\lambda/2$ slot structure it is 16%, and slitted structure 8%. However, the slitted structure is more compact when comparing the $\lambda/2$ slot structure.

When comparing the results to the objectives, it can be concluded the $\lambda/2$ slot structure has better than 30% relative −6 dB impedance bandwidth and, on the other hand, the mutual coupling was smaller than −18 dB around the center frequency.

Mutual coupling reduction by optimizing the dimensions of a patch antenna structure

Another approach to reduce mutual coupling is presented in [V], where the dimensions of two element patch arrays are optimized to gain good matching, when, at the same time, the antenna elements are in good isolation. The antenna structure, with two microstrip patch antennas, is presented with optimal dimensions to achieve good matching and low mutual coupling at the studied 5.8 GHz center frequency. The structure itself is very simple and only includes the two patches on an individual substrate, both air-insulated from the ground plane. CST Microwave Studio is used in the simulations.

The two microstrip patch antenna structure, with the selected coordinate system, is presented in Fig. 52. Both of the patches are matched to a 50 Ω transmission line with SMA-connectors, and no external matching circuit is used. The matching to 50 Ω is done by adding the center of the coaxial feed 2 mm away from the edge of the microstrip patch. The coaxial feeds of the patches have an approximately $\lambda/2$ separation at 5.8 GHz.

Parameter W represents the width of the ground plane in the studied structure and equals 120 mm. Parameter L = 70 mm is the length of the ground plane. The size of the ground plane is the same as used in [IV], and the size of a smart phone ground plane simulated in [X]. As shown in the original paper [V], the characteristics of the antenna structure are more dependent on the interaction between patch elements than dimensions of the ground plane.

The patches are made of Rogers RO4003 RF-laminate with a dielectric constant of ε_r = 3.38, and the laminate has a copper patch, printed only on the upper side. The patches are air-insulated from the aluminium ground plane, and the total height of the patches is 5.5 mm.

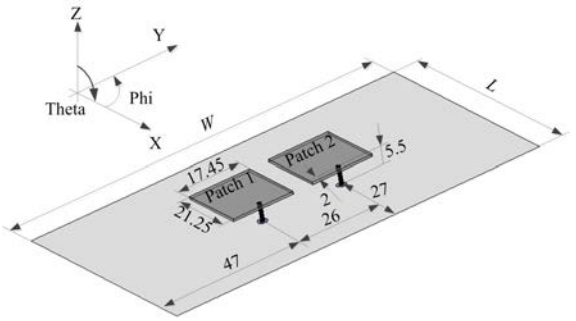

Fig 52. Optimized patch array structure to reduce mutual coupling (V, published by permission of VDE Verlag).

The simulated and measured *S*-parameters are presented in Fig. 53. The mutual coupling itself was calculated from the measured *S*-parameters by using (24). It can be seen that the measured -10 dB impedance bandwidth of the two microstrip patch antennas is 640 MHz. This equals an 11.7% bandwidth related to the 5.8 GHz center frequency. The measured mutual coupling in the same bandwidth is less than -21 dB. The bandwidth when the mutual coupling is less than -20 dB is 950 MHz, corresponding to a 16.4% relative bandwidth. The measured S_{11} of the two patch antennas at the 5.8 GHz center frequency is -23.7 dB, when the mutual coupling is -27 dB. Mutual coupling is slightly increased at both ends of the studied bandwidth, and this is basically caused by the poorer matching of the antennas.

Figure 54 presents the measured radiation patterns in the XY, XZ, and YZ cuts in Theta and Phi planes. The measurements were done by terminating Patch 1 with a 50 Ω load, when the radiation properties of Patch 2 were measured. The maximum gain of 10.9 dBi at the 5.8 GHz center frequency is found in the YZ cut and in the Phi plane. It can be observed that the radiation pattern is more directive in the direction of +20° in the YZ plane, where the maximum gain is found, as well. This directivity is caused by suppressed surface currents between the patches, which attenuate the surface currents on the ground plane in the direction of $-90°$. In the XZ cut and Theta plane, a zero is observed in the radiation pattern in the direction of $-50°$, caused by the surface currents propagating in opposite directions in the patch element and the ground plane.

As studied in the original paper [V], the ground plane width or length does not dramatically affect the antenna matching or mutual coupling performance. This is

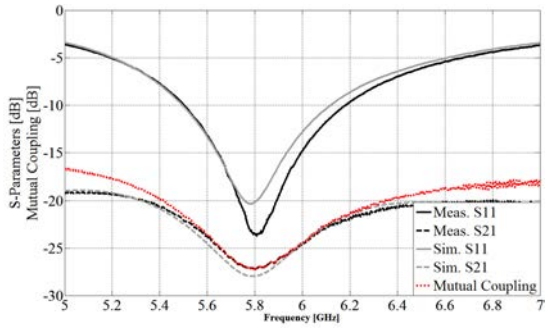

Fig 53. Measured and simulated S-parameters with measured mutual coupling of the optimized patch array structure to reduce mutual coupling (V, published by permission of VDE Verlag).

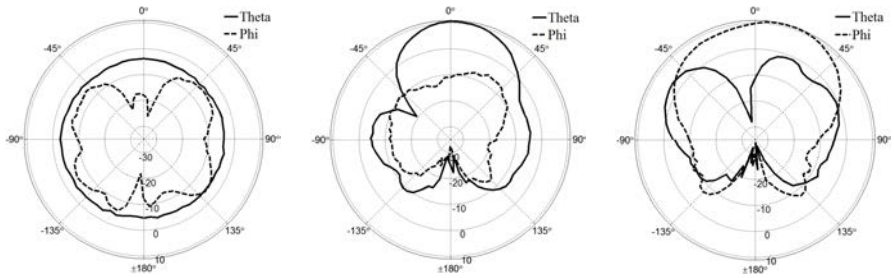

(a) XY (b) XZ (c) YZ

Fig 54. Measured radiation patterns at 5.8 GHz of the patch antennas in low mutual coupling (V, published by permission of VDE Verlag).

because the patches are mutually in resonance and, thus, the size of the ground plane does not play a major role in the performance.

In [184], the slitted ground plane was used to reduce mutual coupling between two adjacent patch elements. The results were showing 4.7% relative -6 dB bandwidth against 21.6% of the optimized patch structure in this section. Additionally, the mutual coupling was less than -20 dB over the operating bandwidth, whereas in [184] mutual coupling was less than -16 dB.

When comparing the results to the objectives in Table 1, it can be concluded that the patch structure with optimized dimensions has much better relative impedance

bandwidth than 10% and, on the other hand, the mutual coupling better than −18 dB over the −6 dB impedance bandwidth.

However, the relative −6 dB impedance bandwidth defined in objectives (>30%) was not achieved. The 21.6% relative −6 dB impedance bandwidth of the patch structure is still good as they are relatively narrow band structures with 0.5–5% bandwith [54]. The improvement in bandwidth is due the fact that the structure has a bigger volume compared to patch antennas in general as they are planar.

4.6 Polarization diversity

Polarization diversity implies a single polarization at the transmitter, with depolarization in the propagation medium. Independent reception is possible with two orthogonal polarizations, and the two resulting signals do not fade in a correlated manner. Polarization diversity is particularly attractive in mobile applications because of the limited space available, whereas the antenna separation d can be very small, even zero (Fig. 47(b)). An analysis of the effects is more complex given in the large angular spread and the mutual interaction between antenna elements and a human body [83]. For the designing of an antenna system for polarization diversity, antenna elements can have identical radiation patterns, but orthogonal polarizations [50].

In mobile radio environments, signals transmitted on orthogonal polarizations exhibit low fade correlation and, therefore, offer the potential for diversity combining. Polarization diversity can be obtained either by explicit or implicit techniques. Note that with polarization, only two branches are available as compared to space diversity, where several branches can be obtained by using multiple antennas. In explicit polarization diversity, the signal is transmitted and received in two orthogonal polarizations, as shown in Fig. 47(b).

With mobile phones, it can be held at random orientations during a call. This results in energy being launched with varying polarizations angles from the vertical to the horizontal. This further increases the advantage of cross-polarization antennas at the base station, since the two antennas can be combined to match the received signal polarization. This makes polarization diversity even more attractive. Finally, it is notable that cross-polarization antennas can be deployed in a compact antenna assembly and do not need a large physical separation as required in space diversity antennas. This is an important advantage where low profile antennas are needed [178].

In mobile terminals, the space becomes limited for multiple antenna configurations. Moreover, the trend for mobile terminals nowadays is to increase the number of operating frequency bands, hence, covering different wireless applications. One way to reduce the number of elements when covering different wireless standards is to use wideband [188, 189] or multi-band antennas as discussed in the introduction of Section 3.4. Therefore, structures with broadband behaviour may represent a very appealing solution for a multi-standard device. Polarization diversity antennas for mobile terminals are presented in [190, 191], being both relatively narrow bands. According to the author's best knowledge, wideband polarization diversity antennas for mobile terminals are not widely presented in the literature.

4.6.1 Wideband polarization diversity antenna for mobile terminals

In the mobile handset, the limited space with more than two antennas is a difficult implement. In addition, the mobile terminal device miniaturization, making the spacing between multi-antenna elements decreases, and the mutual coupling between antenna elements affects the diversity system performance. On the other hand, the diversity system should cover multiple radio interfaces at wide frequency range. Objectives for antenna structures can be found in Table 1.

This section presents wideband planar antenna with polarization diversity for mobile terminals based on [IX]. The antenna consists of two orthogonally oriented planar notch QCAs (QCA 1 and QCA 2), presented earlier in Fig. 19(a). The antennas are located at separate ends of a mobile ground plane. The geometry of the antenna structure, together with its dimensions, is presented in Fig. 55(a). The thickness of the ground plane is 0.8 mm.

A prototype antenna structure is presented in Fig. 55(b). The wideband tapered microstripline balun, used to excite the QCAs, is presented in Fig. 15(b). The feeding of the prototype antenna has been optimized by simulations, taking into account the relative dielectric constant of the substrate (ε = 2.2) used in the balun and the dipole. In addition, the slot length has been optimized to match the increased electric length of the dipole (compare with Fig. 19(a)) affected by the substrate and the thickness of the ground plane.

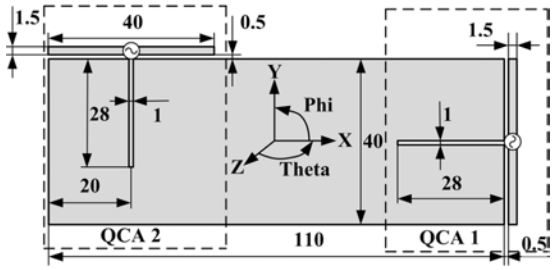

(a)

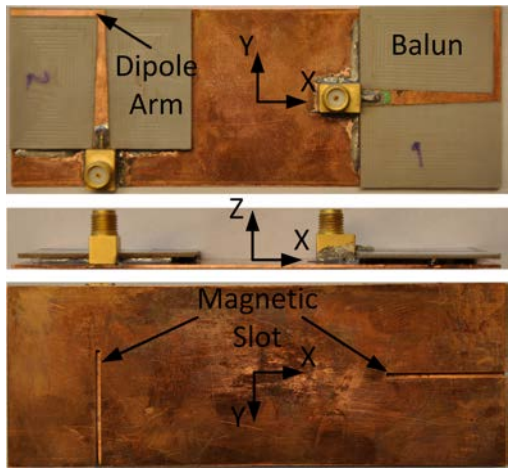

(b)

Fig 55. (a) layout and (b) prototype of the wideband diversity antenna with two QCA antennas for mobile terminals (IX, published by permission of IEEE).

In Fig. 56, the measured S-parameters and the total efficiency of QCA 1 and QCA 2 are presented. As observed, both antennas have an approximate a -6 dB impedance bandwidth that ranges from 1.8 to 4.6 GHz, corresponding to a 87.5% relative bandwidth. This correlates well with the numerical results presented in Fig. 20(c). At the same time, the measured S_{21} at the operating bandwidth is less than -18 dB. The shift in the center frequency, compared to the simulated results in Fig. 3, is caused by the increased electric length of the dipole and the slot.

Furthermore, the measured total efficiency for both antennas is between -3.5 and -0.3 dB (average -0.95 dB) within the studied -6 dB impedance bandwidth. The total

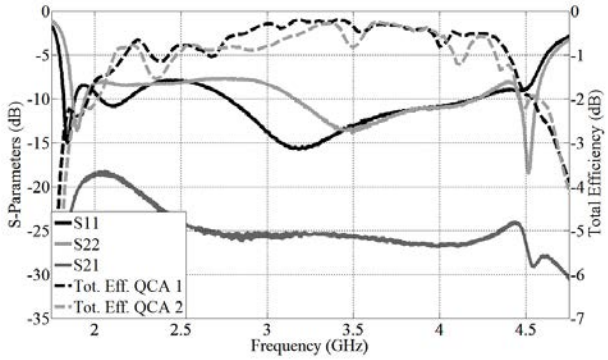

Fig 56. Measured *S*-parameters and the total efficiency of the QCA 1 and QCA 2 elements (IX, published by permission of IEEE).

efficiency is measured by terminating the passive antenna element with a standard 50 Ω load.

The measured radiation patterns of the prototype antenna at 2 and 4 GHz are presented in Fig. 57. The magnitude of the electric field (in decibels) for both antennas is presented with Phi and Theta components. The method to measure radiation patterns is the same as that which is used with the total efficiency. The maximum field, depending on the cut, the frequency, and the measured antenna, is between 0.1 and 4.5 dB. It can be noted that the amplitude of the radiated field varies between the cuts at the two measured frequencies.

In general, when in one polarization, the difference in amplitude is good, the other one has more equal components, and vice versa. As only two center frequencies are compared here, in Section 4.9, the diversity antenna performance in terms of envelope correlation and effective diversity gain within the whole operating bandwidth are presented.

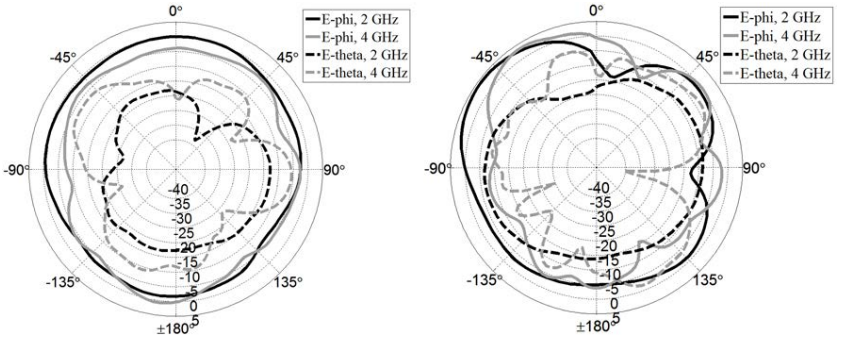

(a)

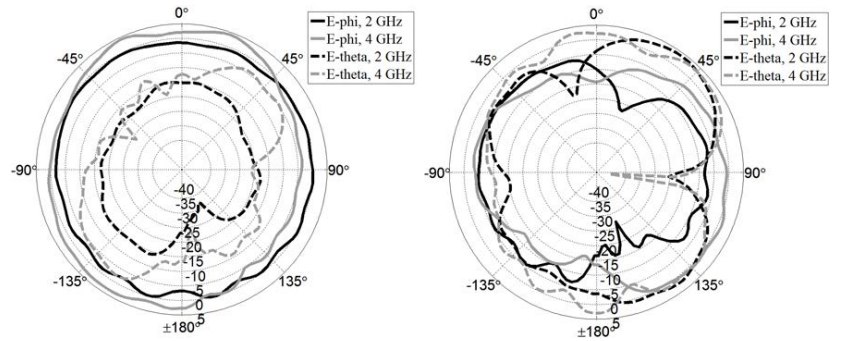

(b)

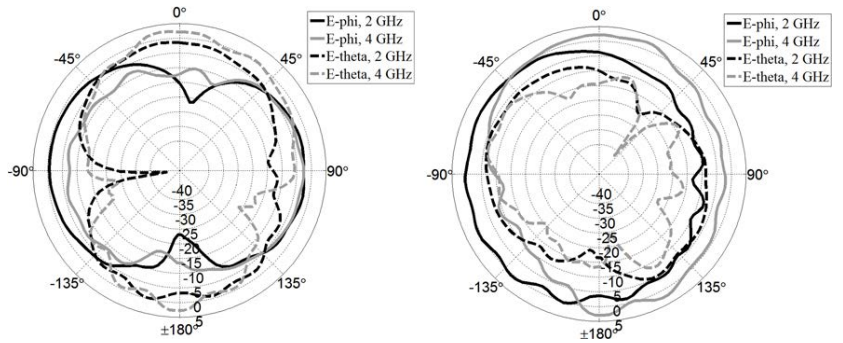

(c)

Fig 57. Measured radiation patterns (in decibels) for Phi and Theta components at 2 and 4 GHz in (a) XY cut, (b) XZ cut, and (c) YZ cut. The left patterns present the radiation properties of the QCA 1 and the right one, QCA 2. (IX, published by permission of IEEE).

Polarization diversity antenna for mobile terminals is presented in [190]. The structure offers 29% relative −6 dB impedance bandwidth against 87.5% of the structure presented in this section. The measured isolation between antennas with orthogonal polarizations in this section was better than 18 dB compared to [190], where maximum isolation was better than 15 dB.

The computed result of the antenna structure in [191] showed maximum total efficiencies −0.25 dB (94.4%), −0.98 dB (79.8%), and −0.67 dB (86.1%), depending on feeding mechanism. The antenna structure presented in this section showed −0.95 dB (80.4%) averaged total efficiency, and was from −3.5 to −0.3 dB over the operating bandwidth.

It can be concluded that the polarization diversity antenna for mobile terminals well satisfied the goals defined in objectives related to the −6 dB impedance bandwidth (> 30%), isolation (> 18 dB), and maximum total efficiency at most −1 dB.

The lower limit of the total efficiency was slightly below the definition −3 dB (> 50%), but the average total efficiency was −0.95 dB, which is better than the defined maximum total efficiency of a wideband antenna −1 dB (< 80%).

With the proposed antenna structure, UMTS (2.1 GHz), DVB-SH S-band (2170–2200 MHz), Bluetooth (2.4 GHz), WLAN (2.45 GHz), LTE (1.8–3.8 GHz), and WiMAX (2.3–3.6 GHz) can be covered.

4.7 Radiation pattern diversity

A fading dip is created when multipath components, which usually come from different directions, interfere destructively. If some of these waves are attenuated or eliminated, the location of the fading dips changes. In other words, two co-located antennas with different radiation patterns see differently weighted multipath components, so that the multipath components interfere differently for the two antennas. This is the principal of radiation pattern diversity. Radiation pattern diversity is usually used in conjunction with spatial diversity; it enhances the decorrelation of signals at closely spaced antennas. Different antenna patterns can be achieved easily by using different types of antennas. But, even identical antennas can have different patterns when mounted close to each other. This effect is due to mutual coupling between the antenna elements [192].

Directional antennas provide radiation pattern diversity by restricting the receive antenna beamwidth to a given angle. If the angle is very small then, at most, one of the multipath rays will fall within the receive beamwidth, so there is no multipath

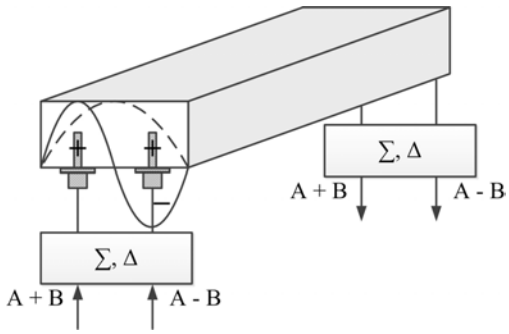

Fig 58. Rectangular waveguide excited with TE_{10} (*dashed line*) and TE_{20} (*solid line*) modes. When excitation polarizations are positive in the (Σ) mode, TE_{10} is excited. When opposite excitation polarizations (Δ), mode TE_{20} is excited. At the end of the waveguide, the opposite signal processing is performed to receive the signal.

fading from multiple rays. However, this diversity technique requires either a sufficient number of directional antennas to span all the possible directions of arrival or a single antenna whose directivity can be steered to the angle of arrival of one of the multipath components. Note also that with this technique, the SNR may decrease due to the loss of multipath components that fall outside the received antenna beamwidth, unless the directional gain of the antenna is sufficiently large to compensate for this lost power [176].

This section discusses the basics of the radiation pattern diversity gained by exciting higher order modes. In a radiation pattern diversity, one antenna element, such as a ground plane of a portable device, can be excited with orthogonal modes. The concept was first presented in the mid 60's within a rectangular waveguide [193]. In the waveguide, the fundamental mode (TE_{10}) and a higher order mode (TE_{20}) are excited as shown in Fig. 58.

Consider the waveguide as a radio channel, with one end representing a transmitter and the other one, a receiver. The Σ represents an excitation with the same amplitude and phase, whereas the Δ represents an excitation where the other probe is in an opposite phase. As both orthogonal modes are excited at the same time at a certain frequency, e.g., at the cut-off frequency of a higher order mode (TE_{20}), the modes can deliver the same or different information through individual channels.

To extend the modes in a rectangular waveguide to modes in a free space, where the free space is called a spherical waveguide [15], radiating modes are operating as a part of a radio channel with different angle of arrival. These modes are comparable to a multi-antenna system in such a way, that, e.g., the principal of the polarization diversity presented in Fig. 47(b), the vertical polarization represents radiating Mode 2 in Fig. 59, whereas the horizontal polarization represents an orthogonal radiating mode, Mode 3, in Fig. 59.

When extending the idea to an N-element antenna array with space diversity, the N orthogonal modes corresponds with the amount of N antenna elements in an array to achieve the same capacity. The difference is that the space needed for a diversity system become more compact by using orthogonal modes, and, thus, is more suitable for mobile applications.

Fig. 59 shows spherical modes with excitations, comparable to ones in a waveguide. Notice how the orthogonal modes respond differently to the LOS (Line-of-Sight) component as to the reflected signal components in a radio channel. Figure 60(b) shows a situation where the LOS component is blocked, but reflected signals in a radio channel can be received by a diversity receiver. This mode corresponds to the spherical modes TM_{01} or TE_{01}, and it is referred to as Mode 2 in Fig. 9(c).

The second mode in Fig. 59(b) receives the LOS component of a radio channel. This mode corresponds to the spherical modes TM_{11} or TE_{11}, and it is referred to as Mode 3 in Fig. 9(d), or it can be referred as Mode 4 in Fig. 60(c). The mode is orthogonal to Mode 2 [194].

As both of the modes are orthogonal, it is easy to receive reflected signals from a different direction with one mode and an LOS component with the other mode. An intelligent receiving/transmitting diversity system can excite several orthogonal modes at the same time or choose a few modes to fit best to a current radio channel conditions.

4.7.1 Radiation pattern diversity with characteristic currents on mobile ground plane

According to the spherical mode theory, it is possible to excite higher order spherical modes when using larger antenna aperture size [18]. In most of the published cases, the fundamental mode of the mobile chassis is excited, which is based on studies presented in [24]. However, the excitation of the higher order modes is not widely studied in the

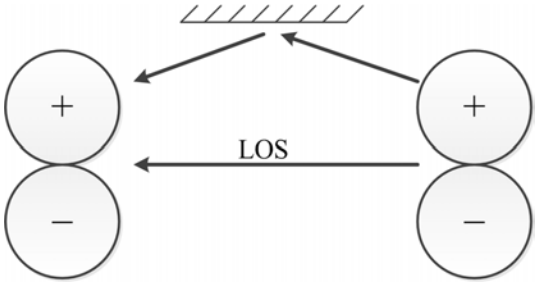

(a) Mode 2, TM_{01}, TE_{01}

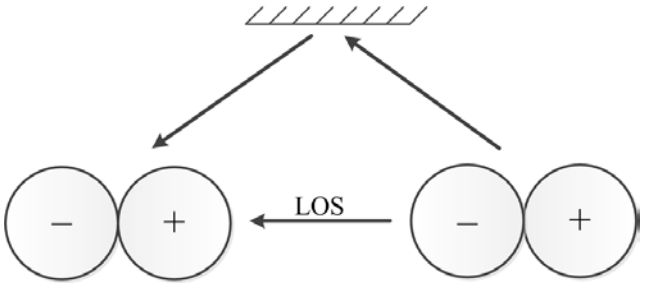

(b) Mode 3, TM_{11}, TE_{11}

Fig 59. Principal of radiation pattern diversity: (a) the LOS component is blocked, but the reflected signals are received, and (b) where the LOS is received and the reflected is neglected. Both of the presented modes are orthogonal to each other to gain radiation pattern diversity.

literature. In this section, orthogonal higher order current modes on a small mobile ground plane are presented, and these modes are compared to the orthogonal radiating modes which are supporting the radiation pattern diversity.

To present the radiation pattern diversity with the characteristic currents based on [I], 8 dipoles are used above a conducting ground plane of a mobile device, as shown in Fig. 66. In Fig. 60, the same fundamental modes can be found as in Fig. 59. Note that the radiation is directive because the excitation dipoles are only on one side of the ground plane. The envelope correlation between different radiated modes in a mobile ground plane can be found in Tables 4 and 5, in Section 4.9.

Additionally, the radiation pattern diversity can be gained with the structure presented in [VI]. There are two different ways to use the excitation; one is symmetrical, as

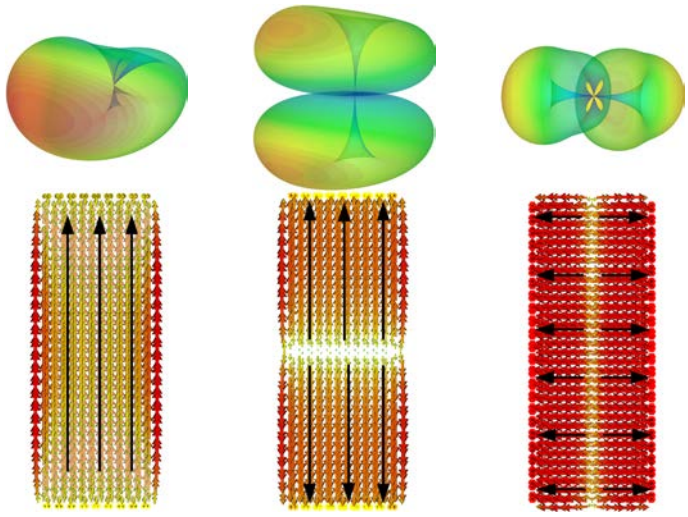

(a) Mode 1 (b) Mode 2 (c) Mode 4

Fig 60. Orthogonal modes in a mobile ground plane excited with 8 elevated dipoles.

described in 4.3, and the other one is asymmetrical feeding. Asymmetrical feeding means that both ports have the same amplitude, but they are in the opposite phase. As can be seen, different excitation supports different modes.

The currents around the ground plane in Fig. 61(b) at 2 GHz create 4 current zeroes for every corner of the ground plane. Notice that this mode is a higher order mode, Mode J_4, presented in Fig. 30. When comparing these currents to Fig. 61(a), it can be observed that the simulated modes are orthogonal, corresponding to a very low envelope correlation, approximately 10^{-6}. However, as only two excitation elements are used here, it limits the amount of the excited modes to two at a studied center frequency.

The radiation pattern diversity in mobile terminals is presented in [76, 195–198], where multiple antenna element configurations are studied to generate orthogonal radiation patterns. A proposal to excite 8 slots to gain orthogonal modes in a mobile ground plane can be found in [75], whereas in [199], a concept for the selective excitation of different characteristic modes on a mobile terminal chassis is presented. [200] presents both approaches with capacitive and inductive coupling to excite ground plane modes. Additionally, [33] presents a study of a loop antenna with four sources, which are excited

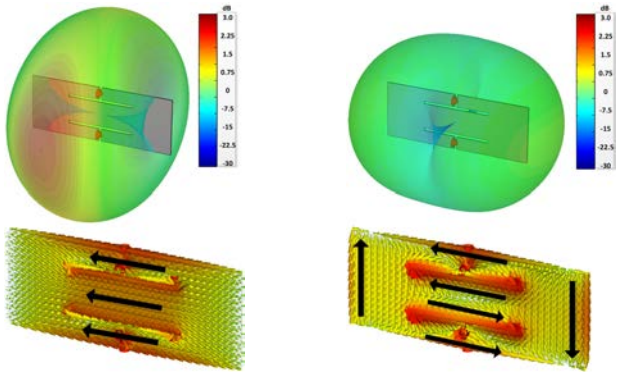

(a) (b)

Fig 61. Simulated orthogonal radiation patterns with surface current distributions of symmetrical folded dipole at 2 GHz with ports (a) symmetrically excited and (b) asymmetrically excited. The envelope correlation between the radiation patterns is 10^{-6}. The scale is in realized gain.

in different phases to gain orthogonal radiating modes. For comparison, these papers are presenting only an excitation of three or four radiating current modes.

It was shown, that excitation of higher order modes with multiple excitation elements, it is possible to achieve orthogonal radiation patterns. As here only 3 modes were shown with excitation by using 8 dipoles, the rest are compared in terms of envelope correlation in Section 4.9. The idea of orthogonal radiating modes is to propose a solution for radiation pattern diversity within a small space, as the size of a mobile terminal is limited.

4.8 MIMO systems

MIMO (Multiple-Input-Multiple-Output) system is presented in Fig. 62, which employs multiple transmit and multiple receive antenna elements, substantially improve the data rates that can be transmitted over the channel and the reliability which they can be received without any additional bandwidth. Higher data rates are achieved by transmitting multiple data streams simultaneously using spatial multiplexing techniques. Increased reliability is achieved by exploiting spatial diversity to significantly reduce the probability that the channel is in a deep fade. While MIMO systems perform

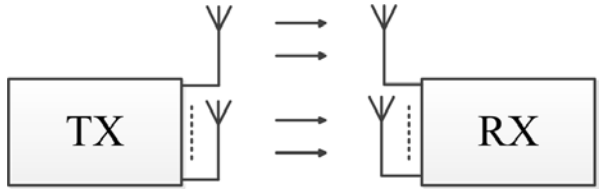

Fig 62. Principal of MIMO radio channel model.

impressively, they also increase the hardware and signal processing complexity, power consumption, and component size in the transmitter and receiver. This increase in complexity has reduced the widespread adoption of MIMO systems.

As an example, one solution to reduce the complexity of a MIMO system is to use antenna selection. It reduces the hardware complexity of a transmitter and receiver by using fewer RF-chains than the number of the antenna element [201].

4.8.1 MIMO diversity and multiplexing

In diversity MIMO, a number of transmitting antenna replicas of the same data stream are transmitted by using different orthogonal channelization codes, but the same scrambling code. Each transmitting antenna uses different channelization codes so that the base station can separate the signals from different antennas and combine them later by using maximal ratio combining. Thus, the scheme doubles the usage of uplink channelization codes when compared to single antenna transmission [201]. This scheme is also referred to as MIMO beamforming. Beamforming provides diversity gain through the coherent combining of the multiple signal paths.

Channel knowledge at the receiver is typically assumed, since this is required for coherent combining. The diversity gain then depends on whether or not the channel is known at the transmitter. When the channel matrix is known, the received SNR is optimized by choosing the vector weights of the channel matrix. When the channel is unknown at the transmitter, the transmit antenna weights are all equal [176].

In the case of MIMO multiplexing, a composite data stream is multiplexed into two or more independent sub-streams that are transmitted from separate antennas by employing different scrambling codes. All of the streams contain different channelization and control codes, so that in the base station they can be interpreted as signals from different independent users [201].

4.8.2 Multi-element antennas and MIMO capacity

The global wireless system reliability and a growing demand for high spectrum efficiency have furthered recent achievements of diversity, smart antennas, and MIMO techniques. Therefore, integrated multi-element antenna arrangements are expected to become more common in the near future in the systems which exploit diversity. The optimization of those arrangements needs aspects of antenna element design, integration, and multi-element antenna design [8]. The integration of multiple antennas into a limited space raises the additional problem of mutual coupling interaction between antenna elements. Mutual coupling may have a significant effect in the MIMO channel capacity [202] and antenna efficiency [203].

The channel capacity is an important indicator to measure quality of a MIMO system. The capacity depends on many things, like the number of transmitting and receiving antennas and their spacing, the multipath environment, and how direction of angle of arrival is spread. Assuming a propagation scenario in which the incident field shows a uniform 3D random distribution, the envelope correlation can be obtained for two antenna system by using scattering parameters at wide frequency range, or then radiation patterns of individual antenna elements at a single frequency [54].

It has been shown that MIMO wireless system can provide increased capacity in rich multipath environment [204]. In MIMO systems, the minimum physical separation between antenna elements for an appropriate limit in correlation between the multitude of received signals is commonly referred to be $\lambda/2$. However, there is no minimum distance condition but rather a definition of the acceptable correlation level to insure the effectiveness of the MIMO system. The correlation level in [2] is defined to be 0.5 when maximum ratio combining is used for the received signal. For example, the distance can be very small, especially in adjacent antenna elements, which are using orthogonal polarization.

In a small mobile terminal, the number of antenna elements may range from two in a small handheld, to four in a personal digital assistant (PDA), and up to sixteen or more in a laptop computer [205]. In mobile or handheld communications, a two-antenna approach to diversity is quite common due to the limited space in a mobile terminal. Two diversity signals are received from two antennas, depending on the diversity techniques employed, and the two signals are combined to maximize the SNR ratio after signal combing.

Mobile wireless communication systems quite often have to operate in such areas as the inside and outside of buildings in a city environment where multipath propagation is a severe problem. Thus, the use of multiple antennas can provide some diversity in these situations, even on a small handset in areas where the signal strength is weak [79].

4.8.3 Antennas for mobile MIMO systems

MIMO systems take advantage of the spatial properties of the propagation channel. Therefore, in the evaluation of MIMO antennas, it is necessary to use a proper characterization of the spatial channel properties. In wireless systems using digital transmission, a multipath echo leads to a spreading of the received signal in time. Much of the signal energy can be recovered in the detection process, through the use of equalizers. Parameters, such as the angular spread of the waves impinging at the receiver, may have a significant influence on the MIMO system performance. The combination of sophisticated signal processing and multiple antennas leads to an adaptation of the MIMO system to the multipath radio channel. In propagation environments, where the MIMO system can be applied, the propagation situation changes rapidly. A meaningful comparison of MIMO antennas can only be drawn if the spatial properties of a realistic propagation channel have been taken into account [10].

Since the MIMO operates at a high level of complexity in order to take advantage of the radio channel space-time recourses, to understand the space-time characteristics of the channel is required to measure the potential performance of practical multi-element antenna link. MIMO terminal performance is a combination of antenna characteristics, signal propagation conditions, RF, baseband hardware, and software [10]. Therefore, they need to be well understood through some form of MIMO OTA test system. The conventional way of testing the antenna characteristics and the signal processing performance does not measure the MIMO device performance realistically.

Due to the fact that the antennas and the propagation channel interact in MIMO systems, the antenna configurations have to be chosen carefully. The antenna type, as well as the arrangement of the elements, strongly influences the performance. Goals are high antenna efficiency and a low correlation by exploiting various propagations paths. The problem arises when multiple antennas need to be integrated into small devices with limited antenna spacing [10]. The challenges for MIMO antenna designing for mobile terminals are discussed in [206].

Diversity and MIMO antennas for wireless devices have been the subject of much attention in the last decade [66, 72, 76, 207–210]. The trend towards mobile terminals nowadays is to increase the number of operating frequency bands, hence, covering different applications. Therefore, a MIMO structure with broadband behaviour represents a very appealing solution for a multi-standard device. Additionally, all of the diversity methods and antennas presented in Section 4.4 can also be employed in MIMO systems.

4.8.4 Wideband multi-element antenna for mobile MIMO systems

This section presents a wideband planar MIMO antenna for mobile terminals, based on original paper [X]. By adding the basic QCA antenna structure with a square slot, presented in Fig. 19(b), to the opposite ends of the ground plane of a mobile terminal as presented in Fig. 63(a), a wideband MIMO antenna structure with high isolation and low correlation can be created. Objectives for antenna structures can be found in Table 1.

The prototype MIMO antenna in Fig. 63(b) is fabricated with a wideband tapered microstripline balun. The relative dielectric constant of the substrate used in the balun is 2.2. The balun has been optimized by simulations, by taking into account the combined effect of the slot and the thickness of the ground plane. To find the best result in terms of larger -6 dB impedance bandwidth, the slot dimensions need to be modified. Thus, the slot length is longer now when compared with the slot in Fig. 19(b). The balun topology which is used is the same as presented in Fig. 15(b).

The simulated and measured S-parameters and the total efficiency of the prototype antenna are shown in Fig. 64. It can be observed that the measured relative -6 dB impedance bandwidth (S_{11}) is 95%, ranging from 2.0 to 5.6 GHz. The measured S_{21} at the same bandwidth is less than -19 dB. The results are well correlated with the numerical results that are presented in Fig. 20(c). The measured total efficiency is between -2.3 and -0.1 dB, having an average of -0.85 dB within the -6 dB impedance bandwidth. The total efficiency is measured by terminating the other antenna element with a standard 50 Ω load.

Figure 65 presents the measured radiation patterns of the QCA 2 element in terms of the total gain at 2 and 5 GHz. Radiation patterns have been measured the same way as the total efficiency. It can be observed that the antenna radiation patterns do not have deep nulls at both frequencies, which is desired in mobile applications.

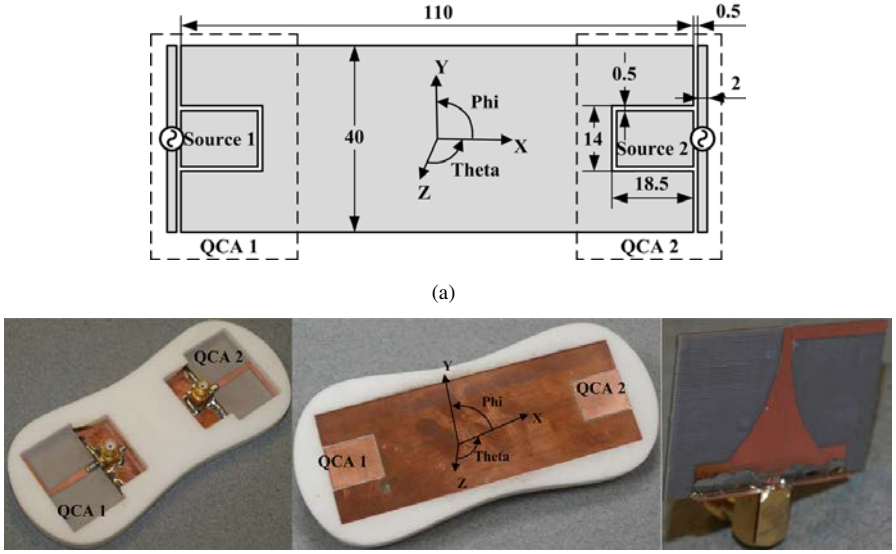

Fig 63. (a) layout and (b) prototype of the wideband MIMO antenna with two QCA antennas for mobile terminals (X, published by permission of IEEE).

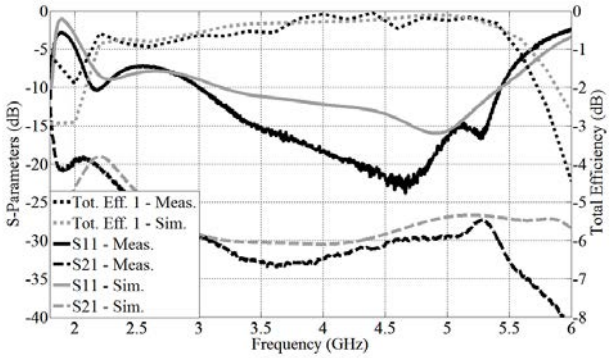

Fig 64. Measured and simulated *S*-parameters and the total efficiency of the QCA 1 and QCA 2 elements for MIMO (X, published by permission of IEEE).

Especially at 2 GHz, the radiation is almost isotropic, which agrees with the radiation of a complementary antenna. The maximum total gains are 2.8 dBi and 5.7 dBi at 2 GHz

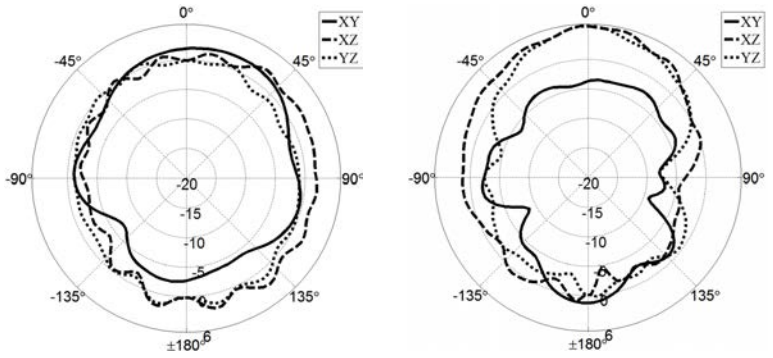

Fig 65. Measured radiation patterns (in dBi) of QCA 2 at (a) 2 GHz and (b) 5 GHz in terms of total gain (X, published by permission of IEEE).

and 5 GHz, respectively. Notice that, as the coordinate system is located in the middle of the antenna structure, the radiation patterns of QCA 1 are images for the QCA 2.

It can be mentioned at the end of the chapter that multi-element antennas presented in the previous sections with space, polarization, and radiation pattern diversity can also be used in an MIMO application because of the good isolation between antenna ports. Also, a compensation of mutual coupling between closely spaced antenna elements is very important to gain a low correlation and, thus, a good MIMO performance.

In [72] a wideband MIMO antenna with space diversity is presented. The antenna system has relative -6 dB impedance bandwidth of 93%, which correlates well with the antenna system presented in this section (95%). On the other hand, the mutual coupling is better than -19 dB over the operating frequency, as the antenna system in [72] presents maximum coupling better than -15 dB. At the same time, the measured average total efficiency is -0.85 dB (82%) from -2.3 dB to -0.1 dB within the -6 dB impedance bandwidth, whereas the antenna in [72] represents total efficiencies from -3.3 dB to -1.3 dB.

It can be concluded that the MIMO antenna for mobile terminals well satisfied the goals defined in objectives related to -6 dB impedance bandwidth better than 30%, isolation better than 18 dB, and the total efficiency at most -1 dB (80%) but slightly smaller than -3 dB (50%). Still, the average total efficiency was -0.85 dB, and it is better than the defined maximum total efficiency of a wideband antenna.

The antenna structure covers the UMTS (2.1 GHz), Bluetooth (2.4 GHz), WLAN (2.45 GHz), DVB-SH S-band (2170–2200 MHz), LTE (2.0–3.8 GHz), and WiMAX (2.3–5.4 GHz) standards.

4.9 Envelope correlation, effective diversity gain, and MIMO efficiency

Section 4.7.1 was discussing the excitation of orthogonal higher order current modes on mobile ground plane to achieve radiation pattern diversity at a single frequency by using multiple excitation elements. In this section the study is continued by calculating the envelope correlation between the excited radiation patterns. Objectives for antenna structures can be found in Table 1.

This section presents parameters enabling the study of envelope correlation, diversity, and MIMO performance in two antenna element systems. These parameters are an effective diversity gain (EDG) and a MIMO efficiency, which both use envelope correlation as a measure to investigate the system performance. All of these parameters can be calculated at a single frequency by using antenna radiation patterns, or in a wide frequency bandwidth by using *S*-parameters.

By using radiation patterns [2], the envelope correlation of two antenna systems can be calculated as follows

$$\rho_e = \frac{\left| \iint\limits_{4\pi} [\vec{F}_1(\theta,\phi) \bullet \vec{F}_2(\theta,\phi)] d\Omega \right|^2}{\iint\limits_{4\pi} \left| \vec{F}_1(\theta,\phi) \right|^2 d\Omega \iint\limits_{4\pi} \left| \vec{F}_1(\theta,\phi) \right|^2 d\Omega}, \tag{25}$$

where $\vec{F}_i(\theta,\phi)$ is the radiated field of the ith excited antenna element, $\bullet$ denotes the Hermitian product, and Ω is a solid angle over a sphere.

Table 3 presents the excitation polarization of the individual dipoles shown in Fig. 66. The size of the ground plane in Fig. 66 is 110 mm x 40 mm, the dipole separation in the vertical plane is 30 mm and in the horizontal plane, 20 mm, and the dipoles are located 10 mm above the ground plane. The multi-element structure can be used to excite orthogonal modes in the radiating ground plane. Each radiating mode, excited by 8 dipoles, can be considered to be one antenna. Later, in Table 4 and 5, the excited modes are compared correspondingly to a two antenna system, based on (25).

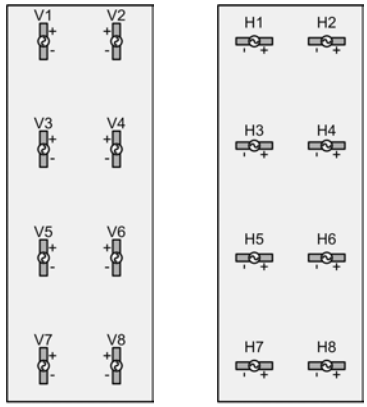

(a) (b)

Fig 66. Orientation of (a) the vertical (V) and (b) the horizontal (H) dipoles above a radiating ground plane (I, published by permission of EurAAP).

Configurations $\mathbf{E_{V1}}$, $\mathbf{E_{V2}}$, and $\mathbf{E_{V3}}$ represent the excitation polarizations for the vertical dipoles ($\mathbf{D_{V1} - D_{V8}}$), whereas, $\mathbf{E_{H1}}$, $\mathbf{E_{H2}}$, and $\mathbf{E_{H3}}$ represent the same configurations for the horizontal dipoles ($\mathbf{D_{H1} - D_{H8}}$). The amplitude value 1 represents a 0° phase shift, whereas -1 represents a 180° phase shift of the signal at the dipole feeding port. The sign of the amplitudes are related to the polarization ($\pm$) shown in Fig. 66.

Table 3. Excitation of the vertical (V) and horizontal (H) dipoles shown in Fig. 66 (I, published by permission of EurAAP).

Dipoles	$\mathbf{E_{V1}}$	$\mathbf{E_{V2}}$	$\mathbf{E_{V3}}$	$\mathbf{E_{H1}}$	$\mathbf{E_{H2}}$	$\mathbf{E_{H3}}$
$\mathbf{D_{V1}/D_{H1}}$	1	1	1	1	1	1
$\mathbf{D_{V2}/D_{H2}}$	-1	1	1	1	1	-1
$\mathbf{D_{V3}/D_{H3}}$	1	1	1	1	1	1
$\mathbf{D_{V4}/D_{H4}}$	-1	1	1	1	1	-1
$\mathbf{D_{V5}/D_{H5}}$	1	1	-1	-1	1	1
$\mathbf{D_{V6}/D_{H6}}$	-1	1	-1	-1	1	-1
$\mathbf{D_{V7}/D_{H7}}$	1	1	-1	-1	1	1
$\mathbf{D_{V8}/D_{H8}}$	-1	1	-1	-1	1	-1

Tables 4 and 5 presents envelope correlations at 2 GHz and 5 GHz with different antenna configurations studied in [I], and shown in Fig. 66. The corresponding excitations are shown in Table 3 with Phi and Theta polarizations. These antenna configurations correspond with different excited current modes on a conducting mobile ground plane. The envelope correlation calculations represents a radiation pattern diversity system presented in 4.7.1.

Table 4. Envelope correlation of Phi and Theta polarization at 2 GHz, between different 8 elevated dipole excitation configurations. The numbers above the diagonal represent the envelope correlation in Phi polarization, whereas, numbers below the diagonal present a correlation in the Theta polarization (I, published by permission of EurAAP).

Config.	$\mathbf{E_{V1}}$	$\mathbf{E_{V2}}$	$\mathbf{E_{V3}}$	$\mathbf{E_{H1}}$	$\mathbf{E_{H2}}$	$\mathbf{E_{H3}}$
$\mathbf{E_{V1}}$	1	$5.9 \cdot 10^{-7}$	$1.7 \cdot 10^{-7}$	0.95	$2.1 \cdot 10^{-7}$	$5.4 \cdot 10^{-7}$
$\mathbf{E_{V2}}$	$2.5 \cdot 10^{-7}$	1	$1.1 \cdot 10^{-7}$	$7.5 \cdot 10^{-7}$	$4.7 \cdot 10^{-7}$	$2.5 \cdot 10^{-6}$
$\mathbf{E_{V3}}$	$2.0 \cdot 10^{-7}$	$1.0 \cdot 10^{-6}$	1	$3.5 \cdot 10^{-7}$	$2.8 \cdot 10^{-7}$	0.73
$\mathbf{E_{H1}}$	$7.0 \cdot 10^{-2}$	$3.4 \cdot 10^{-7}$	$3.6 \cdot 10^{-7}$	1	$2.6 \cdot 10^{-7}$	$6.1 \cdot 10^{-7}$
$\mathbf{E_{H2}}$	$4.1 \cdot 10^{-7}$	$2.2 \cdot 10^{-7}$	$1.3 \cdot 10^{-7}$	$3.2 \cdot 10^{-6}$	1	$1.1 \cdot 10^{-6}$
$\mathbf{E_{H3}}$	$8.9 \cdot 10^{-7}$	$5.6 \cdot 10^{-7}$	0.53	$4.7 \cdot 10^{-7}$	$1.6 \cdot 10^{-6}$	1

Table 5. Envelope correlation of Phi and Theta polarization at 5 GHz between 8 different elevated dipole excitation configurations. The numbers above the diagonal represent the envelope correlation in Phi polarization, whereas, the numbers below the diagonal present a correlation in the Theta polarization (I, published by permission of EurAAP).

Config.	$\mathbf{E_{V1}}$	$\mathbf{E_{V2}}$	$\mathbf{E_{V3}}$	$\mathbf{E_{H1}}$	$\mathbf{E_{H2}}$	$\mathbf{E_{H3}}$
$\mathbf{E_{V1}}$	1	$6.2 \cdot 10^{-6}$	$1.6 \cdot 10^{-7}$	0.31	$4.2 \cdot 10^{-7}$	$4.1 \cdot 10^{-7}$
$\mathbf{E_{V2}}$	$5.3 \cdot 10^{-6}$	1	$4.9 \cdot 10^{-6}$	$3.4 \cdot 10^{-7}$	$1.8 \cdot 10^{-7}$	$2.3 \cdot 10^{-6}$
$\mathbf{E_{V3}}$	$1.5 \cdot 10^{-6}$	$4.7 \cdot 10^{-7}$	1	$1.6 \cdot 10^{-7}$	$2.1 \cdot 10^{-7}$	0.1
$\mathbf{E_{H1}}$	$1.9 \cdot 10^{-2}$	$1.0 \cdot 10^{-7}$	$8.8 \cdot 10^{-7}$	1	$3.6 \cdot 10^{-7}$	$8.6 \cdot 10^{-7}$
$\mathbf{E_{H2}}$	$3.4 \cdot 10^{-7}$	$2.5 \cdot 10^{-7}$	$7.8 \cdot 10^{-7}$	$4.7 \cdot 10^{-6}$	1	$2.2 \cdot 10^{-7}$
$\mathbf{E_{H3}}$	$7.3 \cdot 10^{-7}$	$3.2 \cdot 10^{-7}$	$4.5 \cdot 10^{-2}$	$8.7 \cdot 10^{-7}$	$6.6 \cdot 10^{-7}$	1

As in this dissertation, wideband antenna structures are discussed, the *S*-parameter representation is also an attractive approach. The envelope correlation in terms of the

S-parameters [61] can be studied with the following formulation

$$\rho_e = \frac{|S_{11}^* S_{12} + S_{21}^* S_{22}|^2}{(1-(|S_{11}|^2+|S_{21}|^2))\,(1-(|S_{22}|^2+|S_{12}|^2))}, \tag{26}$$

where $*$ is a complex conjugate, S_{11} and S_{22} represent an impedance matching of antenna 1 and 2, whereas S_{21} and S_{12} are the coupling between the two studied antenna systems. This formula assumes a uniformly distributed radio channel, meaning that the probability to receive a signal in any possible direction on a sphere is equal. Additionally, port 2 terminates with a 50 Ω load, when port 1 is excited, and the antenna system is assumed to be lossless [211].

As discussed in [211], ohmic losses must be very low to ensure good radiation efficiency. To gain such a condition, good matching and low mutual coupling are required to represent a lossless antenna system. In practice, when antenna systems always include losses, the accurate calculations for a lossy system can be found in [212]. The antenna systems in this chapter exhibit high total efficiency with good impedance matching and low mutual coupling, and the inaccuracy in the final results is assumed to be very small. Thus, the lossless envelope correlation (26) is used to calculate the EDG and MIMO efficiency.

The EDG is presented in (27), where low correlation and high radiation efficiency corresponds with good diversity properties. The diversity gain is calculated by using a selection combining criteria with maximum apparent diversity gain (10) at a 1% outage rage [177]. In the calculations, the relation between the complex cross correlation coefficient ρ and the envelope correlation coefficient ρ_e is $|\rho|^2 \approx |\rho_e|^2$ [177]. Finally, the EDG is calculated by multiplying the diversity gain with the radiation efficiency (η_{rad}) of the most efficient antenna element [213].

$$EDG = \eta_{rad} \cdot 10\sqrt{1-|\rho|^2}. \tag{27}$$

Notice that the radiation efficiency of an ideal antenna is 100%, and respectively the radiation patterns are orthogonal to each other. This corresponds to a diversity gain of 10.

Figure 67 presents measured effective diversity gain with corresponding envelope correlation of the polarization diversity antenna structure for mobile terminals presented in [IX]. As can be observed, the antenna system represents excellent diversity properties (>8.0) with a low envelope correlation (<0.01) over the -6 dB impedance bandwidth (1.8–4.6 GHz).

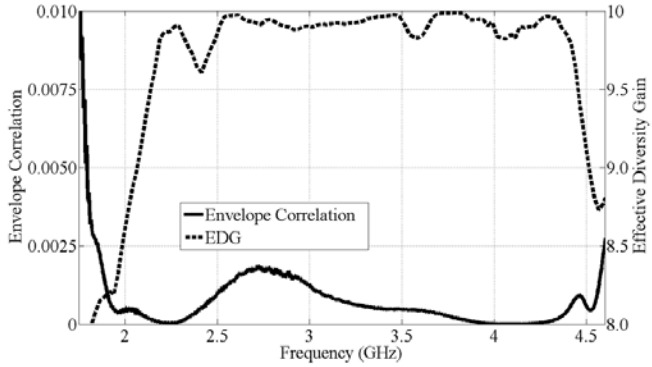

Fig 67. Effective diversity gain and the corresponding envelope correlation of antenna structure, introduced in [IX] (IX, published by permission of IEEE).

The envelope correlation is also needed when studying MIMO efficiency, which is also called MIMO multiplexing efficiency. MIMO efficiency is a measure of the additional SNR (Signal to Noise Ratio) required for a prototype antenna, or an antenna in a real application, to achieve the same capacity as an ideal antenna in an independent and identically distributed (i.i.d.) Rayleigh fading radio channel [64]. In (28), the MIMO efficiency is presented for a 2x2 MIMO system in good SNR condition

$$\eta_{MIMO} = \sqrt{\eta_{rad,1}\eta_{rad,2}(1-|\rho|^2)}, \tag{28}$$

where $\eta_{rad,1}$ and $\eta_{rad,2}$ are the radiation efficiencies of antenna element 1 and 2, respectively. In MIMO efficiency calculations, the relation between the complex cross correlation coefficient ρ and the envelope correlation coefficient ρ_e is the same as previously discussed with the EDG.

Figure 68 shows measured MIMO efficiency with a corresponding envelope correlation for a MIMO system for mobile applications presented in [X]. As in the EDG case, low correlation (<0.04) and good radiation properties leads to an excellent MIMO performance over the studied frequency bandwidth (2.0–5.6 GHz), with MIMO efficiency better than 0.9.

It was shown, that excitation of higher order modes with multiple excitation elements, it is possible to achieve a low correlation between the excited radiation patterns. Totally six orthogonal modes were excited and the radiation patterns were compared in terms of envelope correlation, originally presented in [I].

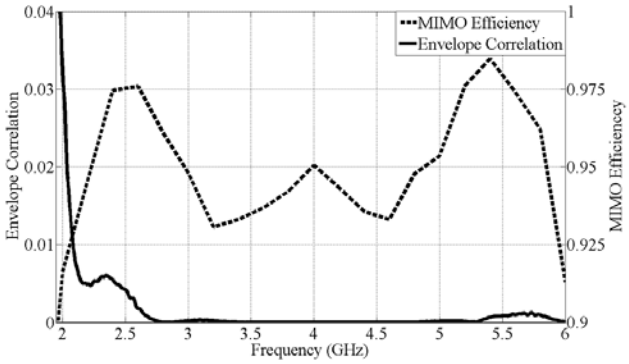

Fig 68. MIMO efficiency and the corresponding envelope correlation of antenna structure introduced in [X] (X, published by permission of IEEE).

By exciting higher order modes with eight short dipoles above a mobile ground plane, in 90% of the excited radiation patterns at 2 and 5 GHz center frequencies, the correlation was less than 0.2. The results correspond with good orthogonality between the excited radiating modes. The idea of orthogonal radiating modes is to propose a solution for radiation pattern diversity within a small space, as the size of a mobile terminal is limited.

When the polarization diversity antenna was studied in [IX], it presented excellent wideband antenna characteristics with good average total efficiency (-0.95 dB) and isolation between the antenna elements (> 18 dB). This led to a correlation smaller than 0.01 with EDG better that 8.0 over the operating frequency (1.8–4.6 GHz), which well satisfies the predefined goals in the objectives.

On the other hand, the MIMO antenna in [X] also presented excellent antenna characteristics over the operating frequency (2.0–5.6 GHz) with an average total efficiency of -0.85 dB, and the isolation between the antenna elements better than 19 dB. As the correlation was smaller than 0.04, with these values the MIMO efficiency was better than 0.9, and, thus, well satisfies the predefined goals in the objectives as well.

4.10 Summary

This chapter presented novel wideband multi-element antennas for mobile applications. By using two symmetrically excited folded dipoles, oriented as mirror images for each

other, it was shown how to create a magnetic boundary condition between these antenna elements and, at the same time, achieve a wide frequency bandwidth.

The correlation between the image theory and the characteristic modes theory, in terms of magnetic and electric boundary conditions, were presented. The image theory was also used to build a prototype antenna. By extending the symmetrical folded dipole to a more practical metal bezel structure, it was shown that the antenna performance is not disturbed. The symmetrical folded dipole and the metal bezel was also discussed in vicinity of a head phantom in terms of SAR-values and S_{11}-parameter.

Next, wideband diversity antennas were discussed and examples for space and polarization diversity techniques were presented. It was shown, by reducing mutual coupling between closely spaced antenna elements, a good isolation was achieved and, thus, antennas can be used in space diversity applications. Wideband polarization and MIMO antennas were presented by combining two quasi-complementary antennas at the opposite end of a mobile ground plane with good matching, isolation, and radiation properties.

The principal of radiation pattern diversity was presented. By exciting orthogonal higher order modes on a mobile ground plane with multiple antenna elements, it is possible to gain low correlation between the radiated modes.

And finally, parameters to study diversity and MIMO performances were presented to show the efficiency of the novel antenna structures presented in the chapter.

As a conclusion, by using symmetrical feeding, the excitation of higher order modes can be avoided. On the other hand, by using well isolated antenna elements, good correlation properties were achieved between the wideband antenna elements, closely spaced to a conducting ground plane. Also excitation of higher order current modes is possible with small antenna to achieve orthogonal radiation patterns in low correlation.

5 Summary of the contributed papers

[I] Small Radiating Ground Plane with Higher Order Modes

In the publication [I], a planar small rectangular radiating ground plane with an excitation study of orthogonal radiating modes is investigated. Eight short elevated dipoles were used to excite the modes in the ground plane with different excitation configurations. Instead of slots, the dipoles are used to couple energy to the ground plane to gain a better surface current performance. The paper shows that the spherical modes excited with the currents on a sphere presented in Section 2.1.4, which is a general case, can also be excited with a planar structure. The paper also presents radiating modes in a planar ground plane excited with the dipoles. The same excited modes can be found in Section 2.2 for comparison. The numerical results were the prediction of low correlation (< 0.2) with 90% of the studied cases corresponding good orthogonality between the modes. The configurations providing low envelope correlation are the ones that are used to gain pattern diversity. The presented approach has no practical solution and the purpose is only to show that it is possible to excite higher order modes on a small radiating ground plane.

[II] Optimized Dimensions of Ultra Wideband Quasi-Complementary Antenna with Switching Capability

In publication [II], quasi- and auto-complementary antennas were compared. By simulations, the structures were optimized to gain wide impedance matching (< -10 dB). After the optimization, the antennas were split in half as a monopole, and situated at the end of a mobile ground plane. With the optimized monopole structure, an impedance matching over the Ultra Wideband (UWB) frequency range (3.1–10.8 GHz) was achieved. The idea of using switches to cover lower frequencies was also presented. By using an open circuit to demonstrate RF-switches, the antenna frequency band was shifted down to around 950 MHz. At the lower frequencies, the antenna structure excites the fundamental radiating mode, Mode 1.

[III] Wideband Planar Slotted Radiating Ground Plane Antenna for Portable Devices

In publication [III], two monopoles for separate frequency ranges were used as coupling elements to excite surface currents in a planar radiating ground plane over a wide frequency range with a 65% relative -6 dB impedance bandwidth. A complementary slot was implemented into the ground plane as a matching element for both monopoles. By studying the surface currents, it can be noticed how both monopoles excite the fundamental radiating mode (Mode 1). The antenna operating principal is the same as in [IX, X], in terms of compensating for the imaginary part of the input impedance, except now, instead of a dipole, a monopole is used to excite the radiating mode. With the antenna structure, DVB-H, GSM, and UMTS standards, 2.45 GHz WLAN, and future LTE-bands can be covered. The main benefit of the antenna structure is a large effective area, so it provides good radiation properties over a wide frequency range.

[IV] Low Mutual Coupling Between Monopole Antennas by Using Two $\lambda/2$ Slots

In publication [IV], two half-wavelength slots cut into the ground plane were used between two monopole antennas to reduce mutual coupling. Low mutual coupling (< -18 dB) over a wide bandwidth was achieved with good radiation properties. The surface currents are propagating in the opposite direction on different sides of the slots, and, thus, mutually cancelling each other at a wide frequency bandwidth. Dramatic improvement was observed in the mutual coupling and the impedance matching. An interesting result was that the mutual coupling was reduced when the antenna spacing was reduced to less than a quarter of a wavelength, compared to the case where the antenna elements had a half-wavelength separation. Thus, by the antenna structure, an excellent diversity performance was gained with closely spaced antennas.

[V] Optimal Dimensions of Two Microstrip Patch Antennas for Low Mutual Coupling at 5.8 GHz

In publication [V], a microstrip patch antenna structure with optimum dimensions was presented. The structure is very simple and only includes the patches with no external matching circuit. Good impedance matching and mutual coupling (< -18 dB)

characteristics were achieved with good radiation properties and, thus, the antenna is suitable for space diversity applications. The simulated effect of the ground plane showed that the low mutual coupling and good impedance matching was only achieved by optimizing the patch dimensions. The principal of the mutual coupling cancelation is that the current path between the feeding points is half of the wavelength shorter than the signal propagating via the patch edges.

[VI] Creation of a Magnetic Boundary Condition in a Radiating Ground Plane to Excite Antenna Modes

In publication [VI], a planar rectangular radiating ground plane antenna with a symmetrical feeding was presented. The antenna consists of two folded dipoles which are planar and orientated as a mirror image. The dipoles are excited symmetrically with an equal amplitude and phase, which creates a magnetic boundary condition along the symmetry line between the folded dipoles. The structure is called a symmetrical folded dipole (SFD). Correctly designed symmetrical feeding counts the mutual coupling between the folded dipoles, and, thus, it can be exploited to improve the matching. The Theory of Characteristic Modes is used to identify the lowest order radiating mode (Mode 1) of the antenna, as discussed in 2.2. The antenna structure is considered to be a wideband multi-element antenna and it is designed to excite Mode 1 within a wide frequency bandwidth. The measurements showed 75% relative -6 dB impedance bandwidth. When using asymmetrical feeding (the amplitude of the sources is opposite) at the same time as a symmetrical one (sources have the same amplitude), it is possible to achieve a radiation pattern diversity, e.g., for a compact mobile MIMO system.

[VII] Performance Comparison of a Symmetrical Folded Dipole Antenna for Mobile Terminals and Its Metal Bezel Extension

In publication [VII], a performance of the symmetrical folded dipole and a metal bezel structure were compared. The metal bezel is extended in width and compared to the original SFD antenna structure presented in [VI]. The purpose of the paper is to show that it is possible to extended the ground plane and bend it's sides up by combining a mobile chassis and a bezel as one antenna element, without changing the antenna performance. Both antennas excite the fundamental mode, Mode 1. The measured

results show that the major difference between the antennas appears because of slightly different cascaded LC-baluns designs that are used as a feeding mechanism.

[VIII] Wideband Multi-element Mobile Terminal Antenna with Symmetrical Chassis Coupling

In publication [VIII], a multiple patch antenna structure was presented. In total, four patches were separated into pairs, where adjacent patches were fed symmetrically with the same amplitude and phase. The configuration was used to couple electromagnetic energy to the mobile chassis at a wide frequency bandwidth. The measurements showed 37.6% relative -6 dB impedance bandwidth. The feeding mechanism excites the radiating mode (Mode 3), presented in Section 2.2. Based on the radiation patterns, the structure offers radiation pattern diversity for MIMO or diversity systems to increase the reliability of the data transmission.

[IX] Planar Wideband Polarization Diversity Antenna for Mobile Terminals

In publication [IX], a planar wideband ground plane antenna is presented for mobile terminals. The antenna consists of two quasi-complementary antenna (QCA) elements located at both ends of a mobile ground plane to gain polarization diversity. One QCA element includes an electric dipole, closely spaced to a ground plane with a magnetic slot. The electric dipole and the magnetic slot compensate each other in terms of the imaginary part of input impedance. By using a dipole as a coupling element to couple energy to the radiating ground plane, the fundamental radiating mode (Mode 1) is excited. The antenna offers a diversity performance in terms of effective diversity gain (EDG) better than 8.0 over a wide frequency range. The antenna also provides excellent relative -6 dB impedance bandwidth (87.5%), low mutual coupling (< -18 dB), good radiation properties in terms of average total efficiency (-0.95 dB), and correlation smaller than 0.01 over the operating bandwidth.

[X] Improved Planar Wideband Antenna Element and Its Usage in a Mobile MIMO System

In publication [X], an improved planar wideband ground plane antenna, based on [IX], is presented. The antenna consists of two quasi-complementary antenna (QCA) elements

located at both ends of a mobile ground plane to gain space diversity. One QCA element includes an electric dipole closely spaced to a ground plane with a magnetic square shaped slot. The structure offers 95% relative -6 dB impedance bandwidth, mutual coupling less than -19 dB, and average total efficiency -0.85 dB, and correlation smaller than 0.04 over the operating bandwidth.

The antenna provides the fundamental mode (Mode 1) with different radiating mechanisms. When in low frequencies, the vertical currents can be found in the ground plane, in the center frequency, the dipole itself is radiating. In higher frequencies, the ground plane radiates again with vertical radiating currents. All the same, the magnetic slot in the ground plane, excited by the electric dipole ([IX] and [X]), offers a soft variation of the imaginary part of the input impedance by avoiding the appearance of strong anti-resonances that would ruin the impedance matching.

The simulations also showed that by scaling the antenna element to a size of a smartphone (120 mm $\times$ 70 mm), and slightly modifying the square slot dimensions, a frequency band from 700 MHz to 2.1 GHz (100%) can be achieved.

Table 6 summaries the characteristics of the antenna structures presented in the original papers compared to the specific objective defined in Section 1.3.2 (Table 1).

Table 6. Summary of the results achieved with the antenna structures presented in the original papers compared to the specific objectives of the dissertation.

	Literature	Specific objectives	Achieved results
Number of modes	4	6	6
Relative -6 dB BW [%]	> 10	> 30	$21.6 \ldots 100$
Mutual coupling [dB]	< -18	< -18	< -18
Average total efficiency [dB]	≥ -3	$-3 \ldots -1$	$-1.83 \ldots -0.85$
Measured correlation	< 0.5	< 0.2	≤ 0.04
EDG	> 7.0	> 7.8	> 8.0
MIMO efficiency [%]	> 0.70	> 0.78	> 0.90

As observed, the specific objectives defined at the beginning of the dissertation was achieved with a fair margin for the antenna structures presented in the dissertation. There is only one exception as one of the antennas, presented in [V], does not fully exceed the relative -6 dB impedance bandwidth. However, impedance bandwidth of the patch structure is still good as patches are relatively narrow band structures (0.5–5%). It

can concluded the antenna still satisfy the 10% relative impedance bandwidth which is defined as a limit for wideband antenna.

6 Discussion

This chapter will shortly discuss the results that are presented in the dissertation and original papers. The chapter is divided into three parts. First, the theoretical implication will discuss and compare the results to the previously published results. The second part will present ideas on how the results can be exploited and what are the benefits from a practical point of view. The final part will explain the future work and which phenomenon will require further investigation.

6.1 Theoretical implication

The theory part of this dissertation presented spherical modes on a conventional sphere, and the results were compared to characteristic modes on a planar mobile ground plane. A clear correlation between the radiating and current modes was observed. The theoretical foundation was compared to the results presented in the original papers.

The dissertation also presented novel wideband and multi-element antenna structures for mobile terminals. Whereas, usually presented wideband antennas combine multiple resonances to gain wideband characteristics, this dissertation concentrated on antenna structures to cover a wide frequency range by exciting only one mode by avoiding the excitation of higher order modes. The excited modes are described in the theoretical foundation. To gain the excitation of only one mode, carefully designed antenna feeding mechanisms were presented, by using well known principles found in literature.

When comparing results to the previously published wideband MIMO and diversity antennas for mobile applications, these kinds of results are not very widely presented in the literature. The radiation pattern diversity, with multiple excitation elements to gain orthogonal radiation patterns, is also not widely studied in literature. The radiation pattern diversity, by using multiple excitation elements, is an attractive technique, as the ground plane of a device functions as an antenna.

6.2 Practical implementations

The results of this dissertation focused on wideband antenna technology in future wireless applications. Whereas, the presented solutions concentrated on mobile terminal

applications, the area of applications is not only limited for such usage. Individual antenna elements which are presented in this dissertation can also be widened to research areas or practical applications, such as wearable body antennas or sensors and textile antennas.

It was shown by measurements that a metal bezel extension, as a practical implementation of a symmetrical folded dipole, the modification did not spoil the performance of the antenna. Additionally, even the metal bezel radiates omni-directionally, the measured SAR-values are still within the standard limits. Thus, the proposed metal bezel structure is a good option in the future to cover multiple radio interfaces with one antenna and, at the same time, leaving space for other equipments in a device, or antennas for wireless standards at higher frequencies.

The radiation pattern diversity with excitation of higher modes represented a compact solution for a MIMO antenna in a mobile or a portable device. As the ground plane is excited with multiple antenna elements, and with different excitation configurations, several orthogonal radiating modes can simultaneously take advantage of multiple independent MIMO channels.

Quasi-complementary antenna elements with wideband characteristics are an attractive solution as only one antenna system is needed, instead of using separate antenna systems for every wireless standard. The quasi-complementary UWB bowtie antenna with switching capability offers one antenna solution for high and low frequencies. It can also be mentioned here that when placing an UWB bowtie to both ends of the ground plane, space diversity systems can be implemented, which operate within a large frequency bandwidth.

As the ground plane in the middle of a mobile chassis has been used as a radiator, the antenna element itself cannot be touched by user's hand or head [174]. As a metal bezel structure was compared to a conventional PIFA in [174], the PIFA element became sensitive for a user's hand or finger, and, thus, needs alternative compensating structures [162, 214]. When the surface currents are concentrated towards a wide area on a mobile ground plane, the antenna becomes less sensitive to the user vicinity. This opens up an opportunity to compensate for the effect caused by the usage environment. This plays an important role when considering practical industrial antenna design, nowadays and in the future.

6.3 Future research topics and challenges

The dissertation was related to a wideband antenna research including multi-element antennas for mobile applications. As the antenna structures were purely studied as an antenna element, many issues related to the mobile antenna designing were left out from the contents. This section discusses these issues, whereas also future research topics for other researchers are presented.

It has been understood that antenna for mobile system should not be treated independently as an isolated element, but instead should be designed by taking such parameters into consideration as propagation, system requirements, and environmental conditions. As this dissertation introduces wideband and multi-element antennas for mobile terminals mostly as an antenna element, except in one case where SAR-values and S_{11} are measured in a close vicinity of a head phantom, the environmental issues will be discussed here.

A diversity application in a handset, the body will usually reduce the radiation pattern correlation. The performance will drop due to the body loss and mismatching [215]. The work of adaptive matching and adaptive control of distributed MIMO antennas is a promising solution to overcome human body detuning and loading [216]. Also multi-element antennas can also be used to compensate the user effect [166, 217].

In [VII], the user effect of the symmetrical folded dipole and the metal bezel was studied in terms of SAR-values and S_{11}-parameters in the vicinity of a head phantom. To get a complete picture of the vicinity of a user, measurements need to be done with a hand and head phantom as well, and with different hand grips. Also, some more parameters to describe the effect of a hand and head phantom should be studied, such as losses in antenna total efficiency, reflection losses, and the Smith chart presentation.

The antenna structures presented in this dissertation were using a mobile ground plane as a radiating element, and, in most of them, slots were cut to the ground plane to couple energy into it. Thus, an effect of slots to the SAR-values needs to be considered as well as the SAR-value is strongly dependent on the ground-plane geometry and the antenna position. In [218], analysis of the human head interaction in handset antennas has been done by studying several cases with slotted ground plane. Measurement results showed that shorted-end slots presented lower SAR values than the open-ended slots. Comparing the values to the reference ground plane without slot, it was demonstrated that slots usually do not increase the SAR values. A general conclusion was that the

SAR-values for slotted ground planes were not increased compared to a ground plane without a slot.

Another thing to consider are differences in a SAR-distribution after adding other components (display, battery, etc.) to the device, and how these components will modify the SAR-values. Usually this means reduction in SAR-values, but SAR can also depend on the electromagnetic field, and how the field is coupling to other components. As metallic parts are used in mobile devices, these might arise problematic from SAR point of view. When the field couples e.g. to a metal chassis or metallic parts in a display, these can act as directive elements and steer the radiated field against the users head by increasing SAR-value. The SAR-distributions should also be taking into account at the very beginning of the system design.

One way to decrease SAR caused by the components (display, battery, etc.), is to increase the number of the grounding pins in the chassis, which, on the other hand, might affect to the ground plane surface current distributions. Another way is to use multiple antenna elements to force the currents propagate into a certain direction. In that manner, the excitation (amplitude, phase) of the multiple antenna elements counts the uncertainties caused by the components on the ground plane. In any case, it is good to mention here that the best way to couple the field or modes to the chassis with multiple antenna elements is not solved in a proper way yet.

Whereas the mobile ground plane is very crowded with different kind of components, obtaining the desired volume and position for the antennas is very difficult. Still, as an antenna is a crucial part of a wireless device, it is needed to be taken into account at the very beginning of a mobile device designing to find the best possible positions for antennas. To gain proper or wanted antenna characteristics within a certain volume, from the antenna designer point of view, this means cooperation with other professionals related to the circuit, material, and component designing. That kind of cooperation will be more and more important in the future when considering designing of mobile and wireless devices.

As mentioned previously, the antenna structures were studied purely as an antenna element. Making simulations and measurements with prototypes closer to the real applications is another issue to make the antenna modeling closer to real applications. This means modeling of such components in the mobile applications like battery, circuitry over the slots in the ground plane, display, speaker, and the chassis itself as it can be metallic. It is also understood that antenna for mobile system should not be treated independently as an isolated element, but instead should be designed by

taking such parameters into consideration as propagation, system requirements, and environmental conditions.

Also the EMC (Electromagnetic Compatibility) aspects, and how they are affecting to the current distributions on a mobile ground plane, are not discussed in the dissertation. In general, there are some coupling between components and antennas in a real mobile device. For example, if circuits are not properly EMC-protected, some harmonics of an oscillator might disturb the transceiver, especially the receiver branch where the signal levels are very low. On the other hand, if the antenna couples field to the transmission or feeding lines, this is once again disturbing the current distributions. One way to prevent the coupling is to isolate the most sensitive components, whereas, if metal boxes are used to reduce EMC, this might cause problems from SAR perspective. Getting back to the previous paragraphs, the EMC issues are needed to be taken into account in the very beginning of the system level design as well.

In the future, such an antenna element as QCA [III, IX, X], which have a wide impedance bandwidth, opens new areas on mm-wave mobile terminal environment, or as an element in a wideband antenna array with certain antenna spacing limitation. When scaling a QCA element by the factor 3 to the size of a modern smartphone (120 mm $\times$ 70 mm), as presented in [X], a frequency range from 700 MHz to 2.1 GHz was achieved. This is opening opportunity to add two smaller scale QCA elements to the opposite end of the ground plane for a space diversity system [X]. On the other hand, a polarization diversity approach is attractive as well, such as presented in [IX].

One of the future challenges is how a radiation pattern diversity system with multiple excitation elements can be implemented in a compact space, as presented in [I]. The applications need a complex feeding network or digital signal processing to excite multiple orthogonal modes at the same time. Also mutual coupling between the multiple excitation elements needs to be investigated to guarantee good antenna performance, unless it can be utilized in the system. The question can also be set whether multiple wideband antenna elements can be used to excite orthogonal modes on a mobile ground plane in wide frequency range.

A MIMO-cube [219] is an interesting approach to excite orthogonal radiating modes. The antenna includes multiple feeding elements to excite orthogonal modes in any orientation and polarization related to the usage or radio channel conditions. Thus, it includes a large degree of freedom of different excitations. As mentioned in the case of radiation pattern diversity, a MIMO-cube provides huge challenges related to the source excitation and mutual coupling compensation between the individual excitation

elements. Related to the idea presented in [I], an approach to investigate a MIMO-cube at a wide frequency range is also a big challenge.

7 Summary

The dissertation presented wideband antennas and multi-element antennas for mobile applications. The subject was first studied with a general approach by providing basic knowledge of the spherical and the characteristic mode theories. The theory part presented numerical results and showed that it is possible to excite the same radiating modes on a planar radiating rectangular ground plane than on a conventional sphere. The introduction to the mode theories was later used in the dissertation, when the results based on the original papers [I] - [X] were analyzed.

The measured results were presented and a good correlation with simulations was observed. The designed antenna structures also correlated with the modal studies that were presented in the theory part. Some fundamental approaches were also taken by only simulation (original papers [I] - [II]) to show the functionality of the original idea.

The antenna structures were first studied without a conducting ground plane. While the ground plane was added close to the radiator, it was shown, by using a magnetic slot in a ground plane, how the excitation of the higher order modes can be avoided to increase the antenna frequency bandwidth and still, keep the antenna as an efficient radiator. The principal to excite the certain modes at a wide frequency bandwidth was cutting slots into a conducting ground plane and using monopoles, dipoles, and folded dipoles to couple energy to the ground plane.

When designing an antenna where a certain mode is wanted to be excited at a wideband frequency range, the antenna feeding and impedance matching plays a crucial part. Symmetrical folded dipoles were used with a symmetrical feeding to create a magnetic boundary condition in [VI] - [VII]. Symmetrical feeding was also used with two patches to excite a current mode on a conducting ground plane [VIII]. As dipoles were used as a coupling element, they required a wideband balun with a wideband impedance transformation to feed the antenna structure itself. The dissertation presented an LC-baluns ([VI] - [VII]) and tapered microstrip line baluns ([IX] - [X]) to feed such antennas within a wide frequency bandwidth.

A coaxial line feed was used in [III] and [VIII] without any baluns or matching circuitry. The slot dimensions of the antenna structure in [III] were modified so that the antenna could be directly connected to the 50 Ω coaxial line. The structures in [IV] and

[V] were also modified, so that no separate matching circuitry was needed, and so the structure can be kept as simple as possible.

Wideband multi-element antennas were presented for space and polarization diversity with excellent correlation, diversity gain, or MIMO efficiency properties ([IX] - [X]). It was also shown how in [I], by using multiple antennas as a feed element, it is possible to excite higher order modes on a mobile ground plane to achieve radiation pattern diversity for compact MIMO applications.

Mutual coupling compensation methods were presented with closely spaced antenna elements for diversity system. A pair of $\lambda/2$ slots between monopole antennas [IV], and by optimizing dimensions of two patch antennas [V] were presented. With both methods, the mutual coupling was significantly reduced at a wide frequency bandwidth, while, at the same time, the matching of antenna elements was greatly improved.

8 Conclusions

Nowadays, and in the future, there are several wireless standards in mobile devices. To come up with these challenges and cover multiple radio interfaces, antenna research will play an important role as they offer a wireless connection to the other devices and mobile services. Wideband mobile antenna designing can be separated into three sub-areas: frequency-tuneable antennas, multi-frequency antennas, and wideband antennas. This dissertation was concentrating on wideband antennas. How to place wideband and multiple antenna elements into a small multi-standard mobile device with limited space was another issue of the dissertation.

The results of this dissertation were focusing on wideband and multi-element antenna structures in mobile applications. It connected together the analysis of spherical modes excited on a sphere and how characteristic modes on a planar mobile ground plane are related to these spherical modes. The results obtained in the theoretical foundation were later compared to the simulated and measured results presented in the original papers [I] - [X]. To the best knowledge of the author, this kind of work has not been previously presented in the literature.

In most of the published papers in the literature, the fundamental chassis mode is excited. One of the dissertation's topics was the excitation of higher order modes by using mobile ground plane as a radiating element. In the theory part of the dissertation, the higher order spherical modes were excited on a conventional sphere, and these modes were compared to the radiation properties of excited current modes on a planar ground plane. It was shown that the same radiating modes can be found on both surfaces with corresponding surface current distributions. The surface currents on a planar ground plane were studied with respect to the characteristic mode theory, and then compared to the obtained spherical vector modes. The number of resonating modes is given by $N = kr_0$, and e.g. a ground plane size used in the dissertation $(40 \times 110)\text{mm}^2$ support 4 modes at 2 GHz.

With different excitation configurations, the surface currents of a planar antenna could be forced to higher order orthogonal forms to obtain low correlation between the radiation patterns. Three vertically and three horizontally polarized modes, totally six modes, were excited. It was shown in [I], that by exciting higher order modes with eight short dipoles above a mobile ground plane, in 90% of the excited radiation patterns at 2

and 5 GHz center frequencies, the correlation was less than 0.2. The results correspond with good orthogonality between the excited modes, as the correlation was defined to be smaller than 0.2.

The excitation of the higher order modes at a single frequency can be considered as radiation pattern diversity. Benefit of this kind of a diversity is that with orthogonally excited radiation patterns, the diversity system can be exploited in a small space, e.g. in a mobile terminal where the size of the device is limited.

As the second topic was wideband antennas, a novel and simple antenna structures were presented in original papers [II] - [III] and [VI] - [X]. It was shown that, by exciting a planar mobile ground plane with efficient feeding network, the radiating current mode in the issue remained over a wide frequency range without the disturbance of higher order modes. This required knowledge of the characteristic current modes of a certain shape of a radiator. By knowing these principal modes and their surface current distributions, the excitation was designed for the desired antenna mode.

One of the presented solutions to achieve a wide frequency range, was the usage of an electrical excitation element (inductive behaviour) close to a conducting ground plane with a magnetic slot cut into it (capacitive behaviour). The solutions were presented in original papers [III] and [IX] - [X]. These two opposite components are cancelling each other in terms of the imaginary part of the input impedance at wide frequency range. The structures are called Quasi-Complementary Antennas (QCA). The QCA structure supports the idea of a single current mode excitation.

Another solution was the usage of symmetrical feeding presented in [VI] and [VIII], where antenna elements were excited with same amplitude and phase to support only one radiating mode. Also by using this method, it is possible to create an artificial magnetic ground plane between two adjacent folded dipoles, as presented in [VI].

The dissertation was focusing on finding wideband antenna structures which relative -6 dB bandwidth is better than 30%. In practise, the relative -6 dB impedance bandwidths of the presented wideband antenna structures were between 37.5–100% over the operating bandwidth, depending on the antenna structure.

When the aforementioned single QCA element was combined as a multi-element structure in [IX] and [X], it enabled to obtain a wideband two element antenna for diversity and MIMO systems. The presented multi-element antenna structure for a mobile diversity system was supporting polarization diversity, whereas the mobile MIMO system supported space diversity.

The wideband multi-element antennas were studied as diversity and MIMO systems within a large relative -6 dB impedance bandwidth ($> 30\%$) with correlation much smaller than 0.2, antenna efficiency is at most -1 dB (80%) but better than -3 dB (50%), and the isolation between the antenna elements better than 18 dB. In Section 1.3.2, the objective for the effective diversity gain was defined to be better than 7.8, and for the MIMO efficiency better than 0.78.

The relative -6 dB impedance bandwidth of these multi-element antenna structures were between 87.5–95%, and an individual antenna had measured average total efficiency of $-0.95\ldots-0.85$ dB over the -6 dB bandwidth. The isolation between the antenna elements was better than 18 dB, when, at the same time, the measured correlation was smaller than 0.04. Thus, the measured EDG was calculated to be better than 8.0, and the measured MIMO efficiency better than 0.9 over the operating bandwidth.

The mutual coupling compensation between two antennas is important to achieve low correlation in MIMO and diversity systems. To obtain this, a mutual coupling between two adjacent antenna elements was defined to be lower than -18 dB. As the dissertation presented wideband antenna elements, methods to compensate mutual coupling at wide frequency range between the closely spaced antenna elements was presented. Following methods were investigated: slots between two monopole antennas [IV], optimizing the dimensions of two patch antennas so that the interaction between the patches is very small [V], symmetrical feeding which counts the coupling between two antenna elements [VI] - [VIII], and orthogonal polarizations [IX]. With all these methods, good isolation between antenna elements was achieved over a wide frequency range.

An interesting result in the monopole study was observed as the mutual coupling was reduced when the antenna spacing was less than a quarter of a wavelength, compared to the case where the antenna element spacing was a half-wavelength. Another interesting result was reach with the patch antenna structure. The structure presents only optimum dimensions of the adjacent patches, and, thus, the structure is very simple and includes no external matching circuit or mutual coupling compensation.

The results related to the original papers [I] - [II] were presented numerically to demonstrate the functionality of the studied methods. In [III] - [X] the numerical and empirical results were presented to show the functionality of the proposed wideband and wideband multi-element antenna structures at a wide frequency range.

In the dissertation, it was shown that the excitation of orthogonal higher order modes on a mobile ground plane is possible with multiple excitation elements. On the

other hand, the defined relative -6 dB impedance bandwidth better than 30% was well exceeded with presented wideband antenna structures. This was achieved by exciting only a single mode by avoiding the excitation of higher order modes.

Additionally, also the presented wideband multi-element antenna structures showed excellent impedance bandwidth, good isolation between the antenna elements, and good total efficiency of an individual antenna element. Good antenna performance led to a good correlation between antenna elements, and, thus, good diversity and MIMO properties. The wideband characteristics of the multi-element antennas were also based on the excitation of single mode by avoiding the excitation of higher order modes.

It can be concluded that the parameters defined in the objectives of the dissertation were obtained with a fair margin, and the comparison of the results to the literature and the state of art justifies the novelty of the work.

References

1. Sánchez-Hernández D (2008) Multiband integrated antennas for 4G terminals. Artech House Publishers.
2. Vaughan R & Andersen J (1987) Antenna diversity in mobile communications. Vehicular Technology, IEEE Transactions on 36(4): 149–172.
3. Gesbert D, Shafi M, Shiu D, Smith P & Naguib A (2003) From theory to practice: an overview of MIMO space-time coded wireless systems. Selected Areas in Communications, IEEE Journal on 21(3): 281–302.
4. Mitola III J & Maguire Jr G (1999) Cognitive radio: Making software radios more personal. Personal Communications, IEEE 6(4): 13–18.
5. Li Q, Li G, Lee W, Lee M, Mazzarese D, Clerckx B & Li Z (2010) MIMO techniques in WiMAX and LTE: a feature overview. Communications Magazine, IEEE 48(5): 86–92.
6. Johnson R & Jasik H (1984) Antenna engineering handbook.
7. Kraus J (1988) Antennas. McGraw-Hill Education.
8. Balanis C (2008) Modern antenna handbook. Wiley.
9. Stutzman W & Thiele G (1998) Antenna theory and design. Wiley.
10. Volakis J (2009) Antenna engineering handbook, volume 67.
11. Balanis C (1997) Antenna theory. Wiley.
12. Svantesson T & Ranheim A (2001) Mutual coupling effects on the capacity of multielement antenna systems. Acoustics, Speech, and Signal Processing, 2001. Proceedings.(ICASSP'01). 2001 IEEE International Conference on 4: 2485–2488.
13. Fletcher P, Dean M & Nix A (2003) Mutual coupling in multi-element array antennas and its influence on MIMO channel capacity. Electronics Letters 39(4): 342–344.
14. Berg M, Sonkki M, Myllymäki S, Tuovinen T & Salonen E (2012) Effect of the mobile terminal antenna efficiency on the cellular network issues. Antennas and Propagation (EuCAP), 2012 Proceedings of the Fourth European Conference on pp. 1–5.
15. Harrington R (2001) Time-harmonic electromagnetic fields. Wiley-IEEE Press.
16. Harrington R & Mautz J (1971) Theory of characteristic modes for conducting bodies. Antennas and Propagation, IEEE Transactions on 19(5): 622–628.
17. Chu L (1948) Physical limitations of omni-directional antennas. Journal of Applied Physics 19(12): 1163–1175.
18. Hansen J (2008) Spherical near-field antenna measurements. Michael Faraday House.
19. Ying Z (2012) Antennas in cellular phones for mobile communications. Proceedings of the IEEE 100(7): 2286–2296.
20. Luhaib S, Quboa K & Abaoy B (2012) Design and simulation dual-band PIFA antenna for GSM systems. Systems, Signals and Devices (SSD), 2012 9th International Multi-Conference on pp. 1–4.
21. Park Y, Kang D & Sung Y (2012) Compact folded triband monopole antenna for USB dongle applications. Antennas and Wireless Propagation Letters, IEEE 11: 228–231.
22. Wong K & Chen W (2009) Small-size printed loop antenna for penta-band thin-profile mobile phone application. Microwave and Optical Technology Letters 51(6): 1512–1517.
23. Gao Y, Zhang Z, Feng Z, Iskander M & Li R (2010) A novel dielectric resonator antenna with new mode and feeding structure. Microwave and Millimeter Wave Technology (ICMMT),

2010 International Conference on pp. 8–10.
24. Vainikainen P, Ollikainen J, Kivekas O & Kelander K (2002) Resonator-based analysis of the combination of mobile handset antenna and chassis. Antennas and Propagation, IEEE Transactions on 50(10): 1433 – 1444.
25. Antonino-Daviu E, Cabedo-Fabres M, Ferrando-Bataller M, Valero-Nogueira A & Martinez-Vazquez M (2005) Novel antenna for mobile terminals based on the chassis-antenna coupling. Antennas and Propagation Society International Symposium, 2005 IEEE 1: 503–506.
26. Villanen J, Icheln C & Vainikainen P (2007) A coupling element-based quad-band antenna structure for mobile terminals. Microwave and Optical Technology Letters 49(6): 1277–1282.
27. Zhang S, Ying Z & He S (2012) Diagonal chassis mode for mobile handset LTE MIMO antennas and its application to correlation reduction. Electromagnetics; Applications and Student Innovation (iWEM), 2012 IEEE International Workshop on pp. 1–2.
28. Martens R & Manteuffel D (2012) A feed network for the selective excitation of specific characteristic modes on small terminals. Antennas and Propagation (EUCAP), 2012 6th European Conference on pp. 1842–1846.
29. Rowell C & Lam E (2012) Mobile-phone antenna design. Antennas and Propagation Magazine, IEEE 54(4): 14–34.
30. Cabedo Fabrés M (2007) Systematic design of antennas using the theory of characteristic modes. Ph.D. thesis, Universidad Politécnica de Valencia.
31. Antonino Daviu E (2008) Analysis and design of antennas for wireless communications using modal methods. Ph.D. thesis, Universidad Politécnica de Valencia.
32. Cabedo-Fabres M, Antonino-Daviu E, Valero-Nogueira A & Bataller M (2007) The theory of characteristic modes revisited: A contribution to the design of antennas for modern applications. Antennas and Propagation Magazine, IEEE 49(5): 52–68.
33. Antonino-Daviu E, Cabedo-Fabres M, Gallo M, Ferrando-Bataller M & Bozzetti M (2009) Design of a multimode MIMO antenna using characteristic modes. Antennas and Propagation, 2009. EuCAP 2009. 3rd European Conference on pp. 1840–1844.
34. Elfergani I, Hussaini A, Abd-Alhameed R, Child M, Jones S & Rodriguez J (2012) Tunable PIFA slot antenna for mobile handset and WLAN applications. Antennas and Propagation (EUCAP), 2012 6th European Conference on pp. 1–4.
35. Liu L & Langley R (2010) Frequency-tunable mobile phone antennas with matching circuits. Antennas and Propagation (EuCAP), 2010 Proceedings of the Fourth European Conference on pp. 1–4.
36. Hu Z, Kelly J, Song C, Hall P & Gardner P (2010) Novel wide tunable dual-band reconfigurable chassis-antenna for future mobile terminals. Antennas and Propagation (EuCAP), 2010 Proceedings of the Fourth European Conference on pp. 1–5.
37. Del Barrio S, Pelosi M, Franek O & Pedersen G (2011) Tuning range optimization of a planar inverted f antenna for the LTE low frequency bands. Vehicular Technology Conference (VTC Fall), 2011 IEEE pp. 1–5.
38. Naser-Moghadasi M, Sadeghzadeh Sheikhan R, Fakheri M, Aribi T, Sedghi T & Virdee B (2012) Miniature hook-shaped multi-band antenna for mobile applications. Antennas and Wireless Propagation Letters, IEEE 11: 1096–1099.
39. Zhuo W, Yan G & Yu D (2010) Reconfigurable multiband antenna design for mobile phones. Signals Systems and Electronics (ISSSE), 2010 International Symposium on 2: 1–4.

40. Wong K & Chang C (2009) Printed $\lambda/8$-PIFA for internal penta-band mobile phone antenna. Antennas and Propagation, 2009. EuCAP 2009. 3rd European Conference on pp. 533–537.
41. Ma J, Yin Y, Hu W & Ren X (2011) Compact planar hexa-band inverted-f antenna for mobile phone application. Microwave and Optical Technology Letters 53(6): 1233–1236.
42. Lee C & Wong K (2010) Planar monopole with a coupling feed and an inductive shorting strip for LTE/GSM/UMTS operation in the mobile phone. Antennas and Propagation, IEEE Transactions on 58(7): 2479–2483.
43. Zhou D, Abd-Alhameed R, See C, Alhaddad A & Excell P (2010) Compact wideband balanced antenna for mobile handsets. Microwaves, Antennas & Propagation, IET 4(5): 600–608.
44. Jeon S & Kim H (2012) Mobile terminal antenna using a planar inverted-e feed structure for enhanced impedance bandwidth. Microwave and Optical Technology Letters 54(9): 2133–2139.
45. Kim M, Lee W & Yoon YJ (2011) Wideband antenna for mobile terminals using a coupled feeding structure. Antennas and Propagation (APSURSI), 2011 IEEE International Symposium on pp. 1910–1913.
46. Lim Y, Yoon Y & Jung B (2012) Small UWB antenna with bandstop function for wireless USB of mobile handsets. Microwave and Optical Technology Letters 54(2): 438–441.
47. Kearney D, John M & Ammann M (2011) Miniature ceramic dual-PIFA antenna to support band group 1 UWB functionality in mobile handset. Antennas and Propagation, IEEE Transactions on 59(1): 336–339.
48. Zhao A & Rahola J (2007) Compact printed patch and bent-patch monopole ultra-wideband (UWB) antennas for mobile terminals. Antennas and Propagation Society International Symposium, 2007 IEEE pp. 5135 –5138.
49. Zhao A & Ollikainen J (2007) Half-sized vertical monopole ultra-wideband (UWB) antennas for mobile applications. Ultra-Wideband, 2007. ICUWB 2007. IEEE International Conference on pp. 497 –501.
50. Vaughan R & Andersen J (2003) Channels, propagation and antennas for mobile communications, volume 50. IET.
51. Vainikainen P, Holopainen J, Icheln C, Kivekas O, Kyro M, Mustonen M, Ranvier S, Valkonen R & Villanen J (2009) More than 20 antenna elements in future mobile phones, threat or opportunity? Antennas and Propagation, 2009. EuCAP 2009. 3rd European Conference on pp. 2940–2943.
52. Berg M (2011) Methods for antenna frequency control and user effect compensation in mobile terminals. Ph.D. thesis, University of Oulu.
53. Holopainen J (2011) Compact UHF-band antennas for mobile terminals: focus on modelling, implementation, and user interaction. Ph.D. thesis, Aalto University.
54. Jofre L, Martínez-Vázquez M, Serrano R & Roqueta G (2012) Handbook on Small Antennas, volume 1. EurAAP Technical Working Group on Compact Antennas.
55. Wang M, Lin L, Chen J, Jackson D, Kainz W, Qi Y & Jarmuszewski P (2011) Evaluation and optimization of the specific absorption rate for multiantenna systems. Electromagnetic Compatibility, IEEE Transactions on 53(3): 628–637.
56. (2008). FCC, SAR evaluation considerations for handsets with multiple transmitters and antennas, KDB 941255 D01.
57. Rao Q & Wilson K (2011) Design, modeling, and evaluation of a multiband MIMO/Diversity antenna system for small wireless mobile terminals. Components, Packaging and Manufac-

turing Technology, IEEE Transactions on 1(3): 410 –419.
58. Shen D, Guo T, Kuang F, Zhang X & Wu K (2012) A novel wideband printed diversity antenna for mobile handsets. Vehicular Technology Conference (VTC Spring), 2012 IEEE 75th pp. 1–5.
59. Liu L & Du Z (2010) A wideband four-element antenna system for mobile terminals. Microwave and Millimeter Wave Technology (ICMMT), 2010 International Conference on pp. 36 –39.
60. See C, Abd-Alhameed R, Abidin Z, McEwan N & Excell P (2012) Wideband printed MIMO/Diversity monopole antenna for WiFi/WiMAX applications. Antennas and Propagation, IEEE Transactions on 60(4): 2028–2035.
61. Blanch S, Romeu J & Corbella I (2003) Exact representation of antenna system diversity performance from input parameter description. Electronics Letters 39(9): 705–707.
62. Kildal P & Rosengren K (2003) Electromagnetic analysis of effective and apparent diversity gain of two parallel dipoles. Antennas and Wireless Propagation Letters, IEEE 2(1): 9–13.
63. Ying Z, Bolin T, Plicanic V, Derneryd A & Kristensson G (2005) Diversity antenna terminal evaluation. Antennas and Propagation Society International Symposium, 2005 IEEE 2: 375–378.
64. Tian R, Lau B & Ying Z (2011) Multiplexing efficiency of MIMO antennas. Antennas and Wireless Propagation Letters, IEEE (99): 183–186.
65. Liflander J. Radiated efficiency: A true measure of antenna performance, (cited 5.12.2012). http://www.pulseelectronics.com/library/white_papers.
66. Vainikainen P, Mustonen M, Kyro M, Laitinen T, Icheln C, Villanen J & Suvikunnas P (2008) Recent development of MIMO antennas and their evaluation for small mobile terminals. Microwaves, Radar and Wireless Communications, 2008. MIKON 2008. 17th International Conference on pp. 1–10.
67. Li H, Xiong J, Ying Z & He S (2010) Compact and low profile co-located MIMO antenna structure with polarisation diversity and high port isolation. Electronics Letters 46(2): 108 –110.
68. Chiu CY & Murch R (2008) Compact four-port antenna suitable for portable MIMO devices. Antennas and Wireless Propagation Letters, IEEE 7: 142 –144.
69. Zhang S, Lau B, Tan Y, Ying Z & He S (2012) Mutual coupling reduction of two PIFAs with a T-shape slot impedance transformer for MIMO mobile terminals. Antennas and Propagation, IEEE Transactions on 60(3): 1521–1531.
70. Rowell C & Lam E (2012) Multiple frequency band and high isolation mobile device antennas using a capacitive slot. Antennas and Propagation, IEEE Transactions on 60(8): 3576–3582.
71. Li Z, Du Z, Takahashi M, Saito K & Ito K (2012) Reducing mutual coupling of MIMO antennas with parasitic elements for mobile terminals. Antennas and Propagation, IEEE Transactions on 60(2): 473–481.
72. Li J, Chu Q & Huang T (2012) A compact wideband MIMO antenna with two novel bent slits. Antennas and Propagation, IEEE Transactions on 60(2): 482–489.
73. Kim I, Kim Y *et al.* (2008) Low-profile wideband MIMO antenna with suppressing mutual coupling between two antennas. Microwave and Optical Technology Letters 50(5): 1336–1339.
74. Yu B, Jung C, Lee H, Park M, Kim B, Wi H, Choi Y, Kim D & Lee B (2012) Closely mounted compact wideband diversity antenna for mobile phone applications. International

Journal of Antennas and Propagation 2012.
75. Martens R, Safin E & Manteuffel D (2011) Selective excitation of characteristic modes on small terminals. Antennas and Propagation (EUCAP), Proceedings of the 5th European Conference on pp. 2492–2496.
76. Chaudhury S, Chaloupka H & Ziroff A (2008) Novel MIMO antennas for mobile terminal. Microwave Conference, 2008. EuMC 2008. 38th European pp. 1751–1754.
77. Harrington R (1960) Effect of antenna size on gain, bandwidth, and efficiency. J. Res. Nat. Bur. Stand 64(1): 1–12.
78. Garbacz R & Turpin R (1971) A generalized expansion for radiated and scattered fields. Antennas and Propagation, IEEE Transactions on 19(3): 348–358.
79. Gadora LC (2002) Handbook of Antennas in Wireless Communications. CRC press.
80. Sedra AS & Smith KC (1998) Microelectronic circuits. Oxford university press.
81. Mongia R, Bahl I & Bhartia P (1999) RF and microwave coupled-line circuits. Boston.
82. Gans M, Kajfez D & Rumsey V (1965) Frequency independent baluns. Proceedings of the IEEE 53(6): 647–648.
83. Saunders S & Aragón-Zavala A (2007) Antennas and propagation for wireless communication systems. Wiley.
84. Wheeler H (1947) Fundamental limitations of small antennas. Proceedings of the IRE 35(12): 1479–1484.
85. Wheeler H (1975) Small antennas. Antennas and Propagation, IEEE Transactions on 23(4): 462–469.
86. Wheeler H (1959) The radiansphere around a small antenna. Proceedings of the IRE 47(8): 1325–1331.
87. McLean J (1996) A re-examination of the fundamental limits on the radiation Q of electrically small antennas. Antennas and Propagation, IEEE Transactions on 44(5): 672.
88. Bourtoutian R, Delaveaud C & Toutain S (2007) Low profile UWB shorted dipole antenna. Antennas and Propagation Society International Symposium, 2007 IEEE pp. 5729–5732.
89. Zhang J & Wang F (2008) Study of a double printed UWB dipole antenna. Microwave and Optical Technology Letters 50(12): 3179–3181.
90. Gao G, Yang X, Zhang J, Xiao J & Wang F (2008) Double-printed rectangular patch dipole antenna for UWB applications. Microwave and Optical Technology Letters 50(9): 2450–2452.
91. Low X, Chen Z & See T (2009) A UWB dipole antenna with enhanced impedance and gain performance. Antennas and Propagation, IEEE Transactions on 57(10): 2959–2966.
92. Li D & Mao J (2012) A koch-like sided fractal bow-tie dipole antenna. Antennas and Propagation, IEEE Transactions on 60(5): 2242–2251.
93. Wong K, Tseng T & Teng P (2004) Low-profile ultra-wideband antenna for mobile phone applications. Microwave and optical technology letters 43(1): 7–9.
94. Jung J, Seol K, Choi W & Choi J (2005) Wideband monopole antenna for various mobile communication applications. Electron. Lett 41(24): 1313–1314.
95. Zhao A & Ollikainen J (2007) Half-sized vertical monopole ultra-wideband (UWB) antennas for mobile applications. Ultra-Wideband, 2007. ICUWB 2007. IEEE International Conference on pp. 497–501.
96. Lee J, Hong S, Shin J & Choi J (2009) A compact ultrawideband monopole antenna for wireless communication application. Antennas and Propagation, IEEE Transactions on 57(9): 2785–2788.

97. Sung Y (2012) UWB monopole antenna with two notched bands based on the folded stepped impedance resonator. Antennas and Wireless Propagation Letters, IEEE 11: 500–502.
98. Wang Y, Lee C, Tian P & Lee S (2003) Novel microstrip-monopole-integrated ultra-wideband antenna for mobile UWB devices. Radio and Wireless Conference, 2003. RAWCON'03. Proceedings pp. 87–90.
99. Wang H & Zhang M (2008) Simulation design of four-arm cavity backed dielectric loaded UWB spiral antenna. Microwave and Millimeter Wave Technology, 2008. ICMMT 2008. International Conference on 4: 1675–1678.
100. Li W, Hei Y, Wei F & Shi X (2011) Planar antenna for 3G/Bluetooth/WiMAX and UWB applications with dual band-notched characteristics. Antennas and Wireless Propagation Letters, IEEE (11): 61–64.
101. Radiom S, Aliakbarian H, Vandenbosch G & Gielen G (2009) An effective technique for symmetric planar monopole antenna miniaturization. Antennas and Propagation, IEEE Transactions on 57(10): 2989–2996.
102. Yao Y, Chen W, Huang B & Feng Z (2008) Novel planar tapered-slot-fed UWB antenna. Microwave and Optical Technology Letters 50(9): 2280–2283.
103. Azim R, Islam M & Misran N (2011) Compact tapered-shape slot antenna for UWB applications. Antennas and Wireless Propagation Letters, IEEE (10): 1190–1193.
104. Jacob S, Shameena V, Mridula S, K Anandan C, Vasudevan K & Mohanan P (2012) Planar UWB antenna with modified slotted ground plane. International Journal of RF and Microwave Computer-Aided Engineering 22(5): 594–602.
105. Xiao B, Wang X & Zhao J (2010) A dual band notched ultra-wideband antenna using complementary split ring resonators. Wireless Communications, Networking and Information Security (WCNIS), 2010 IEEE International Conference on pp. 107–109.
106. Guo L, Wang S, Chen X & Parini C (2010) Study of compact antenna for UWB applications. Electronics letters 46(2): 115–116.
107. Huang C & Su Jr Y (2012) A printed quasi-self-complementary antenna for band-notched uwb applications. Microwave and Optical Technology Letters 54(8): 1879–1882.
108. Merli F, Zurcher J, Freni A & Skrivervik A (2009) Analysis, design and realization of a novel directive ultrawideband antenna. Antennas and Propagation, IEEE Transactions on 57(11): 3458–3466.
109. Guo L, Huang F, Wang Y & Tang X (2010) A band-notched UWB log-periodic dipole antenna fed by strip line. Ultra-Wideband (ICUWB), 2010 IEEE International Conference on 1: 1–4.
110. Wang Y, Lee C, Tian P & Lee S (2003) Novel microstrip-monopole-integrated ultra-wideband antenna for mobile UWB devices. Radio and Wireless Conference, 2003. RAWCON'03. Proceedings pp. 87–90.
111. Martinez-Vazquez M (2005) Small UWB antenna for mobile handsets. Antennas and Propagation Society International Symposium, 2005 IEEE 2: 347–350.
112. Wu C, Tang C & Chen A (2005) UWB chip antenna design using LTCC multilayer technology for mobile applications. Microwave Conference Proceedings, 2005. APMC 2005. Asia-Pacific Conference Proceedings 3: 3–5.
113. Lee Y, Hong S, Kim J, Kim G, Seong W & Choi J (2008) Design of an ultra-wideband internal antenna using symmetrical radiators for mobile application. Antennas and Propagation Society International Symposium, 2008. AP-S 2008. IEEE pp. 1–4.

114. Chien D (2010) A small monopole antenna for UWB mobile applications with WLAN band rejected. ICCE 2010-3rd International Conference on Communications and Electronics pp. 379–383.
115. Seo S & Lee B (2010) Compact UWB diversity antenna for mobile phone applications. Microwave Conference Proceedings (APMC), 2010 Asia-Pacific pp. 2268–2270.
116. Lee JM, Kim KB, Ryu HK & Woo JM (2012) A compact ultrawideband MIMO antenna with WLAN band-rejected operation for mobile devices. Antennas and Wireless Propagation Letters, IEEE 11: 990–993.
117. Chen Z *et al.* (2007) Antennas for portable devices.
118. Kaivanto M (2007) UWB antennas in portable devices. Master's thesis, University of Oulu.
119. Mushiake Y (1992) Self-complementary antennas. Antennas and Propagation Magazine, IEEE 34(6): 23–29.
120. Booker H (1946) Slot aerials and their relation to complementary wire aerials (Babinet's principle). Electrical Engineers-Part IIIA: Radiolocation, Journal of the Institution of 93(4): 620–626.
121. (2002). FCC, The first report and order regarding ultra-wideband transmission system, ET Docket No. 98-153.
122. Tanaka S, Nagatoshi M, Kim Y, Morishita H, Horiuchi S, Narieda S & Atsumi Y (2009) Miniaturised wideband folded bow-tie antenna. Electronics letters 45(6): 295–297.
123. Antonino-Daviu E, Cabedo-Fabres M, Ferrando-Bataller M & Herranz-Herruzo J (2004) Analysis of the coupled chassis-antenna modes in mobile handsets. Antennas and Propagation Society International Symposium, 2004. IEEE 3: 2751–2754.
124. Villanen J, Ollikainen J, Kivekas O & Vainikainen P (2003) Compact antenna structures for mobile handsets. Vehicular Technology Conference, 2003. VTC 2003-Fall. 2003 IEEE 58th 1: 40–44.
125. Villanen J, Ollikainen J, Kivekas O & Vainikainen P (2006) Coupling element based mobile terminal antenna structures. Antennas and Propagation, IEEE Transactions on 54(7): 2142–2153.
126. Antonino-Daviu E, Suarez-Fajardo C, Cabedo-Fabrés M & Ferrando-Bataller M (2006) Wideband antenna for mobile terminals based on the handset PCB resonance. Microwave and optical technology letters 48(7): 1408–1411.
127. Cabedo A, Anguera J, Picher C, Ribó M & Puente C (2009) Multiband handset antenna combining a PIFA, slots, and ground plane modes. Antennas and Propagation, IEEE Transactions on 57(9): 2526–2533.
128. Zhao A & Rahola J (2005) Numerical and experimental study of a quarter-wavelength wideband slot antenna for mobile applications. Microwave Conference Proceedings, 2005. APMC 2005. Asia-Pacific Conference Proceedings 4: 4–7.
129. Muscat A & Zammit J (2008) Reconfigurable antenna structure for a wideband cognitive radio pp. 1–5.
130. Liu L & Langley R (2010) Frequency-tunable mobile phone antennas with matching circuits. Antennas and Propagation (EuCAP), 2010 Proceedings of the Fourth European Conference on pp. 1–4.
131. Hossa R, Byndas A & Bialkowski M (2004) Improvement of compact terminal antenna performance by incorporating open-end slots in ground plane. Microwave and Wireless Components Letters, IEEE 14(6): 283–285.

132. Anguera J, Sanz I, Mumbru J & Puente C (2010) Multiband handset antenna with a parallel excitation of PIFA and slot radiators. Antennas and Propagation, IEEE Transactions on 58(2): 348–356.
133. Lin C, Wong K & Yeh S (2007) Printed monopole slot antenna for multiband operation in the mobile phone. Antennas and Propagation Society International Symposium, 2007 IEEE pp. 629–632.
134. Wong K & Huang C (2008) Compact multiband PIFA with a coupling feed for internal mobile phone antenna. Microwave and Optical Technology Letters 50(10): 2487–2491.
135. Chi Y & Wong K (2008) Compact multiband folded loop chip antenna for small-size mobile phone. Antennas and Propagation, IEEE Transactions on 56(12): 3797–3803.
136. Bhatti R, Im Y, Choi J, Manh T & Park S (2008) Ultrathin planar inverted-F antenna for multistandard handsets. Microwave and Optical Technology Letters 50(11): 2894–2897.
137. Song C, Hu Z, Kelly J, Hall P & Gardner P (2009) Wide tunable dual-band reconfigurable antenna for future wireless devices. Antennas & Propagation Conference, 2009. LAPC 2009. Loughborough pp. 601–604.
138. Cao Y, Yuan B & Wang G (2011) A compact multiband open-ended slot antenna for mobile handsets. Antennas and Wireless Propagation Letters, IEEE 10: 911–914.
139. Zhang T, Li R, Jin G, Wei G & Tentzeris E (2011) A novel multiband planar antenna for GSM/UMTS/LTE/Zigbee/RFID mobile devices. Antennas and Propagation, IEEE Transactions on 59(11): 4209–4214.
140. Sim C, Chao C & He W (2012) A multiband hybrid antenna with double layer structures for mobile devices. Microwave and Optical Technology Letters 54(6): 1543–1548.
141. Cabedo-Fabres M, Antonino-Daviu E, Valero-Nogueira A & Ferrando-Bataller M (2007) Notched radiating ground plane analyzed from a modal perspective. Frequenz 61(3-4): 66–70.
142. (2009). ETSI, Digital Video Broadcasting (DVB), DVB-H implementation guidelines, 2009-06.
143. Holopainen J, Kivekas O, Icheln C & Vainikainen P (2010) Internal broadband antennas for digital television receiver in mobile terminals. Antennas and Propagation, IEEE Transactions on 58(10): 3363–3374.
144. Ulaby F, Michielssen E & Ravaioli U (1999) Fundamentals of applied electromagnetics. Prentice Hall New Jersey.
145. Ma K, Hirose K, Yang F, Qian Y & Itoh T (1998) Realisation of magnetic conducting surface using novel photonic bandgap structure. Electronics Letters 34(21): 2041–2042.
146. Sievenpiper D, Zhang L, Broas R, Alexopolous N & Yablonovitch E (1999) High-impedance electromagnetic surfaces with a forbidden frequency band. Microwave Theory and Techniques, IEEE Transactions on 47(11): 2059–2074.
147. Broas R, Sievenpiper D & Yablonovitch E (2001) A high-impedance ground plane applied to a cellphone handset geometry. Microwave Theory and Techniques, IEEE Transactions on 49(7): 1262–1265.
148. Du Z, Gong K, Fu J, Gao B & Feng Z (2003) A compact planar inverted-F antenna with a PBG-type ground plane for mobile communications. Vehicular Technology, IEEE Transactions on 52(3): 483–489.
149. Zhang Y, von Hagen J, Younis M, Fischer C & Wiesbeck W (2003) Planar artificial magnetic conductors and patch antennas. Antennas and Propagation, IEEE Transactions on 51(10): 2704–2712.

150. Cabedo-Fabrés M, Antonino-Daviu E, Valero-Nogueira A & Ferrando-Bataller M (2005) Wideband radiating ground plane with notches. Antennas and Propagation Society International Symposium, 2005 IEEE 2: 560–563.
151. Cai L, Li Y, Zeng G & Yang H (2010) Compact wideband antenna with double-fed structure having band-notched characteristics. Electronics Letters 46(23): 1534–1536.
152. Yang Y (2008) A double-fed broadband planar antenna for mobile handset application. Microwave and Millimeter Wave Technology, 2008. ICMMT 2008. International Conference on 3: 1238–1239.
153. Gamage J & Jensen I (2007) Double-fed wideband printed monopole antenna. Antennas, 2007. INICA'07. 2nd International ITG Conference on pp. 76–80.
154. Oikonomopoulos-Zachos C (2010) Double layer compact four-port antenna using a symmetrical feeding technique for future MIMO antenna systems at 5.6 GHz. Antennas and Propagation Society International Symposium (APSURSI), 2010 IEEE pp. 1–4.
155. Antonino-Daviu E, Cabedo-Fabres M, Ferrando-Bataller M & Valero-Nogueira A (2003) Wideband double-fed planar monopole antennas. Electronics Letters 39(23): 1635–1636.
156. Tanaka S, Kim Y, Morishita H, Horiuchi S, Atsumi Y & Ido Y (2008) Wideband planar folded dipole antenna with self-balanced impedance property. Antennas and Propagation, IEEE Transactions on 56(5): 1223–1228.
157. King H & Wong J (1977) Effects of a human body on a dipole antenna at 450 and 900 mhz. Antennas and Propagation, IEEE Transactions on 25(3): 376–379.
158. Pelosi M, Franek O, Knudsen M, Christensen M & Pedersen G (2009) A grip study for talk and data modes in mobile phones. Antennas and Propagation, IEEE Transactions on 57(4): 856–865.
159. Berg M, Sonkki M & Salonen E (2009) Experimental study of hand and head effects to mobile phone antenna radiation properties. Antennas and Propagation, 2009. EuCAP 2009. 3rd European Conference on pp. 437–440.
160. Holopainen J, Kivekas O, Ilvonen J, Valkonen R, Icheln C & Vainikainen P (2011) Effect of the user's hands on the operation of lower UHF-band mobile terminal antennas: Focus on digital television receiver. Electromagnetic Compatibility, IEEE Transactions on 53(4): 831–841.
161. Huang T & Boyle K (2007) User interaction studies on handset antennas. Antennas and Propagation, 2007. EuCAP 2007. The Second European Conference on pp. 1–6.
162. Jung J, Kim S, Kong K, Lee J & Lee B (2007) Designing ground plane to reduce hand effects on mobile handsets. Antennas and Propagation Society International Symposium, 2007 IEEE pp. 1040–1043.
163. Berg M & Salonen E (2011) Compensating for the influence of human hand with two switchable antennas. Microwaves, Antennas & Propagation, IET 5(13): 1576–1582.
164. Morishita H (2008) A study on compact antennas and antenna miniaturization for handsets. Antenna Technology: Small Antennas and Novel Metamaterials, 2008. iWAT 2008. International Workshop on pp. 28–31.
165. Manteuffel D (2004) A concept to minimize the user interaction of mobile phones. Antenna Measurements and SAR, 2004. AMS 2004. IEE pp. 1–4.
166. Berg M, Sonkki M & Salonen E (2011) Absorption loss reduction in a mobile terminal with switchable monopole antennas. Antennas and Propagation, IEEE Transactions on 59(11): 4379–4383.

167. Huang L, Schroeder W & Russer P (2005) Theoretical and experimental investigation of adaptive antenna impedance matching for multiband mobile phone applications. Wideband and Multi-band Antennas and Arrays, 2005. IEE (Ref. No. 2005/11059) pp. 13–17.
168. Huttunen A, Myllymaki S, Komulainen M & Jantunen H (2010) Capacitive sensor arrangement to detect external load on a mobile terminal antenna. Progress In Electromagnetics Research 15: 13–18.
169. Crk I, Albinali F, Gniady C & Hartman J (2009) Understanding energy consumption of sensor enabled applications on mobile phones. Engineering in Medicine and Biology Society, 2009. EMBC 2009. Annual International Conference of the IEEE pp. 6885–6888.
170. Speag. DASY4. www.speag.com.
171. (2005). IEEE C95.1-2005 - standard for safety levels with respect to human exposure to radio frequency electromagnetic fields, 3 kHz to 300 GHz.
172. (2008). 47CFR2.1093 part 2: Frequency allocations and radio treaty matters; general rules and regulations, 2.1093 radiofrequency radiation exposure evaluation: Portable devices.
173. Ma J, Yin Y, Hu W & Ren X (2011) Compact planar hexa-band inverted-f antenna for mobile phone application. Microwave and Optical Technology Letters 53(6): 1233–1236.
174. Sonkki M, Berg M, Antonino-Daviu E, Cabedo-Fabrés M, Ferrando-Bataller M & Salonen E (2013) User effect comparison between metal bezel antenna and planar inverted f-antenna for mobile terminal. Microwave and Optical Technology Letters 55(2): 316–322.
175. Tse D & Viswanath P (2005) Fundamentals of wireless communication. Cambridge Univ Pr.
176. Goldsmith A (2005) Wireless communications. Cambridge Univ Pr.
177. Schwartz M, Bennett W & Stein S (1995) Communication systems and techniques. Wiley-IEEE Press.
178. Gipson JD (2002) The communications handbook. CRC Press.
179. Daniel JP (1974) Mutual coupling between antennas for emission or reception–Application to passive and active dipoles. Antennas and Propagation, IEEE Transactions on 22(2): 347 – 349.
180. Jungnickel V, Pohl V & von Helmolt C (2003) Experiments on the element spacing in multi-antenna systems. Vehicular Technology Conference, 2003. VTC 2003-Spring. The 57th IEEE Semiannual 2: 1124–1126.
181. Tounou C, Decroze C, Carsenat D, Monediere T & Jecko B (2007) Diversity antennas efficiencies enhancement. Antennas and Propagation Society International Symposium, 2007 IEEE pp. 1064–1067.
182. Arbabi A, Boutejdar A, Mahmoudi M & Omar A (2006) Increase of characteristic impedance of microstrip line using a simple slot in metallic ground plane. Communications and Electronics, 2006. ICCE '06. First International Conference on pp. 478 –481.
183. Salehi M, Motevasselian A, Tavakoli A & Heidari T (2006) Mutual coupling reduction of microstrip antennas using defected ground structure. Communication systems, 2006. ICCS 2006. 10th IEEE Singapore International Conference on pp. 1–5.
184. Chiu C, Cheng C, Murch R & Rowell C (2007) Reduction of mutual coupling between closely-packed antenna elements. Antennas and Propagation, IEEE Transactions on 55(6): 1732–1738.
185. OuYang J, Yang F & Wang Z (2011) Reducing mutual coupling of closely spaced microstrip MIMO antennas for WLAN application. Antennas and Wireless Propagation Letters, IEEE 10: 310–313.

186. Yang F & Rahmat-Samii Y (2003) Microstrip antennas integrated with electromagnetic band-gap (EBG) structures: A low mutual coupling design for array applications. Antennas and Propagation, IEEE Transactions on 51(10): 2936–2946.
187. Abedin M & Ali M (2005) Effects of a smaller unit cell planar EBG structure on the mutual coupling of a printed dipole array. Antennas and Wireless Propagation Letters, IEEE 4: 274–276.
188. Ding Y, Du Z, Gong K & Feng Z (2007) A novel dual-band printed diversity antenna for mobile terminals. Antennas and Propagation, IEEE Transactions on 55(7): 2088–2096.
189. Li Z, Du Z & Gong K (2008) A novel wideband printed diversity antenna for mobile phone application. Antennas and Propagation Society International Symposium, 2008. AP-S 2008. IEEE pp. 1–4.
190. Wang X, Feng Z & Luk K (2009) Pattern and polarization diversity antenna with high isolation for portable wireless devices. Antennas and Wireless Propagation Letters, IEEE 8: 209–211.
191. Ferrero F, Diallo A, Luxey C & Derat B (2009) Pattern diversity versus polarization diversity in UMTS mobile phones. Antennas and Propagation, 2009. EuCAP 2009. 3rd European Conference on pp. 1522–1525.
192. Molisch A (2011) Wireless communications. Wiley.
193. Lenzing H (1966) An experiment in modal diversity. Antennas and Propagation Society International Symposium, 1966 4: 326 – 333.
194. Manteuffel D (2012) Small terminal antenna concepts for reconfigurable MIMO handsets. Antennas and Propagation (APCAP), 2012 IEEE Asia-Pacific Conference on pp. 15–16.
195. Chaloupka H & Wang X (2004) Novel approach for diversity and MIMO antennas at small mobile platforms. Personal, Indoor and Mobile Radio Communications, 2004. PIMRC 2004. 15th IEEE International Symposium on 1: 637–642.
196. Schroeder W, Famdie T & Solbach K (2005) Utilisation and tuning of the chassis modes of a handheld terminal for the design of multiband radiation characteristics. Wideband and Multi-band Antennas and Arrays, 2005. IEE (Ref. No. 2005/11059) pp. 117–121.
197. Chaudhury S, Schroeder W & Chaloupka H (2007) Multiple antenna concept based on characteristic modes of mobile phone chassis. Antennas and Propagation, 2007. EuCAP 2007. The Second European Conference on pp. 1–6.
198. Chaudhury S, Schroeder W & Chaloupka H (2007) MIMO antenna system based on orthogonality of the characteristic modes of a mobile device. Antennas, 2007. INICA'07. 2nd International ITG Conference on pp. 58–62.
199. Manteuffel D & Martens R (2011) A concept for MIMO antennas on small terminals based on characteristic modes. IWAT 2011 .
200. Martens R, Safin E & Manteuffel D (2011) Inductive and capacitive excitation of the characteristic modes of small terminals. Antennas and Propagation Conference (LAPC), 2011 Loughborough pp. 1–4.
201. Tsoulos G (2006) MIMO system technology for wireless communications. Taylor & Francis Group.
202. Wallace J & Jensen M (2004) Mutual coupling in MIMO wireless systems: A rigorous network theory analysis. Wireless Communications, IEEE Transactions on 3(4): 1317–1325.
203. Manteghi M & Rahmat-Samii Y (2005) Multiport characteristics of a wide-band cavity backed annular patch antenna for multipolarization operations. Antennas and Propagation, IEEE Transactions on 53(1): 466–474.

204. Foschini G & Gans M (1998) On limits of wireless communications in a fading environment when using multiple antennas. Wireless personal communications 6(3): 311–335.
205. Antoniuk J, Moreira A & Peixeiro C (2005) Multi-element patch antenna integration into laptops for multi-standard applications. Antennas and Propagation Society International Symposium, 2005 IEEE 4: 255–258.
206. Manteuffel D (2009) MIMO antenna design challenges. Antennas & Propagation Conference, 2009. LAPC 2009. Loughborough pp. 50–56.
207. Dietrich Jr C, Dietze K, Nealy J & Stutzman W (2001) Spatial, polarization, and pattern diversity for wireless handheld terminals. Antennas and Propagation, IEEE Transactions on 49(9): 1271–1281.
208. Zhang S, Zetterberg P & He S (2010) Printed MIMO antenna system of four closely-spaced elements with large bandwidth and high isolation. Electronics letters 46(15): 1052–1053.
209. Bhatti R, Choi J & Park S (2009) Quad-band MIMO antenna array for portable wireless communications terminals. Antennas and Wireless Propagation Letters, IEEE 8: 129–132.
210. Yang C, Kim J, Kim H, Wee J, Kim B & Jung C (2010) Quad-band antenna with high isolation MIMO and broadband SCS for broadcasting and telecommunication services. Antennas and Wireless Propagation Letters, IEEE 9: 584–587.
211. Diallo A, Luxey C, Le Thuc P, Staraj R & Kossiavas G (2008) Enhanced two-antenna structures for universal mobile telecommunications system diversity terminals. Microwaves, Antennas & Propagation, IET 2(1): 93–101.
212. Hallbjorner P (2005) The significance of radiation efficiencies when using S-parameters to calculate the received signal correlation from two antennas. Antennas and Wireless Propagation Letters, IEEE 4: 97–99.
213. Kildal P, Rosengren K, Byun J & Lee J (2002) Definition of effective diversity gain and how to measure it in a reverberation chamber. Microwave and Optical Technology Letters 34(1): 56–59.
214. Kim S, Jung C, Park M, Lee J, Kim B, Wi H, Choi Y, Lee J, Jung W & Lee B (2012) Ground plane with loop structure for reducing user's hand effect. Antennas and Wireless Propagation Letters, IEEE 11: 450–452.
215. Plicanic V, Lau BK, Derneryd A & Ying Z (2009) Actual diversity performance of a multiband diversity antenna with hand and head effects. Antennas and Propagation, IEEE Transactions on 57(5): 1547 –1556.
216. Plicanic V, Vasilev I, Tian R & Lau B (2011) Capacity maximisation of handheld MIMO terminal with adaptive matching in indoor environment. Electronics Letters 47(16): 900 –901.
217. Valkonen R, Myllymaki S, Huttunen A, Holopainen J, Ilvonen J, Vainikainen P & Jantunen H (2010) Compensation of finger effect on a mobile terminal antenna by antenna selection. Electromagnetics in Advanced Applications (ICEAA), 2010 International Conference on pp. 364–367.
218. Picher C, Anguera J, Andujar A, Puente C & Kahng S (2012) Analysis of the human head interaction in handset antennas with slotted ground planes. Antennas and Propagation Magazine, IEEE 54(2): 36–56.
219. Sarrazin J, Mahé Y, Avrillon S & Toutain S (2009) Pattern reconfigurable cubic antenna. Antennas and Propagation, IEEE Transactions on 57(2): 310–317.
220. Abramowitz M & Stegun I (1964) Handbook of mathematical functions with formulas, graphs, and mathematical tables, volume 55. Dover publications.

Appendix 1
Spherical Bessel functions

The purpose of this appendix is to provide a short introduction to the Spherical Bessel functions that are used in this dissertation. The complete formulation can be found in [220].

Bessel's equations are solutions to the equations of Laplace and Helmholtz in spherical coordinates (also cylindrical). The solutions to the spherical Bessel functions are

1. $j_n(kr)$, the Spherical Bessel function of 1st kind. Representing a radial standing wave, finite at the origin.
2. $n_n(kr)$, the Spherical Bessel function of 2nd kind. Representing a radial standing wave, infinite at the origin.
3. $h_n^{(1)}(kr)$, the Spherical Hankel function of 1st kind. Representing a radial ingoing wave, infinite at the origin.
4. $h_n^{(2)}(kr)$, the Spherical Hankel function of 2nd kind. Representing a radial outgoing wave, infinite at the origin.

where (4) is the function representing an antenna radiation.

The Bessel function of order n+1/2 is used in the solution of the Helmholtz equation in spherical coordinates [15]. In scalar-wave problems, the Spherical Bessel function is defined as

$$b_n(kr) = \sqrt{\frac{\pi}{2kr}} B_{n+1/2}(kr).$$

The zero-order ($n = 0$) Bessel functions are when kr tends to infinity

$$j_0(kr) = \frac{\sin kr}{kr} \qquad h_0^{(1)}(kr) = \frac{e^{jkr}}{jkr}$$
$$n_0(kr) = -\frac{\cos kr}{kr} \quad h_0^{(2)}(kr) = -\frac{e^{-jkr}}{jkr}.$$

Appendix 2
Legendre functions

This appendix shortly presents Legendre function of the first kind and the associated low-order polynomials [18] used in this dissertation. Once again, more detailed formulation can be found in [220].

The Legendre polynomial $P_n(\cos\theta)$ is a spherical harmonic of degree n, which is independent of ϕ. The θ dependence of the spherical component of the Spherical wave function are expressed with following three functions, where $0 \leq \theta \leq \pi$,

$$\overline{P}_n^{|m|}(\cos\theta), \quad \frac{m}{\sin\theta}\overline{P}_n^{|m|}(\cos\theta), \qquad \frac{d}{d\theta}\overline{P}_n^{|m|}(\cos\theta),$$

where $\overline{P}_n^{|m|}(\cos\theta)$ is the normalized associated Legendre function of 1st kind. The normalization is defined by the following equation

$$\overline{P}_n^{|m|}(\cos\theta) = \sqrt{\frac{2n+1}{2}\frac{(n-m)!}{(n+m)!}}P_n^m(\cos\theta),$$

where $P_n^m(\cos\theta)$ is the associated Legendre function. Notice that only functions of non-negative order $|m|$ are applied. $P_n^m(\cos\theta)$ is defined as $n > 0$ and $m \geq 0$ by

$$P_n^m(\cos\theta) = \sin(\theta)^m \frac{d^m P_n(\cos\theta)}{d(\cos\theta)^m},$$

where

$$P_n(\cos\theta) = \frac{1}{2^n n!}\frac{d^n}{d(\cos\theta)^n}(\cos^2\theta - 1)^n$$

is the Legendre polynomial.

The following tables presents low-order Legendre polynomials and their derivations up to the first 2 orders (m) and 3 degrees (n). More polynomials for higher order modes can be found in [18].

Table 7.

$$\bar{\mathbf{P}}_{\mathbf{n}}^{|\mathbf{m}|}\cos\theta$$

	$n=1$	$n=2$	$n=3$
$m=2$		$-\frac{\sqrt{15}}{8}(\cos 2\theta - 1)$	$-\frac{\sqrt{105}}{16}(\cos 3\theta - \cos\theta)$
$m=1$	$\frac{\sqrt{3}}{2}\sin\theta$	$\frac{\sqrt{15}}{4}\sin 2\theta$	$\frac{\sqrt{42}}{32}(5\sin 3\theta + \sin\theta)$
$m=0$	$\frac{\sqrt{6}}{2}\cos\theta$	$\frac{\sqrt{10}}{8}(3\cos 2\theta + 1)$	$\frac{\sqrt{14}}{16}(5\cos 3\theta + 3\cos\theta)$

Table 8.

$$\frac{\mathbf{m}}{\sin\theta}\bar{\mathbf{P}}_{\mathbf{n}}^{|\mathbf{m}|}\cos\theta$$

	$n=1$	$n=2$	$n=3$
$m=2$		$\frac{\sqrt{15}}{2}\sin\theta$	$\frac{\sqrt{105}}{4}\sin 2\theta$
$m=1$	$\frac{\sqrt{3}}{2}$	$\frac{\sqrt{15}}{2}\cos\theta$	$\frac{\sqrt{42}}{16}(5\cos 2\theta + 3)$
$m=0$	0	0	0

Table 9.

$$\frac{\mathbf{d}}{\mathbf{d}\sin\theta}\bar{\mathbf{P}}_{\mathbf{n}}^{|\mathbf{m}|}\cos\theta$$

	$n=1$	$n=2$	$n=3$
$m=2$		$\frac{\sqrt{15}}{4}\sin 2\theta$	$\frac{\sqrt{105}}{16}(3\sin 3\theta - \sin\theta)$
$m=1$	$\frac{\sqrt{3}}{2}\cos\theta$	$\frac{\sqrt{15}}{2}\cos 2\theta$	$\frac{\sqrt{42}}{32}(15\cos 3\theta + \cos\theta)$
$m=0$	$-\frac{\sqrt{6}}{2}\sin\theta$	$-\frac{3\sqrt{10}}{4}\sin 2\theta$	$-\frac{3\sqrt{14}}{16}(5\sin 3\theta + \sin\theta)$

Appendix 3
Vector differential operations of spherical coordinate system

Gradient of a scalar

$$\nabla\psi = \hat{r}\frac{\partial\psi}{\partial r} + \hat{\theta}\frac{1}{r}\frac{\partial\psi}{\partial\theta} + \hat{\phi}\frac{1}{r\sin\theta}\frac{\partial\psi}{\partial\phi}.$$

Divergence of a vector

$$\nabla\cdot\vec{A} = \frac{1}{r^2}\frac{\partial}{\partial r}(r^2A_r) + \frac{1}{r\sin\theta}\frac{\partial}{\partial\theta}(A_\theta\sin\theta) + \frac{1}{r\sin\theta}\frac{\partial A_\phi}{\partial\phi}.$$

Curl of a vector

$$\nabla\times\vec{A} = \frac{\hat{r}}{r\sin\theta}\left[\frac{\partial}{\partial\theta}(A_\phi\sin\theta) - \frac{\partial A_\theta}{\partial\phi}\right] + \frac{\hat{\theta}}{r}\left[\frac{1}{\sin\theta}\frac{\partial A_r}{\partial\phi} - \frac{\partial}{\partial r}(rA_\phi)\right] + \frac{\hat{\phi}}{r}\left[\frac{\partial}{\partial r}(rA_\theta) - \frac{\partial A_r}{\partial\theta}\right].$$

Laplacian of a scalar

$$\nabla^2\psi = \frac{1}{r^2}\frac{\partial}{\partial r}\left(r^2\frac{\partial\psi}{\partial r}\right) + \frac{1}{r^2\sin\theta}\frac{\partial}{\partial\theta}\left(\sin\theta\frac{\partial\psi}{\partial\theta}\right) + \frac{1}{r^2\sin^2\theta}\frac{\partial^2\psi}{\partial\phi^2}.$$

Laplacian of a vector

$$\nabla^2\vec{A} = \nabla(\nabla\cdot\vec{A}) - \nabla\times\nabla\times\vec{A}.$$

Laplacian of a vector in expanded form

$$\begin{aligned}\nabla^2\vec{A} = \hat{r}\Bigg(&\frac{\partial^2 A_r}{\partial r^2} + \frac{2}{r}\frac{\partial A_r}{\partial r} - \frac{2}{r^2}A_r + \frac{1}{r^2}\frac{\partial^2 A_r}{\partial \theta^2} + \frac{\cot\theta}{r^2}\frac{\partial A_r}{\partial \theta} + \frac{1}{r^2\sin^2\theta}\frac{\partial^2 A_r}{\partial \phi^2} \\ &- \frac{2}{r^2}\frac{\partial A_\theta}{\partial \theta} - \frac{2\cot\theta}{r^2}A_\theta - \frac{2}{r^2\sin\theta}\frac{\partial A_\phi}{\partial \phi}\Bigg) \\ &+ \hat{\theta}\Bigg(\frac{\partial^2 A_\theta}{\partial r^2} + \frac{2}{r}\frac{\partial A_\theta}{\partial r} - \frac{A_\theta}{r^2\sin^2\theta} + \frac{1}{r^2}\frac{\partial^2 A_\theta}{\partial \theta^2} + \frac{\cot\theta}{r^2}\frac{\partial A_\theta}{\partial \theta} \\ &+ \frac{1}{r^2\sin^2\theta}\frac{\partial^2 A_\theta}{\partial \phi^2} + \frac{2}{r^2}\frac{\partial A_r}{\partial \theta} - \frac{2\cot\theta}{r^2\sin\theta}\frac{\partial A_\phi}{\partial \phi}\Bigg) \\ &+ \hat{\phi}\Bigg(\frac{\partial^2 A_\phi}{\partial r^2} + \frac{2}{r}\frac{\partial A_\phi}{\partial r} - \frac{1}{r^2\sin^2\theta}A_\phi + \frac{1}{r^2}\frac{\partial^2 A_\phi}{\partial \theta^2} + \frac{\cot\theta}{r^2}\frac{\partial A_\phi}{\partial \theta} \\ &+ \frac{1}{r^2\sin^2\theta}\frac{\partial^2 A_\phi}{\partial \phi^2} + \frac{2}{r^2\sin\theta}\frac{\partial A_r}{\partial \phi} + \frac{2\cot\theta}{r^2\sin\theta}\frac{\partial A_\theta}{\partial \phi}\Bigg).\end{aligned}$$

Notice that $\nabla^2\vec{A} \neq \hat{a}_r\nabla^2 A_r + \hat{a}_\theta\nabla^2 A_\theta + \hat{a}_\phi\nabla^2 A_\phi$, since the orientation of the unit vectors $\hat{r}$, $\hat{\phi}$, and $\hat{\theta}$ varies with the r, ϕ, and θ coordinates.

Original articles

I Sonkki M, Antonino-Daviu E, Ferrando-Bataller M, Salonen E (2011) Small Radiating Ground Plane with Higher Order Modes, In: IEEE 5th European Conference on Antennas and Propagation (EuCAP2011): 1243–1247. Taken from IEEE Explore.

II Sonkki M, Ferrando-Bataller M, Antonino-Daviu E, Salonen E (2010) Optimized Dimensions of Ultra Wideband Quasi-Complementary Antenna with Switching Capability, In: 4th European Conference on Antennas and Propagation (EuCAP2010): 1–4. Taken from IEEE Explore.

III Sonkki M, Antonino-Daviu E, Ferrando-Bataller M, Salonen E (2011) Wideband Planar Slotted Radiating Ground Plane Antenna for Portable Devices, In: Wiley's Microwave and Optical Technology Letters 53(12): 2854–2858.

IV Sonkki M, Salonen E (2010) Low Mutual Coupling Between Monopole Antennas by Using Two $\lambda/2$ Slots, In: IEEE Antennas and Wireless Propagation Letters 9: 138–141.

V Sonkki M, Antonino-Daviu E, Ferrando-Bataller M, Salonen E (2009) Optimal Dimensions of Two Microstrip Patch Antennas for Low Mutual Coupling at 5.8 GHz, In: 3th European Conference on Antennas and Propagation (EuCAP2009), 23th-27th March 2009, Berlin, Germany, VDE VERLAG GMBH · Berlin · Offenbach, Germany, 2009: 3515–3518.

VI Sonkki M, Cabedo-Fabrés M, Antonino-Daviu E, Ferrando-Bataller M, Salonen E (2011) Creation of a Magnetic Boundary Condition in a Radiating Ground Plane to Excite Antenna Modes, In: IEEE Transactions on Antennas and Propagation 59(10): 3579–3587.

VII Sonkki M, Antonino-Daviu E, Ferrando-Bataller M, Salonen E, (2012) Performance Comparison of a Symmetrical Folded Dipole Antenna for Mobile Terminals and Its Metal Bezel Extension, In: IEEE 6th European Conference on Antennas and Propagation (EuCAP2012): 1913–1916.

VIII Sonkki M, Antonino-Daviu E, Ferrando-Bataller M, Salonen E (2010) Wideband Multi-element Antenna with Symmetrical Chassis Coupling, In: 4th European Conference on Antennas and Propagation (EuCAP2010): 1–3. Taken from IEEE Explore.

IX Sonkki M, Antonino-Daviu E, Ferrando-Bataller M, Salonen E (2011) Planar Wideband Polarization Diversity Antenna for Mobile Terminals, In: IEEE Antennas and Wireless Propagation Letters 10: 939–942.

X Sonkki M, Antonino-Daviu E, Cabedo-Fabrés M, Ferrando-Bataller M, Salonen E, (2012) Improved Planar Wideband Antenna Element and Its Usage in a Mobile MIMO System, In: IEEE Antennas and Wireless Propagation Letters 11: 826–829.

Book orders:
Granum: Virtual book store
http://granum.uta.fi/granum/

UNIVERSITY OF OULU P.O.B. 7500 FI-90014 UNIVERSITY OF OULU FINLAND

ACTA UNIVERSITATIS OULUENSIS

ISBN 978-952-62-0107-8 (Paperback)
ISBN 978-952-62-0108-5 (PDF)
ISSN 0355-3213 (Print)
ISSN 1796-2226 (Online)

UNIVERSITY of OULU
OULUN YLIOPISTO